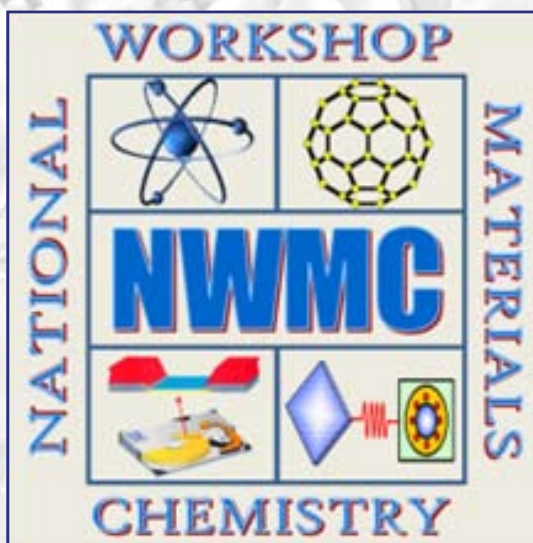


Proceedings of
DAE-BRNS
3rd NATIONAL WORKSHOP ON
MATERIALS CHEMISTRY (OPTICAL MATERIALS)
NWMC-2015 (OPT-MAT)



November 20-21, 2015

Organised by
Society for Materials Chemistry, India
&
Chemistry Division
Bhabha Atomic Research Centre

Supported by
Board of Research in Nuclear Sciences
Department of Atomic Energy
Government of India

NWMC - 2015



**Proceedings of DAE - BRNS
3rd National Workshop on Materials Chemistry
(Optical Materials)**

NWMC-2015 (OPT-MAT)

**Bhabha Atomic Research Centre
Mumbai, India**

November 20-21, 2015

Organised by

**Society for Materials Chemistry, India
&
Chemistry Division**

**Bhabha Atomic Research Centre
Trombay, Mumbai - 400 085, India**

Supported by

**Board of Research in Nuclear Sciences
Department of Atomic Energy
Government of India**

Proceedings of

DAE-BRNS 3rd National Workshop On Materials Chemistry (Optical Materials)
NWMC - 2015 (OPT-MAT)

Organised by

Society for Materials Chemistry, India & Chemistry Division
Bhabha Atomic Research Centre
Trombay, Mumbai - 400 085
India

November 2015

Printed, Designed and Processed by

Ebenezer Printing House

5 Hind Service Industries

Shivaji Park Sea-face, Dadar (W)

Mumbai-400 028. Tel. 24462632/3872

E-mail: outworkeph@gmail.com



SOCIETY FOR MATERIALS CHEMISTRY (SMC)
(Reg. No. - Maharashtra, Mumbai/1229/2008/GBBSD)
c/o Chemistry Division
Bhabha Atomic Research Centre, Mumbai-400 085, India

Executive Council

President

Dr. S. K. Sarkar

Vice-Presidents

Dr. V. K. Jain

Prof. Sandeep Verma

Secretary

Dr. P. A. Hassan

Treasurer

Dr. Sandeep Nigam

Members:

Dr. K. Ananthasivan

Dr. (Smt.) A. Banerjee

Dr. K. Bhattacharya

Dr. D. Das

Dr. G. K. Dey

Dr. P. Sujata Devi

Dr. C. P. Kaushik

Dr. T. Mukherjee

Dr. M. C. Rath

Dr. (Smt.) S. S. Rayalu

Prof. S. D. Samant

Dr. A. K. Tyagi

Dr. R. K. Vatsa

Co-opted Members:

Prof. A. K. Ganguli

Prof. A. Ajayaghosh

Dr. A. K. Tripathi

Prof. S. Ram



Message

You may be aware that UNESCO has declared 2015 to be the International Year of Light (IYL 2015) and to celebrate this a DAE-BRNS National Workshop on (NWMC-2015:OPT - MAT) being organized by Society for Materials Chemistry (SMC) working closely with Chemistry Division, BARC during November 20-21, 2015. This being the third one in our endeavor to organize the workshop series on Materials Chemistry

SMC is an organization devoted to promote education, advancement and applications of Material science and technology in India. At the outset let me express my gratitude to each and every members of SMC for their unstinted support and cooperation in the growth of the Society. Formed eight years back, SMC today is a well-knit vibrant family with members about 1000.

The role of light in our lives is both pervasive and primordial. Ultraviolet light probably had a role in the very origins of life, and light-driven photosynthesis underlies all but the most primitive of living things today. For humans, sight is the most crucial of the senses for perceiving the world around us. Indeed, the highly evolved vertebrate eye is one of the most exquisite light detectors ever created. Yet light is influencing the way we live today what we could never have imagined just a few decades ago. The importance of raising global awareness about how light-based technologies can promote sustainable development and provide solutions to global challenges in energy, education, agriculture, health care and security.

In this regard, Optical Materials continue to play vital role in enabling development of newer technologies in many areas for the benefit of society and have a great role to play in the economy of the country in general. The focus of this Workshop will be on the synthesis and characterization of different types of optical materials and how their properties can be tuned for various applications. About 200 young researchers working in the field of chemistry, physics and materials science from BARC as well as other units of DAE, National laboratories, and Institutes/Universities, will be immensely benefited.

I hope that NWMC-2015:OPT-MAT will provide a stimulating environment among the peer and the young to open up newer frontiers in material chemistry. Once again, as President of SMC, I extend most warm and hearty welcome to all the delegates and wish the workshop every success in achieving its intended objectives.

Dr Sisir K Sarkar
President , SMC

Web : www.smc-india.in; Email: socmatchem@gmail.com

Fax: 022-25505151

Phone : 022-25595330/022-25592001

NWMC-2015 (OPT-MAT)

Workshop Organising Committee

Chairman

Dr. V. K. Jain

Convener

Dr. V. Sudarsan

Secretary

Dr. Sandeep Nigam

Treasurer

Dr. G. Kedarnath

Members

Dr. S. K. Sarkar

Dr. (Smt.) S. R. Bharadwaj

Dr. A. K. Tripathi

Dr. A. K. Tyagi

Dr. R. K. Vatsa

Dr. P. A. Hassan

Dr. C. M. Das

Dr. Rakesh Verma

Dr. M. S. Kulkarni

Dr. R. Mishra

NWMC-2015 (OPT-MAT)

Local Organising Committee

Registration

Dr. Sandeep Nigam (convener)
Dr. Seemita Banerjee (Co-convener)
Dr. Sipra Chowdhury
Dr. C. A. Betty
Dr. R. Sasikala
Mrs. Alpa Shah
Ms. Archana P. Gaikwad
Mr. Rakesh Shukla

Catering

Shri. R. Manimaran (Convener)
Dr. Soumitra Das (Co-convener)
Dr. S. N. Achary
Shri. Suresh Chopade
Shri. Kamal chaudhari
Smt. Nisha Kushwaha
Shri. P. B. Sonavane

Transport

Dr. K. C. Barick (Convener)
Shri. Siddhartha Kolay (Co-convener)
Shri. Adish Tyagi
Dr. C. A. Amarnath
Dr. Prasad P. Phadnis
Shri. Bijaideep Dutta
Shri. Mohsin Jafer

Finance Sub-Committee:

Dr. G. Kedarnath (Convener)
Dr. R. S. Nighthoujam (Co-convener)
Dr. Mrinal R. Pai
Shri. Asheesh Kumar Tiwari

Banner and Auditorium

Dr. Vinita Grover gupta(Convener)
Shri. R. K. Mishra (Co-convener)
Dr. Dimple Dutta
Sh. N. Manoj
Sh. Amey wadawale
Sh. J. K. Gautam
Kum. Bandhan Saha

Publication

Dr. Sandip Dey (Convener)
Dr. A. M. Banerjee (Co-convener)
Dr. K. Bhattacharya
Smt. K. G. Girija
Dr. B.P. Mandal
Dr. Gautam Kole
Mr. Manoj Pal

Accommodation

Dheeraj Jain (Convener)
Shri. Jitendra Nuwad (Co-convener)
Dr. Shilpa Sawant
Shri. A.N. Shirsat
Shri. Suhas B. Phapale
Shri. Deepak Tyagi
Mr. Manoj Pal

PREFACE

Light plays a very important role in the development and progress of mankind. By considering the potential of light based technologies for solving problems and challenges in the fields of energy, education, agriculture and health, UN general assembly has proclaimed the year 2015 as international year of light and light based technologies. As a part of celebration on International Year of light 2015, Society for Materials Chemistry and Chemistry Division are very pleased to jointly organise the 3rd DAE-BRNS workshop on Materials Chemistry with optical materials as the focusing theme (NWMC-2015-OPT-MAT) at BARC. The workshop aims to create a platform for interaction between young scientists and research scholars working in the area of optical materials with the experts in the field.

Any material that can modify propagation or flow of light can be generally called as optical material. The modification includes processes like reflection, refraction, absorption, emission splitting of light beams etc. Efficiency of all the above mentioned processes depends on the nature of the material and wavelength of light propagating through the material. A basic understanding of interaction of light with material is essential for evaluating the efficiency of above mentioned processes and suitability of a material for a particular process. With the emergence of nano-science and nano-technology another dimension, has been added to the light matter interaction.

The two day workshop on Materials Chemistry will cover different aspects of optical materials. This include topics such as materials for spectroscopy, bio-imaging, bio-sensing, superamolecular assemblies, lasers, radiation dosimeter, solid state lighting etc. In addition to this the workshop will also cover synthesis of different types of materials ranging from single crystals, bulk powder and nanomaterials. We hope the deliberations in this workshop will be quite useful to the participants and will provide them an opportunity to expand their understanding of the subject.

The workshop organizing committee sincerely thank all the invited speakers who whole heartedly agreed to spare their valuable time and knowledge, in spite of their busy schedule. Financial support from BRNS is gratefully acknowledged. We are grateful to workshop organizing committee for their valuable suggestions and support. We also thank all the staff members of Chemistry Division for their dedicated and untiring efforts towards organizing this event. We wish all the participants a pleasant stay in Anushaktinagar and fruitful interactions during the workshop

(V. Sudarsan)

Convener, NWMC-2015

(V. K. Jain)

Chairman, NWMC-2015

Scientific Programme - NWMC - 2015 (OPT-MAT)
(November 20-21, 2015)

Friday 20-11-2015 (Day 1)		
8.30-9.30		Registration
9.30-9.45		Inauguration
9.30-10.30	Keynote Lecture	Prof. George Thomas, IISER, Thiruvananthapuram
10.30-11.00		Tea
11.00-13.00		Session I - Synthesis of Optical Materials Chairman: Dr. G. K. Dey
	IT-01	Dr. S. C. Gadkari, BARC Single Crystals as Optical Devices
	IT-02	Dr. A. K. Tyagi, BARC Synthesis of Optical Materials by Chemical Methods
	IT-03	Dr. Kedarnath, BARC Metal-organic Complexes: Optical Applications
13.00-14.00		Lunch
14.00-16.00		Session II: Bio-materials and Supramolecular Assemblies Chairman: Dr. S. K. Gupta
	IT-04	Dr. S. K. Majumder, RRCAT Photonics for Depth-Sectioning of Layered Biological Tissue
	IT-05	Dr. (Mrs.) Jyotirmayee Mohanty, BARC Optical Properties of Supramolecular Assemblies
	IT-06	Dr. Sri Sivakumar, IIT, Kanpur Ln ³⁺ Doped Nanostructures for Solid State Lighting and Bio-Imaging Applications
16.00-16.15		Tea
16.15-18.15		Session III: Lasers and Spectroscopic Applications Chairman: Dr. S. K. Sarkar
	IT-07	Dr. Sushil Mujumdar, TIFR Anderson Localization Random Lasers
	IT-08	Dr. D. V. Udupa, BARC Optical Materials for Spectroscopy Applications

	IT-09	Dr. K. S. Bartwal, RRCAT Optical Materials for Laser Applications
20.00 -21.00		Dinner
<i>*18:45 - 19:45 Society for Materials Chemistry - Annual General Body Meeting</i>		
Saturday 21-11-2015 (Day 2)		
9.30-11.30		Session IV: Glasses and Photonic Crystals Chairman: Dr. S. K. Kulshreshtha
	IT-10	Prof. N. Veeraiah, Acharya Nagarjuna University Non-linear Optical Studies on Some Specific Glasses and Glass Ceramics
	IT-11	Dr. Manoj Mohapatra, BARC Use of Eu (III) ion as a PL Probe to Understand the Radiation Induced Changes in Borosilicate Glass Matrices
	IT-12	Dr. Rajesh V. Nair, IIT, Ropar Tailoring Light-Matter Interactions Using 3d Photonic Crystals
11.30-11.45		Tea
11.45-13.05		Session V: Luminescent Materials Relevant to DAE Chairman: Dr. V. Natarajan
	IT-13	Dr. N. S. Rawat, BARC Thermo-luminescent Materials
	IT-14	Dr. M. S. Kulkarni, BARC Optically Stimulated Luminescent Materials
13.05-14.00		Lunch
14.00-16.00		Session VI: Rare Earth Based Phosphors Chairman: Dr. D. Das
	IT-15	Dr. V. Mahalingam, IISER, Kolkatta Lanthanide-doped Luminescent Nanocrystals: Synthesis, Properties and Applications
	IT-16	Dr. Pushpal Ghosh, Central University, Sagar Recent Trends in Rare-Earth Doped Nanophosphors
	IT-17	Dr. M. Anitha, BARC A Review on Rare Earth Based Phosphors
16.00-17.00		Panel discussion
17.00-17.30		Tea
17.30-18.00		Valedictory function

Contents

Keynote Lecture

Playing with Excitons in Semiconductor Quantum Dots

K. George Thomas

School of Chemistry, Indian Institute of Science Education and Research,
Thiruvananthapuram, 695 016, India
E-mail: kgt@iisertvm.ac.in

Quantum confinement effects in semiconductor nanocrystals allowed newer possibilities in tuning their physical properties by varying the size and shape. Photoexcitation of semiconductor quantum dots can generate a bound electron hole pair called exciton. The first part of the talk will provide an overview on various approaches for tuning the excitonic emission in II-VI and III-V semiconductor quantum dots. The second part of the talk will highlight our recent efforts to understand the interfacial properties of type I and II semiconductor quantum dots. Heterojunctions of type II quantum dots possess novel properties that are fundamentally different from those of individual components. Examples of designing various types of heterojunctions by bringing two dissimilar semiconductor quantum dots in contact will be discussed. Such systems can assist the spatial separation of excitons upon photoexcitation. The last part of the presentation will discuss on the optical properties of quantum dots (QDs) with emphasis on the (i) role of crystal structure and surface composition on luminescence (ii) resonance energy transfer and (iii) light induced electron transfer. We have observed that the luminescence properties of CdSe QDs are affected by its crystal structure. The zinc blende CdSe QDs exhibited excellent photostability and high photoluminescence quantum yield compared to hexagonal wurtzite which make the former system ideal for various applications which demand high emission yield. Photoinduced energy and electron transfer from InP QDs to surface bound chromophores were investigated using steady state as well as time resolved absorption and emission spectroscopic techniques. Our results indicate that InP is a versatile material for light harvesting and charge transport applications, meeting various photophysical requirements.

References

- [1] K. B. Subila and K. George Thomas (submitted 2015)
- [2] K. B. Subila, G. Kishore Kumar, S. M. Shivaprasad and K. George Thomas, *J Phys Chem Lett*, **2013**, 4, 2774-2779.
- [3] P. V. Nair and K. George Thomas *J Phys Chem Lett*, **2010**, 1, 2094-2098.
- [4] A. Thomas, P. V. Nair and K. George Thomas, *J Phys Chem C*, **2014**, 118, 3838-3845.
- [5] R. Vinayakan, T. Shanmugapriya, P. V. Nair, P. Ramamurthy and K. George Thomas *J Phys Chem C*, **2007**, 111, 10146-10149.
- [6] A. Thomas, K. Sandeep and K. George Thomas (submitted 2015).



Prof. George Thomas has made significant contributions in several areas of photosciences and nanomaterials and his group is currently focusing on the studies related to light-matter interaction at the nanoscale. Some of his recent efforts include (i) understanding the interfacial properties of hybrid nanomaterials, (ii) design of plasmonic materials for surface enhanced spectroscopy (iii) supramolecular organization of molecules on surface.

Hereceived his PhD degree in Chemistry from the University of Kerala and afterwards worked as senior scientist in the Photosciences & Photonics Section of the National Institute for Interdisciplinary Science & Technology (CSIR) from July 1994 to April 2010. In May 2010, he accepted an invitation from the newly established Indian Institute of Science Education and Research Thiruvananthapuram (IISER-TVM) and joined as a Professor. His research interests are in the areas of photochemistry and material science.

Prof. George Thomas is a recipient of several awards and distinctions: these include the J C Bose National Fellowship (2014), Shanti Swarup Bhatnagar Prize in Chemical Sciences (2006), MRSI-ICSC Superconductivity & Materials Science Annual Prize (2015). He is an elected fellow of Indian National Science Academy, New Delhi (2015) and Indian Academy of Sciences, Bangalore (2007) and Honorary Professor of the Jawaharlal Nehru Centre for Advanced Scientific Research, Bangalore. He is currently serving as the Dean of Academics of IISER-TVM and the Vice-President of the Asian and Oceanian Photochemistry Association (APA). He is one of the associate editors of the Bulletin of Material Sciences published by the Indian Academy of Sciences, Bangalore and the member of editorial advisory committee of the Journal of Physical Chemistry of the American Chemical Society. He has published around hundred peer-reviewed original research articles and four chapters in books and one of the inventors of a US patent. Seventeen students completed their doctoral degree under his supervision.

Single Crystals as Optical Devices

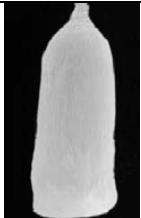
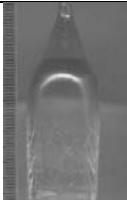


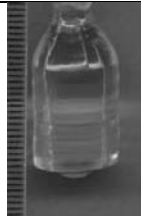
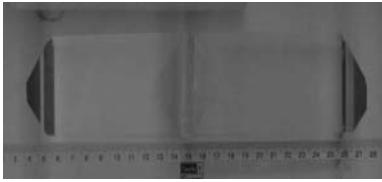

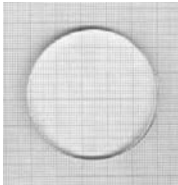
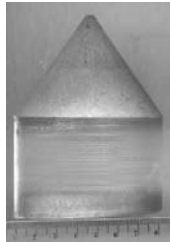
S. C. Gadkari

Technical Physics Division, Bhabha Atomic Research Centre, Trombay,
Mumbai-400085

E-mail: gadkari@barc.gov.in

Abstract

Single crystals of several optical materials are grown in the *Crystal Technology Section* of the Technical Physics Division, BARC. These crystals find applications as scintillators and dosimeters in nuclear radiation detection/measurements, laser host materials, IR windows and in non-linear optical applications. Growth of some of the oxide scintillators like, $Gd_3Ga_3Al_2O_{12}:Ce$, $YAlO_3:Ce$, $Lu_2SiO_5:Ce$, etc for gamma-ray spectroscopy, $Al_2O_3:Cr$, $NaBi(WO_4):Yb$ for laser hosts, $Li_6Y(BO_3)_3:Ce$ for neutron detection and $Li_2B_4O_7:Ag$ as sensitive dosimeters will be discussed. Optical, thermo-luminescence, photo-luminescence and scintillation properties of these crystals will be discussed with a view to develop devices for various applications. The growth of single crystals from melts, recent efforts in the development of detectors and results of experiments conducted to detect thermal neutrons will be described in the talk.

Scintillator Crystals for Nuclear radiation Detection Applications				
				
Gd ₃ Ga ₃ Al ₂ O ₁₂ :Ce crystal under UV-Light	YAlO ₃ :Ce crystal	Lu ₂ SiO ₅ :Ce crystal under UV-Light	Li ₆ Y(BO ₃) ₃ :Ce crystal under UV-Light	Li ₂ B ₄ O ₇ crystal
Crystals for Optical Devices				
				
KH ₂ PO ₄ Crystal for Second Harmonic Generator	Al ₂ O ₃ :Cr Laser Host	CaF ₂ – IR Window	Large Size LiF	



Dr. Sanjay C. Gadkari received his Masters degree in Physics in 1980 from the University of Indore (MP) securing the First Rank. He joined Bhabha Atomic Research Centre in 1981 and received his Ph.D. from the University of Mumbai. At present, he is 'Outstanding Scientist' and Head of Crystal Technology Section in the Technical Physics Division, Bhabha Atomic Research Centre. He is also a Senior Professor and member of the 'Board of Studies in Physical Sciences' in the 'Homi Bhabha National Institute'. Over the last three decades he has been working on several technologies for material synthesis, growth of single crystals, thin films, and development of gas sensors, nuclear radiation detectors, and electronic and UHV based instruments. He has to his credit over 250 research papers in journals, book chapters, technical reports, conference talks, etc. He is a recipient of 'K. Suryanarain Rau Memorial Award-2001', 'DAE Group Achievement Award-2007', 'Crystal Growth Award-2012', 'DAE Group Achievement Award-2013', and 'MRSI-Medal-2014', for his work in the area of thin films based gas sensors and crystal technology. He is a Fellow of the 'Maharashtra Academy of Sciences' and life member of several professional societies including 'The National Academy of Sciences India', 'Materials Research Society of India', 'Institute of Smart Structure and Systems', 'Indian Vacuum Society', 'Society for Materials Chemistry', 'Luminescence Society of India', etc.

Synthesis of Optical Materials By Chemical Methods

A. K. Tyagi

Chemistry Division, Bhabha Atomic Research Centre, Mumbai 400 085

E-mail: aktyagi@barc.gov.in

Abstract

Synthesis of high quality samples is an important step in the field of materials science, and the optical materials are no exception. A wide range of chemical methods for synthesis of optical materials, along with their merits and demerits will be discussed. In addition, the criteria for selection of host materials and suitable guest ions will be elaborated. Simple strategies to prepare dispersible optical materials and composite based optical materials will also be discussed in this talk. Several applications of the prepared samples will be discussed, such as bio-imaging and optical-sensing of toxic metal ions in potable water.

1. Introduction

Functional materials have assumed very prominent position in several high tech areas. Such materials are not classified on the basis of their origin, nature of bonding or processing techniques but are classified on the basis of functions which they can perform [1]. This is a significant departure from the earlier schemes in which materials were described as metals, alloys, ceramics, polymers, glass etc. Luminescent materials are also a class of functional materials. In this class, various luminescent materials are clubbed together, irrespective of their origin, chemical bonding and structure, as they have one thing in common i.e. emission of light. Optical material is a broader term which encompasses parent host materials, optically active ion, wavelength shifter, lasers, plasma display, solid state lighting, phosphors, and materials for bio-imaging and environmental application. Depending upon the applications, optical materials are used in powder or single crystal or thin film forms or even flexible forms. The advent of shape and size dependent properties has further empowered this class of functional material. A rational approach to design new luminescent functional materials is based on interplay of synthesis and crystallographic structure [2]. In view of this the synthesis of optical materials with desired composition, purity and shape has become increasingly important. In addition to shape, size, the extent of agglomeration and purity are also important parameters, which influence the

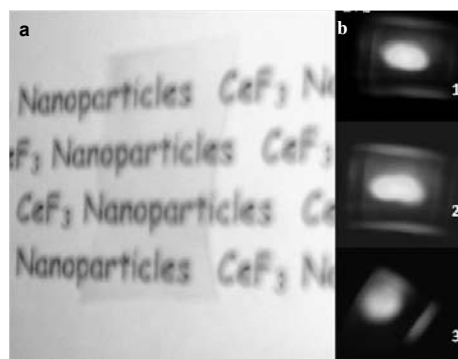


Fig. 1. (a) Picture of unirradiated transparent polymer film embedded with CeF_3 : 5.0 mol% Tb^{3+} . (b) Bright green and blue emission from (1) CeF_3 : 5 mol% Tb^{3+} /PMMA, (2) CeF_3 : 5 mol% Tb^{3+} /PVA and (3) CeF_3 : 2.5 mol% Dy^{3+} /PMMA on UV irradiation [8]

optical properties. Of late, soft chemical methods have emerged significantly in the field of functional materials. These methods are low energy synthesis methods which are often used under ambient or slightly above ambient conditions. This includes combustion synthesis, template method, solvent assisted synthesis, sono-chemical, micellar methods, hydro & solvothermal methods, microwave synthesis and solid state metathesis etc. The merits and demerits of solid state method for synthesis of optical materials will be discussed. The criteria for selection of host materials and guest ions will be elaborated. Among the various optical materials, the inorganic host materials doped with rare earth (RE) ions are being contemplated for several applications such as solid state lighting, medical diagnosis, biological and chemical probes. It is well known that the rare earth ions are known for sharp emissions as the 4f electrons are shielded by outer filled orbitals. We have been using RE ions as dopants in a number of host lattices based on garnet, spinel, zircon, scheelite, tysonite and perovskite structures.

2. Experimental

A wide variety of samples were prepared by chemical methods. Powder X-Ray Diffraction was used for structural characterization whereas the morphology of these materials was investigated by using High Resolution Transmission Electron Microscopy. The static luminescence measurements were carried out at room temperature using Hittachi F-4500 instrument. The lifetime investigations were carried out on an Edinburgh F-LSP920. A microsecond 100W Xe flash lamp was used as the excitation source. The CIE color coordinates (x , y) were calculated with the equidistant wavelength method based on the photoluminescence emission spectra. Some of the salient results are discussed in subsequent sections.

3. Results and discussion

3.1 Lanthanide based luminescent ions

Lanthanide ions doped in inorganic hosts are technologically important and are potential candidates for making, phosphor lamps, digital displays, optical amplifiers, lasers etc. For most of these applications trivalent lanthanide ions are used. In most of the trivalent lanthanide ions, the absorption and emission arise from transitions within the 4f levels, which are well shielded by the 5s and 5p levels. Hence the corresponding transitions are only slightly affected by the environment. Further, these transitions are parity forbidden and due to mixing of 4f levels with 5d levels, the transitions do occur, thereby resulting in longer excited state life times and sharp peaks. The long luminescent life times of the lanthanide ions make the laser action relatively easy to achieve with cheap pump sources. Luminescent properties of the lanthanide ions can be significantly improved by incorporating them in suitable hosts like inorganic semiconductors or insulators. The strong host absorption in these materials followed by transfer of energy to the lanthanide ions, result in improved quantum yields of luminescence from such materials. Some specific lanthanide based luminescent materials are discussed below:

3.2 YPO₄:Eu³⁺ nanoparticles

Appropriate amounts of Y₂(CO₃)₃·3H₂O and Eu₂O₃ were dissolved in dilute HCl and the excess HCl was evolved out by repeated heating and drying. This was then mixed with 20 ml of ethylene glycol and heated to 100 °C in a round bottom flask. At this temperature 15 ml of ethylene glycol containing NH₄H₂PO₄ was added and the resulting solution was heated to 160 °C for 2 h. After two hours of heating, the white precipitate obtained, was washed with acetone and ethanol and dried. The XRD pattern (not shown) is characteristic of highly crystalline YPO₄ phase with tetragonal structure. The emission spectrum for as prepared YPO₄:Eu³⁺ (5%) nanoparticles dispersed in methanol, obtained after exciting the samples at 230 nm showed peaks around 591 and 615 nm which are characteristic of ⁵D₀→⁷F₁ (magnetic dipole allowed) and ⁵D₀→⁷F₂ (electric dipole allowed) transitions respectively of Eu³⁺ ions. In crystalline YPO₄, Y³⁺ ions are having D_{2h} symmetry and hence in YPO₄:Eu³⁺ nanoparticles, Eu³⁺ ions will also have D_{2h} symmetry and this favors both electric and magnetic dipole transitions. Strong Eu³⁺ emission has been observed from the samples on exciting at the charge transfer peak maximum. These results demonstrate the fact that this method can be effectively used for synthesizing nanoparticles which are dispersible in methanol and water [3].

3.3 Rare earth ion doped zinc aluminate and zinc gallate nanoparticles

For the preparation of ZnGa₂O₄:Tb³⁺/Eu³⁺ nanoparticles Ga metal, zinc acetate, and Tb₄O₇/Eu₂O₃ were used as starting materials [4]. Appropriate amounts of Ga metal and Tb₄O₇/Eu₂O₃ were dissolved in concentrated HCl and HNO₃ mixture and the excess acid was removed by repeated evaporation by adding water. This solution was transferred to a two-necked RB flask, containing appropriate amount of zinc acetate. Ethylene glycol (15 ml) and distilled water (10 ml) were added to this mixture. The solution was slowly heated up to 100 °C followed by the addition of approximately 2 g of urea dissolved in 10 ml of ethylene glycol. It was then heated to 120 °C and maintained for 2 hours for the nucleation and growth of the nanoparticles. After the reaction the precipitate was collected by centrifugation and washed. For stabilizing the nanoparticles with oleic acid the same procedure was employed, except that around 2g of sodium oleate dissolved in ethylene glycol was added drop wise to the reaction medium immediately after the starting of precipitation at 120 °C. All the products were investigated by XRD and TEM. The emission spectra for 2% and 5% Tb³⁺ doped ZnGa₂O₄ nanoparticles, obtained after exciting the samples at 280 nm were recorded. Weak emission spectra were obtained from these samples on direct excitation of the Tb³⁺ ions at 350 nm (⁷F₆→⁵G₅ transition). However on excitation at 280 nm (4f→5d transition of Tb³⁺ ions) sharp emission peaks around 540 nm and 490 nm characteristic of the ⁵D₄→⁷F₄ and ⁵D₄→⁷F₃ transitions of Tb³⁺ are clearly observed. In addition to this, there is a broad peak around 427 nm, characteristic of the host is also observed. Dispersability of the ZnGa₂O₄:Eu³⁺ (5%) nanoparticles in organic solvents has been achieved by stabilizing the nanoparticles with oleic acid. FTIR pattern of the samples confirmed the presence of oleic acid with the nanoparticles. Emission spectrum obtained from such oleic acid stabilized ZnGa₂O₄:Eu³⁺ (5%) nanoparticles dispersed in chloroform shows strong emission characteristic of ⁵D₀→⁷F₁ and ⁵D₀→⁷F₂ transitions of Eu³⁺

ions along with broad emission around 430 nm characteristic of the host. These results suggest that the present synthesis method can be used to prepare nanoparticles that can be dispersed in organic solvents. Such materials are potential candidates for making polymer based red light emitting materials.

3.4 $\text{CePO}_4:\text{Ln}^{3+}$ ($\text{Ln}^{3+} = \text{Tb}^{3+}$ and Dy^{3+}) nano-leaves

The starting chemicals used for the synthesis of CePO_4 , $\text{CePO}_4:\text{Tb}^{3+}$ (5%) and $\text{CePO}_4:\text{Dy}^{3+}$ (5%) nano-leaves were $\text{Ce}_2(\text{CO}_3)_3 \cdot 5\text{H}_2\text{O}$, Tb_4O_7 and Dy_2O_3 by the method discussed above. The XRD patterns (not shown) for undoped and 5 at.% Tb^{3+} doped CePO_4 samples match with that of monoclinic structure of CePO_4 . Strong Tb^{3+} emission along with Ce^{3+} emission has been observed from these nano-leaves. Presence of both Ce^{3+} and Tb^{3+} emission from these samples suggests that the energy transfer between the host CePO_4 and Tb^{3+} is incomplete. This is understandable, as the energy transfer takes place through dipole-dipole interaction, Ce^{3+} ions, which are near to the Tb^{3+} ions, can only transfer the excited energy to Tb^{3+} ions [5].

3.5 Luminescence properties of oxides having Ce^{3+} ions

Cerium is commonly known to adopt either +4 or +3 oxidation states. It has been observed that the common oxidation states of cerium in oxides and phosphate matrices are +4 and +3, respectively. On the other hand, the oxides and phosphates having cerium in +3 and +4 oxidation states, respectively, are rather limited. In our group, several mixed oxides having cerium in +3 oxidation state have been prepared by employing a facile two-step synthesis method. CeScO_3 was prepared by using this method [6]. This material showed broad blue emission upon excitation at 345 nm. In order to further improve the emission properties of this material, it was doped with Tb^{3+} which resulted in green emission along with broad blue emission indicating that the energy transfer from CeScO_3 host to Tb^{3+} guest ions is not complete.

3.6 Fluoride based luminescent materials

Metal fluorides are in general wide band gap insulators with very low vibrational energies and low probability of interconfigurational transitions due to which they contribute in optical applications based on vacuum ultraviolet (VUV) and near-infrared (NIR) region. It is very well known that high phonon energies of the host lattices are primarily responsible for non-radiative relaxation in cases of rare-earth ions. Hence, fluoride lattices are superior in comparison to oxide based host lattices and therefore the quenching of the excited states of the lanthanide ions is least. This leads to a low probability of non-radiative decay for rare-earth ions and consequently the luminescence quantum yields are higher than in the oxides and most other inorganic lattices. In view of this several fluoride based luminescent materials have been synthesized in our group [7-9].

To proceed with this idea at first a simple system YF_3 as a host lattice was selected. Redispersible $\text{YF}_3:\text{Ln}^{3+}$ ($\text{Ln}^{3+}: \text{Eu}^{3+}, \text{Tb}^{3+}, \text{Dy}^{3+}, \text{Sm}^{3+}$) and $\text{YF}_3:\text{Ce}^{3+}/\text{Ln}^{3+}$ nanoparticles were synthesized by a simple polyol route using ethylene glycol as a solvent. Formation and

stabilization of the nanoparticles by ethylene glycol was confirmed by X-ray diffraction and FT-IR spectroscopy respectively. By substituting Ce^{3+} as a sensitizer in $\text{YF}_3:\text{Ln}^{3+}$, these nanopowders efficiently absorb UV-light (~ 256 nm) due to Ce^{3+} absorption and produce various luminescent colors on single excitation wavelength. Lifetime measurements suggests that there is considerable reduction in lifetime of Ce^{3+} emission when substituted along with activators and increase in lifetimes of activators (except Eu^{3+}) which supported the energy transfer process [5].

Thus, these results suggest that the Ce^{3+} ion based host lattices shows potential for applications. Also, upon incorporation of these luminescent materials to a suitable polymer matrix, the flexibility for a variety of applications ranging from biological to optoelectronics increases considerably. Two promising polymer matrices in this regards are PMMA (Poly methyl methacrylate) and PVA (Poly vinyl alcohol). Bright green luminescence was observed by $\text{CeF}_3:\text{Tb}^{3+}$ and blue luminescence by $\text{CeF}_3:\text{Dy}^{3+}$ nanoparticles upon host (CeF_3) excitation. It was observed that there is no energy transfer in the case of singly doped Eu^{3+} in CeF_3 though codoping with Dy^{3+} and Tb^{3+} gave good Eu^{3+} emission peaks. Hence, it has been postulated that in presence of Ce^{3+} , quenching of emission in Ce^{3+} and Eu^{3+} co-doped systems occur. The concentrations of Tb^{3+} , Dy^{3+} and Eu^{3+} in CeF_3 were carefully optimized to yield CIE co-ordinates (0.33 and 0.36) very close to broad daylight. PVA and PMMA based transparent nanocomposites of some representative were prepared and these films were shown to emit bright luminescence upon UV irradiation (Fig.1). Energy transfer did not get adversely affected in these polymer films. Hence this shows that these phosphors films have the potential to be developed into solid state lighting devices. The biological applications of luminescent nanoparticles are rapidly developing area of nanotechnology that lead to new possibilities in the diagnosis and treatment of various human diseases including cancers. For this purpose Gd^{3+} based fluoride host lattice was explored. After careful characterization the system was studied for its luminescence properties. Based on steady state and time resolved luminescence studies, efficient energy transfer was observed from host (Gd^{3+}) to guest ions (Eu^{3+} and Tb^{3+}) when excited at 275 nm. The best luminescence properties were observed for the nominal compositions $\text{GdF}_3:5.0$ mol% Eu^{3+} and $\text{GdF}_3:2.5$ mol% Tb^{3+} . Triply doped sample, $\text{GdF}_3:\text{Eu}^{3+}, \text{Tb}^{3+}$ and Dy^{3+} (2.0 mol% each) was found to have CIE co-ordinates (0.31 and 0.34) and correlated color temperature (6502 K) very close to broad day light. Thus, this material is expected to have promising applications as a single phase white light phosphor for UV- based solid state lighting applications. The surface of the nanoparticles was coated with silica, ethylene glycol and oleic acid to achieve better targeting. The

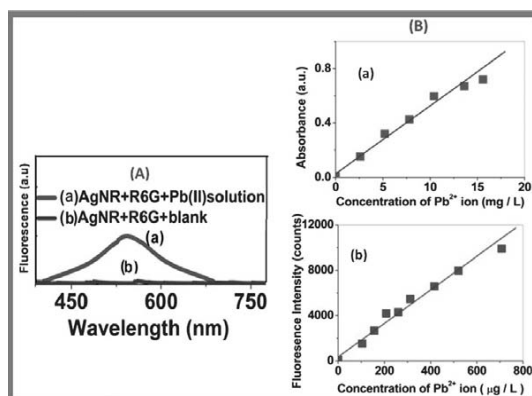


Fig. 2: Fluorescence spectra of solutions containing Ag NR-R6G hybrids in (a) the presence of Pb^{2+} and (b) absence of Pb^{2+} ions. Inset (B) shows calibration curves [10]

nanoparticles have shown encouraging results with cell labeling and imaging studies (on MCF-7) thus suggesting their potential in bio-imaging. The fluorescence intensity was found to be dependent on the surface modifying/coating agent which is in the order of ethylene glycol>oleic acid>silica. These results were further validated using Confocal Microscopy in terms of localization of these functionalized nanoparticles.

3.7 Optical sensors

Sensors are devices that are used to detect and respond to specific external stimuli. It converts some physical parameter into a measurable signal. A sensor should exhibit accuracy, selectivity and repeatability. In addition, it is desired that it should work over a wide range of analyte concentration. The optical sensors are mostly based on measurement of fluorescence from luminescent medium in the presence an analyte which can be a toxic metal ion or organic contaminants. Lead metal ions are of great concern and the monitoring of their concentration in the environment has become extremely important. In view of this, a new inorganic-organic hybrid assay of Ag nanorods (AgNR)-Rhodamine 6G (R6G) was developed for the sensitive and selective determination of Pb^{2+} ions in aqueous solutions [10]. The sensing is based on the photoluminescence of R6G. The sensor was rapid as the measurements were carried out within 3 min of addition of the test solution to the AgNR-R6G hybrid. Moreover, the system showed excellent stability at tested concentration levels of Pb^{2+} ions (Fig. 2). The naked eye detection of the colour was possible with 1 mgL^{-1} of Pb^{2+} ions. The present method has a detection limit of 50 mgL^{-1} of Pb^{2+} .

4. Conclusions:

In view of their wide range of applications, for the synthesis of optical materials (both oxide and fluoride based) different methods have been discussed. The specific synthesis method facilitated the luminescent particles in nano regime with desired size and shape. In addition, by suitable surface modifications, they could be dispersed in different solvents. Luminescence spectroscopy results showed that some of these materials can be used as a phosphor material as they reflected through their desired properties. Some of the materials were also evaluated for their applications in solid state lighting, optical sensor and bio-imaging.

Acknowledgements:

I wish to thank several of my students, colleagues and collaborators who have been associated with this work.

References

- [1] "Functional Materials: Preparation, Processing and Applications" (Eds. S. Banerjee and A. K. Tyagi) Elsevier Publishers, **2012** (ISBN: 978-0-12-385142-0).
- [2] R. Shukla, S. K. Gupta, V. Grover, V. Natarajan and A. K. Tyagi, Dalton Trans., **2015**, 44, 10628-10635.
- [3] K. Srinivasu, R. S. Ningthoujam, V. Sudarsan, R. K. Vatsa, A. K. Tyagi, P. Srinivasu, A. Vinu, J. Nanosci. Nanotech., **2009**, 9, 3034-3039.

- [4] D. P. Dutta, R. Ghildiyal and A. K. Tyagi, *J. Phys. Chem. C*, **2009**, 113, 16954-16961.
- [5] A.K. Gulnar, V.Sudarsan, R. K. Vatsa, A. K. Tyagi, R. C. Hubli, U. K. Gautam and A.Vinu, *Cryst. Growth Des.*, **2009**, 9, 2451-2456
- [6] F. N. Sayed, V. Grover, S. V. Godbole, A. K. Tyagi, *RSC Adv.*, **2012**, 2, 1161-1167.
- [7] R. Shukla, A. Arya and A. K. Tyagi, *Inorg. Chem.*, **2010**, 49, 1152.
- [8] F. N. Sayed, V. Grover, V. Sudarsan, B.N. Pandey, R. K. Vatsa and A. K. Tyagi, *J. Colloid Interf. Sci.*, **2012**, 367, 161-170.
- [9] F. N. Sayed, V. Grover, K.A. Dubey, V. Sudarsan and A.K. Tyagi, *J. Colloid and Interf. Sci.*, **2011**, 353, 445-453.
- [10] A. K. Tyagi, J. Ramkumar and O. D. Jayakumar, *Analysts*, **2012**, 137, 760-764.



Dr. A. K. Tyagi joined Bhabha Atomic Research Centre, Mumbai in 1986 through BARC-Training School. Presently he is heading the Solid State Chemistry Section at ChD, BARC and is a Professor of Chemistry at Homi Bhabha National Institute, DAE.

His research interests are in the field of preparation, structural elucidation and structure-property correlation of a wide range of materials, which include functional materials, nano-materials and nuclear materials.

Dr. Tyagi has been a visiting scientist to several countries such as Germany, USA, France, Canada, Japan, Russia, China, Portugal, Singapore, Australia, Sweden, Spain, Israel and Malaysia.

In recognition of his contribution to the field of materials chemistry, Dr. Tyagi has been conferred with several prestigious awards such as DAE-Homi Bhabha Science and Technology Award, MRSI Medal; CRSI Medal; Gold Medal of Indian Nuclear Society; Rheometric-ITAS Award; Dr. Laxmi Award of ISCAS; IANCAS-Dr Tarun Datta Memorial Award; R. D. Deasi Memorial Award of Indian Chemical Society; DAE-SRC Outstanding Researcher Award; Rajib Goyal Prize in Chemical Sciences; CRSI - Prof. CNR Rao National Prize in Chemical Sciences; ISCB Award for excellence in Chemical Sciences, MRSI-ICSC Materials Science Senior Award, CCRS Award for excellence in Chemical sciences; and ISCA-Platinum Jubilee Lecture Award in Materials Science. He is a Fellow of the Maharashtra Academy of Sciences; National Academy of Sciences India; Indian Academy of Sciences; Royal Society of Chemistry, and Asia Pacific Academy of Materials.

Metal-organic Complexes: Optical Applications

G. Kedarnath

Chemistry Division, Bhabha Atomic Research Centre, Mumbai-400 085

E-mail: kedar@barc.gov.in

Metal-organic (organometallic and metalloorganic) compounds either on their own or indirectly in the form of nanomaterials derived from them received considerable attention due to their applications in optoelectronics such as light emitting diodes (LEDs) [1], biological imaging [2] and solar cells [3], *etc.* The use of the former in OLEDs and biological labelling can be attributed to their emission properties results due to charge transfer transitions between metal to ligand or ligand to metal which can be tuned by changing the oxidation state of the metal, and coordination sphere around the metal and substitution of ligands, *etc.* Molecular rigidity of organometallic compounds is one of the attributes which decreases the molecular vibrations leading to minimization of non-radiative processes and heat losses, subsequently enhancing the emission properties of the compounds.

Heavier transition metal complexes (e.g. Ru, Os, Ag, Pd, Pt, Ir, *etc.*) find applications in phosphorescence based organic light emitting diodes (OLEDs) as they can utilize both singlet and triplet excitons. The possibility of emission from triplet excited state is corroborated by the enhancement of intersystem crossing (ISC) as a consequence of greater spin-orbit coupling owing to high Z atom in heavier transition complexes. For instance, the best OLEDs prepared to the date employ a phosphorescent molecule, [(ppy)₂Ir(acac)] (ppy = metalated 2-phenylpyridine, acac = acetylacetonate) (Fig. 1a) for doping into a wide energy gap host, 3-phenyl-4(1'-naphthyl)-5-phenyl-1,2,4-triazole exhibit external quantum efficiency of 19% and luminous power efficiency of (60±5)% [1].

Similarly, trivalent lanthanide complexes also find potential applications in OLEDs, phosphors and bio-imaging owing to their sharp emission, high quantum yield and longer luminescence lifetimes. The sharp emission properties are due to buried nature of f orbitals while higher quantum efficiency owing to ease of populating the higher excited state through sensitization with the help organic ligands in these complexes. For example, [Eu(tta)₃(phen)] (tta = 2-thenoyltrifluoroacetate) is a red emitting β-diketonate complex of Eu(III) which has quantum efficiency of 36.5% (Fig. 1b) [4].

In addition to transition metal and lanthanide complexes, luminescent main group metal complexes can also be used in OLEDs since they provide better stability or rigidity through stronger chelation as heavy main group elements permit valence expansion and accommodate multidentate ligands due to the availability of unoccupied outer nd orbitals. For instance, AlQ₃ (Q = 8-hydroxyquinolinolate) [5] has been used as a green emitter

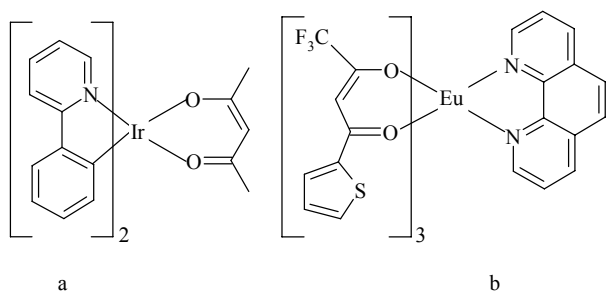


Fig. 1. Molecular structures of a) $[(ppy)_2Ir(acac)]$ and b) $[Eu(tta)_3(phen)]$.

and a common electron-transport layer in OLEDs due to its exceptional electron transport mobilities. The symmetrical arrangement of ligands around aluminium offers high thermal stability and low probability of exciton quenching. They also exhibit strong spin-orbit coupling which increase lifetime of the excited state of the complex.

The charge transfer properties of transition metal complexes also make them important component of dye sensitized solar cell (DSSC) as a sensitizer for injecting electrons into mesoporous TiO_2 films. For instance, *cis*- $[Ru(4,4'$ -dicarboxy-2,2'-bipyridine) $](NCS)_2]$ is one of the most used sensitizer in DSSC and also known as N3 dye [3].

Organometallic compounds find a number of optical applications either on their own as mentioned above or in the form of nanomaterials synthesized either by thermolysis of the former as single source molecular precursors or as metal and/or chalcogen carriers. Nanomaterials exhibit unique size and shape dependent physicochemical properties compared to their bulk counterparts which form the basis for their applications in various disciplines of science and technology. Optical properties are one of the most fascinating attributes of nanomaterials and find applications in optoelectronics, bio-imaging and solar cells, *etc.* The optical properties of nanomaterials depend on size, shape, surface properties, doping and surrounding environment. For instance, the absorption and emission maxima of CdSe quantum dots prepared by thermolysis of $[Cd(SeCH_2CH_2NMe_2)_2]$ are blue shifted with their decreasing size (Fig. 2) [6]. Such type of trend is observed when the nanostructures are confined at least in one of the three dimensions and are quantum confined with respect to size. Therefore, these size dependent optical properties allow the tunability of emission properties over wide range of electromagnetic spectrum and hence their applications in light emitting diodes and bio labelling. The efficiency of luminescent nanomaterials is determined by their quantum yield. Similarly, band gap is also size dependent as it increases with decreasing size of nanomaterials and is inversely related to the square of the particle size. For example, Zn_3P_2 quantum dots with sizes of 2.9 to 8.8 nm synthesized by hot injection of Et_2Zn and tris-(trimethylsilyl)phosphine in HDA/ODE showed band gap values ranging from 2.27 to 1.68 eV [7]. The size dependent band gap tunability of nanomaterials has an important role in several architectures of solar cells like multi junction solar cells and quantum junction solar cells, *etc.*

Likewise, shape of the nanomaterial also influences their optical properties. As mentioned above, size dependent band gap tunability is an important consequence of quantum confinement effect. But, the degree of confinement increases with the number

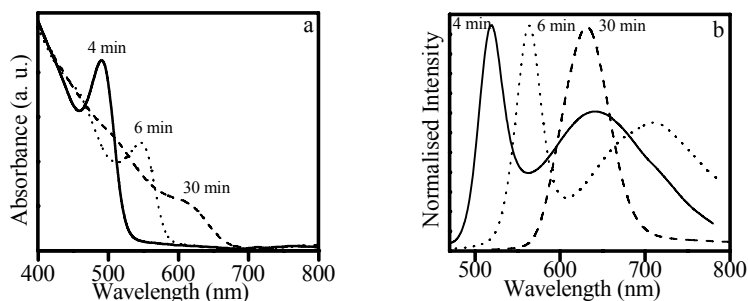


Fig. 2. a) Absorption and b) emission spectra of CdSe nanoparticles obtained by thermolysis of $[Cd(SeCH_2CH_2NMe_2)_2]$ at 187 °C in HDA/TOPO recorded at 4, 6 and 30 minutes of preparation.

of dimensions in which an exciton of semiconductor nanostructure is confined indicating the shape dependent properties of the nanostructures. For instance, spherical nanocrystals show plane polarized emission while nanorods/wires have linearly polarized emission with large Stokes shift compared to the former.

The latter property makes the elongated structures more suitable for applications in LEDs due to reduced reabsorption of light in such structures to enhance the efficiency of these devices. Similarly, spherical nanocrystals show better luminescence compared to nanorods having the same diameter as the surface to volume ratio is higher in the latter case which increases the chance of more trap states and hence reduced luminescence. Hence, spherical nanocrystals are better suited for bioimaging compared to nanorods due to higher quantum efficiency of the former.

The tunability of optical properties and rigidity of metal-organic complexes by changing the coordination and the ligands around the metal atom has generated intense interest for optoelectronic applications and stimulated the demand for new complexes which can exhibit better photophysical properties. The metal-organic complexes also contribute indirectly to the optical applications through their utilization in the preparation of high quality nanomaterials of different size and shape.

References:

- [1] C. Adachi, M. A. Baldo, M. E. Thompson and S. R. Forest, *J. Appl. Phys. Chem.*, **2001**, 90, 5048.
- [2] Q. Zhao, C. Huang and F. Li, *Chem. Soc. Rev.*, **2011**, 40, 2508.
- [3] M. K. Nazeeruddin, A. Kay, I. Rodicio, R. Humphry-Baker, E. Mueller, P. Liska, N. Vlachopoulos, M. Grätzel., *J. Am. Chem. Soc.*, 1993, 115, 6382.
- [4] F. R. G. e Silvaa, J. F. S. Menezes, G. B. Rocha, S. Alves, H. F. Brito, R. L. Longo and O. L. Malta, *J. Alloys and Compounds*, 2000, **303-304**, 364.
- [5] S. -H. Liao, J. -R. Shiu, S. -W. Liu, S. -J. Yeh, Y. -H. Chen, C. -T. Chen, T. J. Chow and C. -I. Wu, *J. Am. Chem. Soc.*, **2009**, 131, 763.
- [6] G. Kedarnath, S. Dey, V. K. Jain, G. K. Dey and B. Varghese, *Polyhedron*, **2006**, 25, 2383.
- [7] M. Q. Ho, R. J. Alan Esteves, G. Kedarnath and I. U. Arachchige, *J. Phys. Chem. C*, **2015**, 119, 10576.



Dr. G. Kedarnath, Scientific Officer (F), after passing M.Sc. (Chemistry) with distinction from Central University, Hyderabad was selected for 43rd batch of training school. After graduation from training school, he joined BARC and has been working on designing and development of single source molecular precursors for metal chalcogenide nanomaterials and thin films. In addition, interesting organotellurium chemistry with platinum group metals has also been developed. His investigations on chemistry of platinum(0) complexes with pyridyl telluroate ligands have led to serendipitous discovery of an unique complex, [Pt(Tepy)₂(Te)(PPh₃)] containing tellurium(0) as a ligand.

He was awarded Ph. D. (Chemistry) in 2010 by University of Mumbai. He acquired postdoctoral experience at Virginia Commonwealth University, Richmond, USA for a year where he has carried out synthesis and characterization of crystalline and luminescent Zn₃P₂ quantum dots. His originality in research is manifested from his publications in high impact factor peer reviewed international journals. He is also a reviewer of ACS and RSC publishers. He has delivered lectures in inorganic chemistry course for University of Mumbai and CAT-I trainees of B.A.R.C. He is a recognized Ph. D. (Chemistry) guide of HBNI and is a recipient of Scientific and Technical Excellence Award of DAE in 2013.

Photonics for Depth-Sectioning of Layered Biological Tissue

Shovan K. Majumder and Khan Mohammad Khan

Optical Spectroscopy and Diagnostic Lab, Raja Ramanna Centre for Advanced Technology, Indore 452013

E-mail: shkm@rrcat.gov.in; shovan.k.majumder@gmail.com

Abstract

There is a growing current interest in developing techniques for selective monitoring of optical signatures from different layers of a biological tissue. A brief overview of various depth-sensitive optical spectroscopic techniques for the analysis of layered biological tissues is presented in this article.

Background and Motivation:

There is enough evidence that the morphological and biochemical changes taking place in the different layers of a tissue as it transforms from normal to diseased are quite different.[1,2] It is, therefore, expected that the resulting changes in optical properties that may be manifested in the optical signatures of the respective tissue layers are also not the same.[1-3] In recent years, there is an increasing interest in selective monitoring of these optical changes with the hope that it may help facilitate diagnosis by providing improved diagnostic feedback.[1-9] However, implementation of this objective warrants a means that can disentangle the optical signals generated in the different tissue layers. One approach, developed earlier,[10] uses mathematical models based on photon transport theory to retrieve the layer specific optical signatures from the mathematical analysis of the set of measured optical spectra. However, the approach is largely based on various assumptions which require prior knowledge about many of the input parameters and often a large array of input variables that are needed to describe various competing events occurring during light propagation inside tissue. A further limitation of this mathematical approach is that the results generated by most of the models used are often difficult to validate through experiments. The other largely followed approach is to develop optical systems which are depth-sensitive and can resolve optical signals arising from the different tissue layers. Over the years a variety of techniques of varying rigor have been proposed [1-9] for disentangling the optical signals generated in the different tissue layers. Each of these techniques has its share of contribution towards meeting the current demands of disease management and deserves values in their own right. Since one common fundamental characteristic measure of all these techniques is the probing depth, based on this important parameter we will group these into two broad categories: i) techniques for shallow depth probing ($\leq 500 \mu\text{m}$) and ii) techniques for deep probing (few mm).

Depth-sensitive measurements in shallow depth ($\leq 500 \mu\text{m}$):

The depth resolution of the techniques in this category ranges from few hundreds of nanometres to tens of micrometers. The probing depths, however, are confined to few hundreds of micrometers ($\sim 300\text{-}500 \mu\text{m}$).

Confocal detection:

Confocal is the most widely researched[6,9] of the various depth-sensitive techniques reported thus far and also perhaps one of the first to be developed for probing sub-surface depths. Its major attraction comes from its intrinsic ability to attain micron scale depth-resolution (typically $\sim 5\text{-}20 \mu\text{m}$) with a comparatively straightforward instrumentation. In a typical confocal configuration, a point illumination on the sample is imaged onto the detector through a pinhole placed before the detector.[6] The practical performance of a confocal system is governed by the choice of an objective lens (for focusing and collecting light) and a pinhole (used in the image plane of the system for rejecting out-of-focus contribution). An objective lens of high numerical aperture (NA) tightly focuses the laser beam on to the surface of the target sample thereby leading to improved resolutions (axial as well as lateral), though, at the cost of reduced overall probing depth. In practice, there is a trade-off between the resolution and the depth to be probed. Likewise, a smaller sized pinhole also improves the resolution by rejecting the out-of-focus contributions of light, but the signal to noise ratio (SNR) gets poorer. However, the best performance of the system is achieved by using an oil-immersion objective lens with an index-matching fluid which removes the spherical aberration[9] by minimizing the refractive index discontinuity.

In tissue analysis, the confocal has been used not only for the characterization of skin[11] but also for estimating the skin water content[12]. The technique has also been used for exploring the possibility of differential diagnosis of cancer.[13] A handheld confocal Raman micro-spectrometer has been developed for dermatologic applications.[14] However, it is important to note that though confocal offers several advantages, two important issues limit its universal use. First, the inverse relation between the resolution and the probing depth, and the second, the light diffraction that limits the resolution. Therefore, in applications like thin film characterization where the overall depth to be probed is around few hundreds of nanometres ($z \leq \lambda$), one requires to choose a different option like total internal reflection optical spectroscopy.[5]

Total Internal Reflection (TIR) optical spectroscopy:

In TIR[5], a light ray enters into a rarer medium from a denser medium with an incident angle greater than the critical angle. During the process, although there should not be any transmission of energy across the interface in the rarer medium but the boundary conditions imply that there is an exponentially decaying electric field (called the evanescent wave). This field generates the optical spectrum of that medium. Since, the penetration depth (d_p) of the field is a function of the wavelength of the incident light (λ) and the

angle of incidence (θ_i), the depth-sensitive optical spectra can be obtained by varying θ_i . The range of the probing depths with the technique typically varies from hundreds of nanometres to few microns.[5] In a typical TIR optical spectroscopy based experimental set-up, a laser beam is incident on the sample through a transparent internal reflection element (IRE)[5] having a refractive index higher than that of the sample and with an NA same as that of the objective lens used for light collection. Although, the technique offers excellent depth resolution (~ 100 nm), it has found limited applications[5, 15-16] due to the complex instrumentation of the TIR system having various bulky optics. Further, the technique also fails to probe depths beyond $20 \mu\text{m}$.[5]

Angled excitation-collection (AEC) configuration

In this technique, the excitation is done via normal incidence and the collection is performed through a path making an angle with the normal. The point of incidence remains the same for both the paths. Since, the obliquely incident light travels mostly in the superficial regions and the light with normal incidence penetrates comparatively deeper in the sub-surface regions, therefore by varying the angle between the two paths, one may obtain the variations in the relative intensities of different peaks of the spectra corresponding to different angles. The angles can be properly calibrated with the probing depths in order to correlate the measured spectra with the depths. In practice, a typical value of probing depth is found to be $\sim 300 \mu\text{m}$.¹⁷ The studies on the AEC configuration are very limited due to its inability of filtering the diffuse component of the light which leads to poorer SNR.[17-18]

Polarized optical spectroscopy (POS)

For a layered turbid media, the light collected from the top layers partially retains its sense of polarization due to little effect of scattering whereas at the bottom layers it is completely depolarized due to increased diffusion (an effect of multiple scattering). The underlying principle, therefore, can be used to probe depths by measuring the spectra with polarization which is either parallel or perpendicular to the inherent polarization of the excitation light. We at RRCAT, Indore demonstrated the technique, for the first time, in fluorescence spectroscopy.[19] Smith et al.[8] revisited this in Raman spectroscopy. Apart from its ability of non-contact depth-sensitive measurements, an additional advantage offered by the technique is that it can provide information of molecular orientation and symmetry of the vibrating bond. However, the SNR degrades with depths and a sharp depth resolution cannot be defined in this technique. Further, the probing depth is also limited to $\sim 500 \mu\text{m}$.

Depth-sensitive measurements in deep probing ($\sim 500 \mu\text{m}$ - ~ 5 mm)

The simplest approach for deep probing is to use the confocal technique with a low NA objective lens, albeit at the cost of reduced axial resolution.[2] Although the probing depth one thus get is comparatively larger than that with high NA lens, but interrogating a depth beyond ~ 1 mm in a tissue is difficult with this arrangement. This is because

beyond this depth, multiple scattering takes over and the signal is largely swamped by the diffused photons. Therefore, the only way of deep probing is to selectively collect the diffused photons through the well known technique called source-detector separation. [3].

Source-detector separation

In this technique,[3, 20-21] optical spectra are measured from those points (lying onto the surface of the sample) which are spatially away from the point of light incidence. The rationale is that the signals originating from the deeper layers are spread over a wider area due to multiple scattering in comparison to that from shallower layers. In other words, the deeper born signal is collected efficiently when it is collected from a point which is away from the point of illumination in comparison to a point lying in the vicinity of the illumination. In practice, the collection of signal is performed through multiple optical fibers co-aligned with multiple points located at the periphery of a ring whose centre is the point of illumination. This is done to multiply the signal strength which in turn improves the SNR. If the illumination and collection points interchange their positions then the configuration becomes inverse in nature, although it still provides the same set of information. In the inverse configuration, the illumination ring is generally formed by using an axicon thereby making the whole set-up less bulky. Other advantages of the inverse configuration include the flexibility in choosing (in principle) any spatial offset, requirement of reduced exposure time (~15 s) and minimal risk of crossing the damage threshold of the sample among others. Both the configurations have been shown to probe depths ranging from 1 mm to 5 mm or more in various turbid media.[20-21]

Studies at RRCAT

We at RRCAT, Indore have been actively pursuing the activity on depth-sensitive optical spectroscopy and imaging for biomedical applications. The objective is to innovate on various depth-sensitive optical techniques to aid in the non-destructive and rapid characterization of the molecular, biochemical and structural properties of human tissues with the intent of improving our understanding of cancer and to make cancer care accessible at the point of care setting. Much of our current efforts have been directed towards this objective. For example, recently we combined depth-sensitive Raman spectroscopy (RS) and optical coherence tomography (OCT)[2] for revealing both biochemical and morphological structure of layered tissues (see Fig. 1). For achieving the depth-sensitivity in RS we adopted a confocal configuration with a low NA (=0.4) objective lens. The objective lens was chosen in such a way so that both RS and OCT might be able to provide almost equal probing depths (up to ~1 mm) for a two layered tissue comprising ~250 μm thick epithelial over a relatively thick stromal layer. The use of a low NA objective lens, though, degraded the depth resolution of the RS to a value of ~210 μm , it was enough to separate the Raman signatures of the individual tissue layers as shown in Fig. 2. In the Fig., one can observe significant differences in the measured Raman spectra corresponding to two different depths. For example, while the

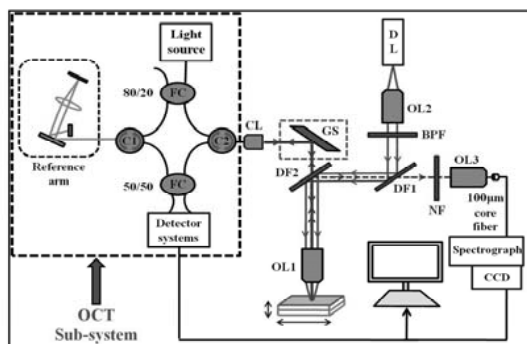


Fig. 1. An experimental arrangement of a RS-OCT system.

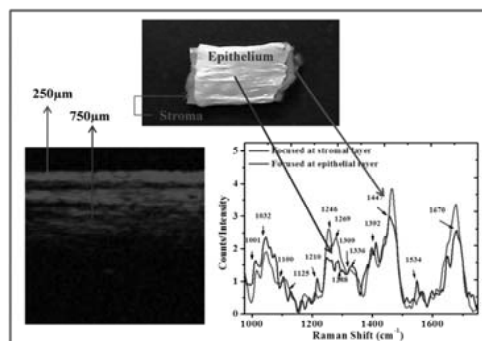


Fig. 2. OCT image and Raman spectra of biological tissue

stromal layer has strong Raman signal for the band centered at 1670 cm^{-1} (corresponding to collagen /amide-I) and the bands at ~ 1246 and 1269 cm^{-1} (amide-III), the intensities of the Raman bands at ~ 1001 , 1032 , 1210 and 1534 cm^{-1} (believed to be associated with aromatic amino acids) are higher in the spectrum corresponding to epithelial layer. In a similar manner, we also combined the OCT with a depth-sensitive fluorescence set up developed using a low NA objective lens.[22]

Since, the use of a confocal scheme with a low NA objective did not allow us to go to a depth beyond $\sim 1\text{ mm}$, we recently proposed cone-shell Raman spectroscopy as a novel technique for non-contact, depth-sensitive measurement of layered biological tissue up to a depth of $\sim 3\text{ mm}$. [4] The technique employs three identical axicon lenses to achieve the configuration of cone-shell Raman excitation and solid cone collection of the backscattered Raman light (see Fig. 3). Apart from the ability of probing a few mm depths, the depth selection can be achieved through adjustment of only the excitation arm which is a coveted feature providing the ease of its use. For determining the depth of focus of the CSRS system, the Raman spectra were measured by axially moving a $20\text{ }\mu\text{m}$ thick sheet of polymethylacrylate (PMMA) across the focus of the Raman excitation beam and then fitting a Gaussian to the plot of the intensities of the characteristic Raman peak of PMMA (at 1450 cm^{-1}) versus the axial distance. The full width at half maximum (FWHM) of the fitted Gaussian, measured to be $\sim 0.9\text{ mm}$, was taken as a practical estimate of depth resolution of the system. For measuring the spot size at the focal plane, the focus of the Raman excitation beam was laterally scanned over a clean edge of a PMMA layer of thickness $20\text{ }\mu\text{m}$ and the fall in the intensity of the 1450 cm^{-1} Raman peak was noted. An error function was fitted to the measured Raman intensities. The lateral movement of sample stage corresponding to the point where the intensity dropped to $1/e^2$ was taken as a measure of the spot size which was found to be $250\text{ }\mu\text{m}$. The performance of the CSRS system was evaluated by measuring the depth-sensitive Raman spectra from a biological system having a layered structure. For the measurement of the Raman spectra from various depths of the samples investigated, the focal plane of

the Raman excitation beam was moved axially by varying the separation between the two axicons in the excitation arm. It was found that despite significant differences in the Raman spectra at different depths, there was considerable mixing of spectral signatures even for the top and bottom layers although the layers have distinctly different bio-chemical make-ups. In order to retrieve the characteristic Raman spectra of the two layers, the Raman spectra measured at the two depths (i.e. top and bottom) were subjected to the method of scale-subtraction. A comparison of these spectra with those recorded from the native tissues comprising the top and bottom layers of the tissue sample clearly revealed that there was very good match between the Raman bands of the retrieved spectra of the top and bottom layers with those measured separately from the corresponding tissue types.

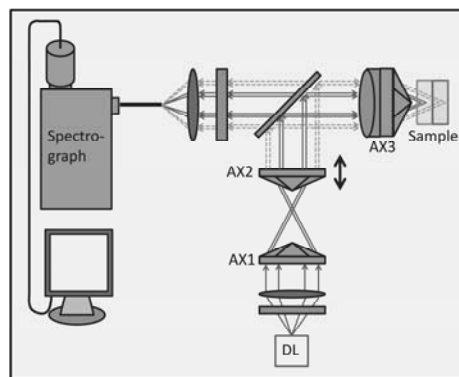


Fig. 3. The cone-shell Raman spectroscopic system

Acknowledgement:

The authors would like to thank Dr. P. K. Gupta, Associate Director, RRCAT for his keen interest in this activity. They also thank other colleagues of RRCAT for their help at various stages.

References:

- [1] R. A. Schwarz et al., D. Arifler, S. K. Chang, I. Pavlova, I. A. Hussain, V. Mack, B. Knight, R. Richards-Kortum, and A. M. Gillenwater, *Opt. Lett.* **2005**, *30*, 1159.
- [2] K. M. Khan, H. Krishna, S. K. Majumder, K. D. Rao and P. K. Gupta, *J. Biophot.*, **2014**, *7*, 77.
- [3] P. Matousek, I. P. Clark, E. R. C. Draper, M. D. Morris, A. E. Goodship, N. Everall, M. Towrie, W. F. Finney and A. W. Parker, *Appl. Spectrosc.*, **2015**, *59*, 393.
- [4] K. M. Khan, S. K. Majumder, and P. K. Gupta, *J. Biophot.*, **2015**, doi: 10.1002/jbio.201400125.
- [5] D. A. Woods and C. D. Bain, *Analyst*, **2012**, *137*, 35.
- [6] R. Tabaksblat, R. J. Meier and B. J. Kip, *Appl. Spectrosc.*, **1992**, *46*, 60.
- [7] P. Matousek, M. Towrie, A. Stanley and A. W. Parker, *Appl. Spectrosc.*, **1999**, *53*, 1485.
- [8] Z. J. Smith and A. J. Berger, *Opt. Lett.* **2005**, *30*, 1363.
- [9] N. J. Everall, *Appl. Spectrosc.*, **2009**, *63*, 245.
- [10] L. Wang, S. L. Jacques and L. Zheng, *Comput. Methods Programs Biomed.*, **1995**, *47*, 131.
- [11] P. J. Caspers, G. W. Lucassen, R. Wolthuis, H. A. Bruining and G. J. Puppels, *Biospectroscopy*, **1998**, *4*, S31.
- [12] P. J. Caspers, G. W. Lucassen, E. A. Carter, H. A. Bruining and G. J. Puppels, *J. Invest. Dermatol.*, **2001**, *116*, 434.

- [13] J. Choi, J. Choo, H. Chung, D. G. Gweon, J. Park, H. J. Kim, S. Park and C. H. Oh, *Biopolymers*, **2005**, 77, 264.
- [14] C. A. Lieber and A. Mahadeven-Jansen, *Opt. Express*, **2007**, 15, 11874.
- [15] R. Iwamoto, M. Miya, K. Ohta and S. Mima, *J. Chem. Phys.*, **1981**, 74, 4780.
- [16] R. Iwamoto, K. Ohta, M. Miya and S. Mima, *Appl. Spectrosc.*, **1981**, 35, 584.
- [17] T. J. Pfefer, A. Agrawal, and R. A. Drezek, *J. Biomed. Opt.*, **2005**, 10, 44016.
- [18] T. F. Cooney, H. T. Skinner and S. M. Angel, *Appl. Spectrosc.*, **1996**, 50, 836.
- [19] N. Ghosh, S. K. Majumder, H. S. Patel and P. K. Gupta, *Opt. Lett.*, **2005**, 30, 162.
- [20] P. Matousek, *Appl. Spectrosc.*, **2006**, 60, 1341.
- [21] P. Matousek and N. Stone, *J. Biophot.*, **2013**, 6, 7.
- [22] K. M. Khan, H. Krishna, S. B. Dutta, S. K. Majumder, K. D. Rao, and P. K. Gupta, *Proc. DAE-BRNS National Laser Symp.*, **2014**, 187.



Dr. Shovan Kumar Majumder is senior Scientist (SO-H) at Raja Ramanna Centre for Advanced Technology (RRCAT), and Professor at Homi Bhabha National Institute (HBNI). He leads the activity on Optical Spectroscopy and Imaging for Biomedical Diagnosis at RRCAT.

Dr. Majumder received his graduate and postgraduate degrees in Physics from Jadavpur University, Kolkata. After successful completion of one-year Orientation Course from Bhabha Atomic Research Centre (BARC) Training School, Mumbai, he joined RRCAT in the year 1992. He received his Ph.D. degree from Devi Ahilya University, Indore for his work on the use of Optical Spectroscopy for Cancer Diagnosis. He worked as a visiting scientist at Vanderbilt University, USA where he did the post doctoral research in the same field. Dr. Majumder's main research interest is development and evaluation of optical spectroscopic techniques for biomedical diagnosis and imaging. His other interests include use of various statistical pattern recognition techniques for the development of diagnostic algorithms for classification of tissue pathologies and development of optical techniques for monitoring the authenticity and the quality of food and pharmaceutical products.



Shri Khan Mohammad Khan obtained his B.Sc. in Mathematics and Physics from the MDS University, Ajmer in 2007. He obtained his M.Sc. in Physics from the Rajasthan University, Jaipur in 2009. He received his M. Tech degree from the Homi Bhabha National Institute, Mumbai in 2011. Currently he is working at Raja Ramanna Centre for Advanced Technology (RRCAT), Indore and actively involved in the development and evaluation of depth-sensitive optical techniques for biomedical diagnosis and imaging.

Optical Properties of Supramolecular Assemblies

Jyotirmayee Mohanty

Radiation & Photochemistry Division, Bhabha Atomic Research Centre

Mumbai, 400 085, India

E-mail: jyotim@barc.gov.in

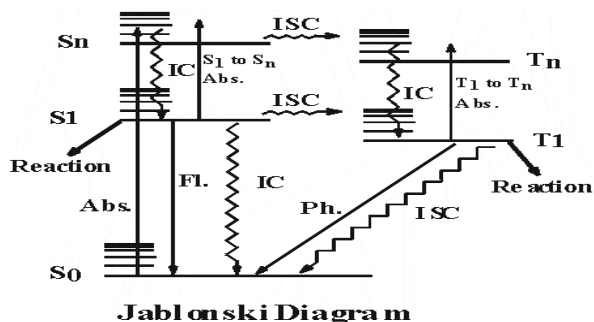
Introduction

Optical properties are concerned with the physical and chemical processes induced by the absorption of electromagnetic radiations (i.e. light) in the visible region in a molecular system. The interaction of light with a molecule leads to the excitation of an electron from a lower to higher electronic state and the excited molecule is energetically unstable with respect to ground state. There are a number of different possible de-excitation pathways by which the excited molecule relaxes to dissipate its excitation energy.¹ The most favorable relaxation pathway depends on the type of molecule and the nature of electronic state involved. The relaxation/excited state processes may be classified into two broad categories: (1) radiative process such as fluorescence and phosphorescence, where the excited species comes back to the ground state by emitting a photon and (2) nonradiative processes such as vibrational relaxation, internal conversion (IC), intersystem crossing (ISC), photoionization, photodissociation, etc., where the excess energy is transferred in the form of heat to the solvent bath around.[1]

Excited state processes

In photochemistry, the molecular electronic states of an organic molecule are classified in terms of spin multiplicities (either as singlet states (S) or triplet states (T)). Since the ground state of a polyatomic molecule is usually a singlet state (S_0), on absorption of photon these molecules are initially excited to some higher energy singlet state, S_n (due to spin selection rule). In condensed phase, the molecules in the S_n state quickly (in $\sim 10^{-11}$ to $\sim 10^{-12}$ sec.) dissipate some of their excess energy to the surrounding media following IC process to come down to the zero vibrational level of the first excited singlet (S_1). [1]

The S_1 state thus formed can return to the ground state (S_0) by a radiative process called fluorescence or by a competitive nonradiative IC process. A fraction of the S_1 state can also switch over to the triplet manifold by ISC process, which will eventually populate the zero vibrational level of T_1 . All these radiative and nonradiative processes in the S_1 state mostly occur



in the time scales of $\sim 10^{-7}$ to 10^{-9} sec. The T_1 state formed in the different ways mentioned above can ultimately come down to the ground S_0 state, either by a radiative transition called phosphorescence, or by a nonradiative ISC process, occurring in the time scales of $\sim 10^{-3}$ to 10^{-6} sec. The different excited states of the molecules can also participate in some chemical reactions, whereby the chemical identity of the molecule will be destroyed. Most of the photoinduced chemical reactions are known to occur in the T_1 state of the molecule, primarily because of the longer lifetime (μs to ms .) of the T_1 state. Some fast reactions are also possible in the S_1 state of the molecules, having lifetimes in the ns scale. If sufficient population of the S_1 and T_1 states can be made using high intensity laser excitation, absorption processes corresponding to S_1 to S_n (singlet-singlet transient absorption) and T_1 to T_n (triplet-triplet transient absorption) can also be observed using suitable probe light. All the different processes occurring in an excited molecule can be nicely and conveniently presented using a pictorial diagram as shown above. Such a pictorial presentation of the photophysical and photochemical processes occurring in the excited state of a molecule is known as the Jablonski diagram.[1]

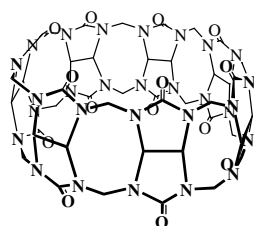
Characterization of the excited state molecules

Due to differences in charge distribution in the various energy states of a molecule, the electronically excited species can be completely different in its chemical and physical behavior as compared to the normal ground state molecule. To understand the effect of absorption of light by a molecule, it is important to know the optical absorption and fluorescence emission characteristics of the molecule under study as the excited state of a molecule is usually characterized by its absorption, emission spectra, lifetime (τ) and quantum yield (ϕ).¹ Study of absorption and emission spectra of the molecule provides important information regarding energies, electronic configuration of excited state, lifetime, rates and mechanism of excited state interconversion, etc. The fluorescence quantum yield (ϕ_f) is the ratio of the number of emitted photons to the number of absorbed photons and the lifetime of an excited state molecule is defined as the average time during which the molecule can stay in that state. A number of methods developed on the basis of the physical properties of the transient species are available for their detection. Generally, UV-vis absorption spectrometer, steady-state and time-resolved fluorescence spectrophotometers are employed to determine the photophysical parameters.

Factors affecting absorption and fluorescence properties

Because of the variation of electron density in the ground and excited states, an interaction with environment causes a large change in the electron density, as a result an energy shift is observed in absorption and fluorescence spectra.¹ Moreover, the fluorescence quantum yield and lifetime of most molecules are indeed extremely sensitive to the microenvironment of the molecule. It should be emphasized that, in the condensed phase, many parameters can affect the spectral peak positions, quantum yields and lifetimes: temperature, pH, solvents (polarity, viscosity, hydrogen bonding), rigidity, substituents, noncovalent interactions, etc.

Supramolecular Assembly



Cucurbit[7]uril

Supramolecular assembly refers to the association of two or more molecules in an organized manner through noncovalent interactions. In recent past, there is an upsurge in the research area of supramolecular assemblies of organic guests using various macrocyclic receptors and biomolecules as they provide a unique way to control the sophisticated nanoarchitectures to create supramolecular functional materials. One of the many different strategies for making supramolecular assemblies takes the advantage of non-covalent host-guest interaction, the method which can direct and thread molecular components according to designs under proper selection criteria to form well-ordered architectures. Since the supramolecular assemblies are held together by comparatively weak non-covalent interactions, the preferential affinity of these forces and the stoichiometric arrangements of the complexes bring out significant modulation in the optical properties of the guests. As a result, they find a wide range of applications in materials and medicines such as in constructing fluorescence sensors, on-off switches, photonic devices, in controlled uptake and release of potential drugs, surface-functionalized nanoparticles and many others.

Cucurbit[*n*]urils (CB_{*n*}), a relatively new class of macrocyclic receptor molecules, consist of methylene-bridged glycoluril monomers having highly symmetrical hydrophobic cavities accessible through two identical carbonyl laced portals. Depending upon the number of monomer units, different homologues of cucurbit[*n*]urils (CB_{*n*}; *n* = 5-10) with varying cavity and portal dimensions are known.[2] They have gained immense research interest because of their ability to host, in a highly selective manner, certain types of guest molecules such as metal cations, protonated alkyl and aryl amines, cationic dyes and surfactants through ion-dipole interaction and hydrophobic interactions. Among CB analogues, CB7 is highly water soluble and forms stable inclusion complexes with guest molecules like adamantyl amine, methyl viologen cations, fluorescent dyes, etc. through complete or partial encapsulation of the guests. On the other hand, the cavity of CB8 is large enough to accommodate more than one guest molecules to form 1:2 or 1:1:1 ternary host-guest complexes.[2] The host-guest complexes are mainly characterized by the changes in the absorption and fluorescence properties of the fluorescent dyes upon complexation with CB7. The presentation will cover some of the recent work on the spectacular optical properties of cucurbituril-assisted supramolecular assemblies of few organic dyes having technological and biological importance and their projected applications toward the aqueous-based dye laser, photofunctional devices, molecular architectures and controlled drug delivery.

Cucurbituril complexed Rhodamines: Water-based supramolecular dye laser systems

Rhodamines are arguably the most important fluorescent dyes as shown by their classical and contemporary applications, for example, in dye lasers, as quantum counters, in

single-molecule detection, as imaging agents for biomolecules, in fluorescence correlation spectroscopy (FCS), and in high-throughput screening assays. Addition of CB7 to the aqueous solution of rhodamines such as rhodamine 6G (Rh6G), rhodamine B (RhB) and ketone red S (KRS)) results in the immediate formation of a strong 1:1 host-guest inclusion complex with high binding constant ($K > 10^5 \text{ M}^{-1}$). It has been observed that there is a drastic increase (factor 30) in photostability of Rh6G dye and enhancement in the fluorescence yield (> 2 -fold) of RhB and KRS in water upon complexation with CB7 (Fig. 1).[3]

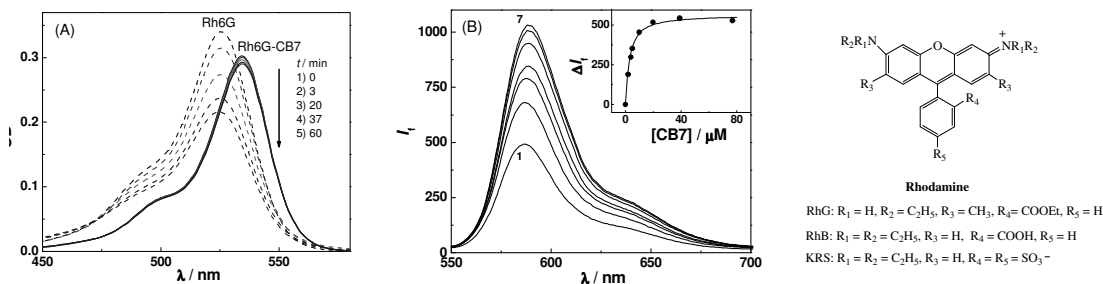


Fig. 1. (A) Photobleaching of Rh6G (ca. 4 μM) in aerated water in the absence (dotted lines) and presence (solid lines) of 1 mM CB7 followed through the decrease of the visible absorption with increasing time of pulsed 532-nm Nd-YAG laser irradiation. (B) Fluorescence spectra of KRS (~1.3 μM) in aqueous solution with CB7. [CB7]/μM: (1) 0.0, (2) 2.0, (3) 4.0, (4) 5.0, (5) 10.0, (6) 19.8 and (7) 39.0. Inset: Fluorescence titration curve of KRS in the presence of CB7. Right panel shows the chemical structure of rhodamine dyes.

Enhanced stability, increased solubility and prevention of aggregation/adsorption of organic dyes in aqueous solution are the crucial parameters for a dye laser system and is nicely demonstrated by the operation of a supramolecularly assisted aqueous dye laser system of rhodamine dyes with CB7 as the macrocyclic host additive. The effect of CB7 on the performance of rhodamine dye solutions has been investigated by using dye laser setup with respect

to the practically relevant parameters like lasing efficiency, lasing stability and beam quality. Large increase in lasing efficiency is observed with addition of micromolar concentration of CB7 to the aqueous so-

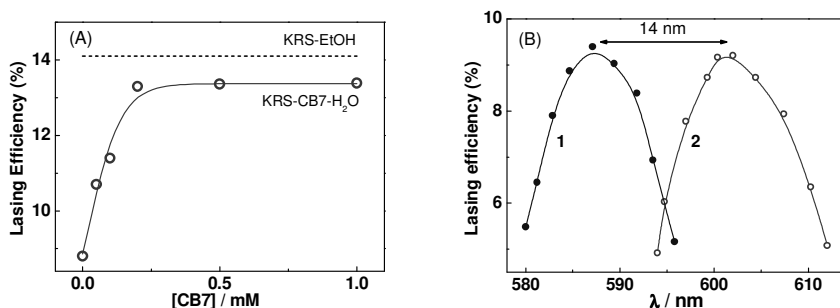


Fig. 2. (A) Dependence of the lasing efficiency of KRS (200 μM) on CB7 concentration. (B) Tuning curves of KRS in EtOH (1) and in the presence of 200 μM CB7 (2) at a pump energy of 6.3 mJ.

lution of kiton red dye (Fig. 2), predominantly due to the deaggregating action of CB7 on the dye. The resulting supramolecular dye lasers are environmentally more benign, more laboratory-safe, and less maintenance-sensitive than the presently employed dye laser systems based on organic solvents.[3]

Supra-biomolecular interaction: Enhancer strategy

Fluorescent dyes serve as probes for biomolecular systems and in selected cases, such as the triphenylmethane (TPM) dyes, as promising drugs for photodynamic therapy and as antimicrobial agents. The increase in fluorescence intensity of brilliant green (BG; a representative TPM dye) with CB7 clearly indicates the binding interactions between them (*cf.* Fig. 3).[4] The partial complexation of a single aryl ring of BG may account for the moderate fluorescence enhancement (6-fold) with the synthetic receptor, it opens up the opportunity for the dye to undergo an additional interaction with a second, biomolecular one: bovine serum albumin (BSA) protein. Upon complexation of BG with BSA alone (without CB7), the fluorescence intensity of BG enhances about 45-fold (*cf.* Fig. 3). We have examined the molecular recognition between the preformed CB7•BG supramolecular complex and BSA. A dramatic increase in the fluorescence yield by a factor of about 300 (Fig. 3) has been observed (relative to free BG), which suggests that the fluorescence enhancements affected by the individual components (factor of 6 for CB7 and factor of 45 for BSA) are cumulative (multiplicative) in nature, or lie even slightly above. Conversely, it has been shown that the binding strength (one order of magnitude increase) as well as the fluorescence properties (factor of 300-fold enhancement) of BG with BSA can be dramatically enhanced by the addition of CB7 as a macrocyclic host molecule.⁴ For BG, the formation of the ternary host-protein-dye complex (Fig. 3) can be in part mechanistically rationalized, because the macrocyclic host cavity is too small to encapsulate the entire dye, thereby leaving additional aryl sites for interaction with the protein. The resulting cooperative binding of a dye and potential drug with biological

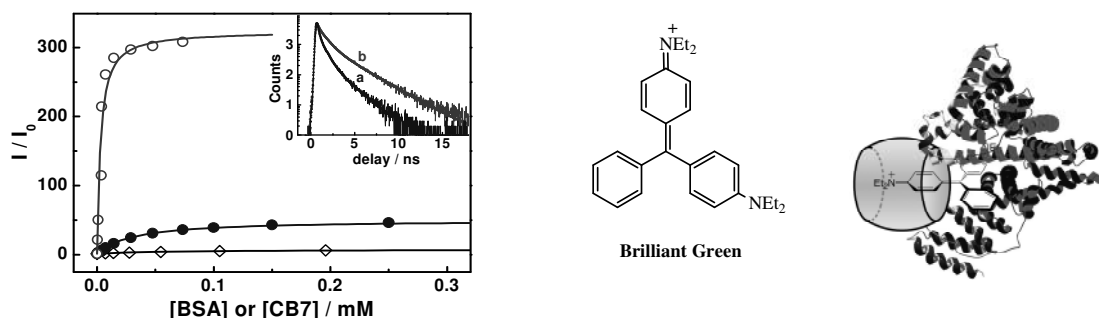


Fig. 3. Plots of the fluorescence intensity ratio (I/I_0) for 1 mM BG with increasing receptor concentration: Addition of CB7 only (◇), BSA only (●), and BSA in the presence of 1 mM CB7 (○). Inset: corresponding fluorescence decays ($\lambda_{ex} = 635 \text{ nm}$, $\lambda_{mon} = 730 \text{ nm}$) for (a) 250 μM BSA only (b) 50 μM BSA in the presence of 1 mM CB7. Middle panel shows the chemical structure of BG. Right panel shows the sketch of the fluorescent ternary complex CB7•BG•BSA.

target molecules opens a new approach to improve medicinal activity or the sensitivity of fluorescent sensor applications by a supramolecular “enhancer” strategy.

Stimuli-responsive fluorescent supramolecular capsule and its rupture

Thioflavin T (ThT) is a benzthiazolium dye ($\phi_f = 0.0003$) that has been extensively applied in the early detection of amyloid fibril formation in tissues to diagnose chronic disorders such as Alzheimer’s and Parkinson’s diseases. Steady-state and time-resolved fluorescence studies illustrate significant enhancements/modifications in the fluorescence yield (40-fold), lifetime and spectral features of ThT on interaction with CB7 and has been assigned to the formation of 1:1 and 2:1 host-guest complexes between the dye and the CB7 leading to the specific structural arrangements. The macrocyclic host-guest interactions impart structural rigidity bringing out restrictions on the torsional motion in the dye, thus modulating the excited state properties.[5]

The binding interactions are mainly non-covalent in nature which makes it convenient to tune the complexes by a wide range of stimuli including competitive binders, pH, temperature, light, redox control, etc. Considering the cases of cation receptor properties of CB7 hosts, an increase in the ionic strength of the solution would lower the extent of the ion-dipole interactions affecting the stability of the complex, especially for cationic guests, thus releasing the free dye in the solution. The addition of metal cations to the 1:1 CB7•ThT complex displays the expected competitive binding interactions with CB7, leading to the decrease in the fluorescence intensity from ThT. However, addition of metal ions to the 2:1 (CB7)₂•ThT complex leads to unusual enhancement in the fluorescence emission (~270 fold in the presence of Ca²⁺ and 160 fold in the presence of Na⁺; Fig. 4).⁶ A detailed photophysical characterization with supporting data from NMR and anisotropy measurements has led to the revelation of a novel stimulus responsive cooperative metal ion binding to the stoichiometrically selected (CB7)₂•ThT complex, demonstrating a highly fluorescent supramolecular nano-capsule (Fig. 4). The first example of such an unusual assembly became feasible due to the stoichiometry and

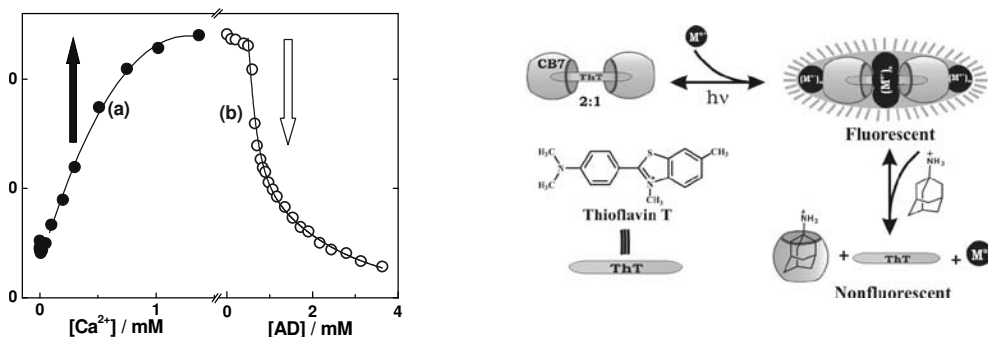


Fig. 4. Changes in the fluorescence intensity of (CB7)₂•ThT complex in presence of Ca²⁺ (trace a) and followed by the addition of AD (trace b). Right panel shows the formation and breakage of highly fluorescent supramolecular capsule.

the structural arrangement of the host-guest complex with two CB7 portals providing strong negative charge density for the metal ions to group and seal the complex, thus rigidizing and protecting the incorporated dye. The rupture of the capsular complex was demonstrated with a strong competitive guest, 1-amantadine hydrochloride, which helped in disrupting the capsule to release the dye (Fig. 4). [6] By proper design criteria of the guest chromophores, the methodology can be explored for the binding and release of drug molecules and for application in fluorescence on-off systems and will have immense potential as building blocks for molecular architectures displaying unique properties.

References

- [1] J. R. Lakowicz, *Principles of Fluorescence Spectroscopy*, 3rd ed.; Springer: New York, **2006**.
- [2] A. C. Bhasikuttan, H. Pal, J. Mohanty, *Chem. Commun.*, **2011**, 47, 9959-9971.
- [3] (a) J. Mohanty, W. M. Nau, *Angew. Chem. Int. Ed.*, **2005**, 44, 3750-3754; (b) J. Mohanty, H. Pal, A. K. Ray, S. Kumar, W. M. Nau, *ChemPhysChem*, **2007**, 8, 54-56; (c) J. Mohanty, K. Jagtap, A. K. Ray, W. M. Nau, H. Pal, *ChemPhysChem*, **2010**, 11, 3333-3338.
- [4] A. C. Bhasikuttan, J. Mohanty, W. M. Nau, H. Pal, *Angew. Chem. Int. Ed.*, **2007**, 46, 4120-4122.
- [5] S. Dutta Choudhury, J. Mohanty, H. P. Upadhyaya, A. C. Bhasikuttan, H. Pal, *J. Phys. Chem. B*, **2009**, 113, 1891-1898.
- [6] S. Dutta Choudhury, J. Mohanty, H. Pal, A. C. Bhasikuttan, *J. Am. Chem. Soc.*, **2010**, 132, 1395-1401.



Dr. (Mrs.) Jyotirmayee Mohanty obtained her M. Sc. in Chemistry from Utkal University, Odisha in 1992 and joined Bhabha Atomic Research Centre, Mumbai, India, in 1994 after one year advanced orientation course conducted by the institute. After her Ph.D. from the University of Mumbai in 2002, she carried out her postdoctoral research at MPIBPC, Göttingen and JUB, Bremen, Germany, 2002-2004. Her current research interests focus on the dynamics of noncovalent supra-biomolecular assemblies, tuning their molecular properties and exploring their photofunctional activities towards various applications. In fact, she has initiated the research activities on the fascinating chemistry of cucurbiturils in India and a number of her recent publications in high impact international journals (*J. Am. Chem. Soc.*, *Angew. Chem. Int. Ed.*, *Chem. Commun.*, *Chem. Eur. J.*, etc.) including patents and reviews are the testimony to her contribution in this area. She is a recipient of the Distinguished Lectureship Award-2009 from the Chemical Society of Japan, APA-Prize for Young Scientist-2010, Samanta Chandra Sekhar Award-2011 from Odisha Bigyan Academy, Scientific & Technical Excellence Award-2011 from DAE, and the Fellow of Maharashtra Academy of Sciences and National Academy of Sciences, India. She has also received the prestigious Humboldt Fellowship for Experienced Researchers from Alexander von Humboldt Foundation.

Ln³⁺ Doped Nanostructures for Solid State Lighting and Bio-Imaging Applications

Sri Sivakumar

Department of Chemical Engineering, IIT Kanpur

E-mail: srisiva@iit.ac.in

Introduction

Ln³⁺-doped nanomaterials have fascinating optical properties such as large stoke shift and sharp emission with high quantum yield, lesser light scattering and deeper tissue penetration (NIR region) which find potential applications in photonics and bio-imaging.[1-2] In addition, they possess up-conversion fluorescence in which low energy photons are converted into higher energy photons. Lanthanide ions can be doped into various hosts such as -oxides, -fluorides, -vanadates, -phosphates, -tungstates, and -molybdates of lanthanides.² In particular, Zircon type LaVO₄ nanomaterials is proven to be a good host for luminescent lanthanide ions, however it possesses lesser thermodynamic stability compared to monazite LaVO₄ at elevated temperature and pressure. Current work discusses the stabilization of zircon La_{1-x}Eu_xVO₄ by doping smaller size lanthanide ions (e.g. Eu³⁺ ions). Furthermore, we have designed a unique approach wherein as prepared up-converting nanoparticles (Yb³⁺/Er³⁺ doped in LaVO₄, GdVO₄, YVO₄, and Gd₂O₃) are encapsulated inside PEGylated polymer capsules using layer-by-layer assembly for bio-imaging applications. In the second part, stability of Mg_{1-x}Eu_xO_{1+3/2} nanostructures is also explored as a function of Eu³⁺ doping concentrations. The doping of Eu³⁺ ions in MgO is quite challenging due to aliovalency and size mismatch of dopant. We have used sol-gel technique for the kinetic stabilization of Eu³⁺ ions in MgO and have provided relationship between the doping concentration and the stability of the doped material. In the third part, effect of morphology on the luminescence of Eu³⁺ ions in NaLa_{1-x}Eu_x(WO₄)₂ have been studied. Finally, we have demonstrated the suppression of undesired emissions to obtain pure green emission from Tb³⁺ ions using hetero-inverse opal structures.

Experimental

Formation of Mg_{1-x}Eu_xO_{1+3/2}[3]A_{1-x}Ln_xVO₄ (A=La, Gd, Y and Ln = Yb, Er, Tb, Eu) [4-5], and NaLa_{1-x}Eu_x(WO₄)₂ silica inverse opal hetero-structure⁶ are given elsewhere.

Results and Discussion

In the first part, effect of Eu³⁺ doping on the stability of Mg_{1-x}Eu_xO_{1+3/2} and La_{1-x}Eu_xVO₄ have been studied. X-ray diffraction data (Fig.1a) of as prepared and heat treated Mg_{1-x}Eu_xO_{1+3/2} samples provide evidences of doping of Eu³⁺ ions into MgO upto 1 atom percent and phase segregation is observed above a critical annealing temperature,

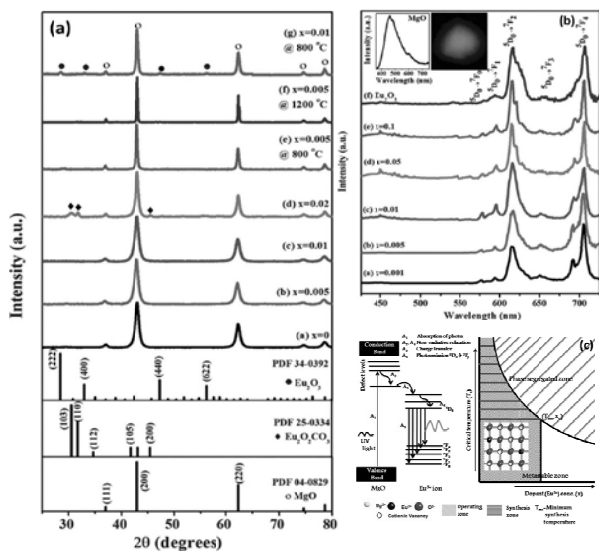


Fig. 1(a) XRD patterns and photoluminescence emission spectra of $Mg_{1-x}Eu_xO_{1+3/2}$ ($x=0.001-1.0$) at $\lambda_{ex} = 270$ nm (c) Schematic showing the effect of Eu^{3+} -doping on the stability of MgO

which progressively decreases with increase in doping concentration. $Mg_{1-x}Eu_xO_{1+3/2}$ samples exhibit characteristic strong red emission of Eu^{3+} via energy transfer from MgO matrix to Eu^{3+} ions (Fig. 1b). The stability of $Mg_{1-x}Eu_xO_{1+3/2}$ decreases with increase in doping concentration as shown in proposed schematic (Fig. 1c). On the other hand, zircon type $LaVO_4$ have been stabilized by doping with suitable smaller size Eu^{3+} ions. With increase in doping concentration both temperature (heat treatment at higher temperatures) and pressure (deduced from DFT) required for phase transformation increases (Fig. 2a) suggesting the enhanced stability with doping. This has been further confirmed by emission spectra of

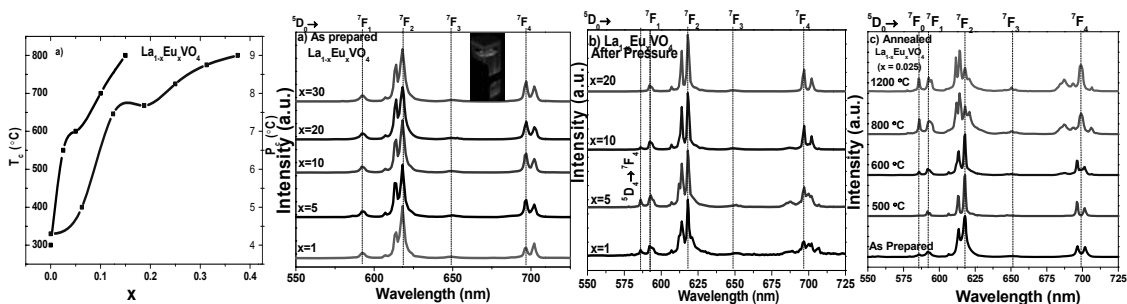


Fig. 2.(a) Phase transition temperature and pressure as a function of Eu^{3+} and PL spectra of $La_{1-x}Eu_xVO_4$ (b) as prepared (c) pressure treated and (d) heat treated ($x=0.025$) samples at $\lambda_{ex} = 310$ nm

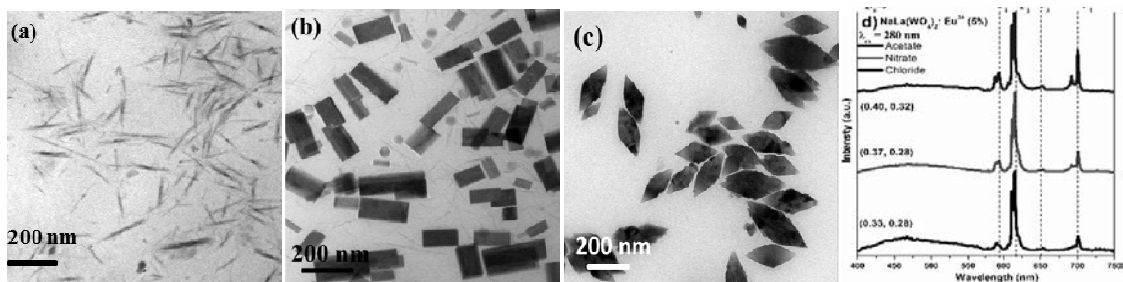


Fig.3 Transmission electron micrographs of $NaLa_{1-x}Eu_x(WO_4)_2$ nanostructures prepared by (a) chloride (b) nitrate and (c) acetate precursor salts of lanthanide (d) PL emission spectra at $\lambda_{ex} = 280$ nm

$\text{La}_{1-x}\text{Eu}_x\text{VO}_4$ samples subjected to high pressure and temperatures (Fig. 2b-d). In second part, morphological evolution of $\text{NaLa}_{1-x}\text{Eu}_x(\text{WO}_4)$ has been studied. Fig. 3 a-c display transmission electron micrographs (TEM) of $\text{NaLa}_{1-x}\text{Eu}_x(\text{WO}_4)$ nano-needles, cuboidal, and rugby ball shape morphologies prepared by chloride, nitrate, and acetate prepared precursor salts of lanthanides. The photoluminescence emission spectra shown in Fig. 3d suggest change in emission behavior of Eu^{3+} ions with morphologies due to differences in the local environment of Eu^{3+} ions in three different morphologies.

Biological studies

Fig. 4a shows unique approach for encapsulating upconverting nanoparticles ($\text{Yb}^{3+}/\text{Er}^{3+}$ doped in LaVO_4 , GdVO_4 , YVO_4 , and Gd_2O_3) inside PEGylated polymer capsules prepared using layer-by-layer assembly⁷: (1) Sol-gel coating of lanthanide doped nanoparticles over silica (sacrificial template), (b) LbL assembly using PEI, PSS/PAH (8 layers), (c) PEGylation, (d) Core removal using HF, and (e) EDC-NHS conjugation of antibodies. Fig. 4(b) demonstrates CLSM image of bright upconverting emission from Er^{3+} ions in A498 cells ($\lambda_{\text{ex}}=980$ nm). Fig. 4(c) shows green fluorescence from nanoparticles-loaded ($\text{LaVO}_4:\text{Tb}^{3+}$) polymer capsules with various cells e.g. HeLa (cervical cancer), A498 (kidney cancer), H460 (lung cancer), MCF-7 (breast cancer), L929 (fibroblast), IC-21 (macrophages) and Schwann cells indicating internalization in all cell types (MTT assay showed biocompatibility). Similar observation was obtained in the case of PEGylated polymer capsules encapsulating lanthanide GdVO_4 , YVO_4 and Gd_2O_3 nanoparticles.

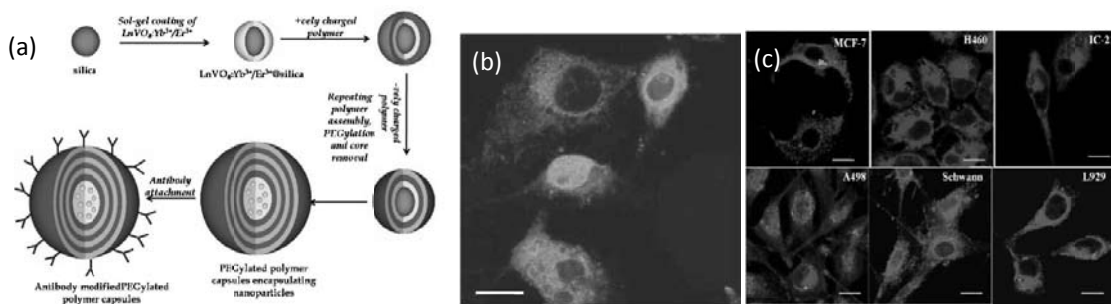


Fig. 4. (a) Schematic illustration of the antibody modified PEGylated polymer capsules encapsulating $\text{LnVO}_4:\text{Yb}^{3+}/\text{Er}^{3+}$ nanoparticles ($\text{Ln} = \text{La}, \text{Gd}, \text{Y}$) and CLSM image of (b) upconverting PEGylated polymer capsules encapsulating $\text{LaVO}_4:\text{Yb}^{3+}/\text{Er}^{3+}$ nanoparticles internalized in A498 cells and (c) representing internalization of PEGylated polymer capsules (~ 500 nm) encapsulating $\text{LaVO}_4:\text{Tb}^{3+}$ nanoparticles with different types of cells (scale bar = $20 \mu\text{m}$).

$\text{SiO}_2:\text{Tb}^{3+}$ Inverse Opal Heterostructure for Green Colour Purification

$\text{SiO}_2:\text{Tb}^{3+}$ inverse opal single film- and double film heterostructure inverse opals were fabricated by convective self-assembly method using 390 and 500 nm of polystyrene spheres.⁶ The process yielded two single inverse opals (termed as 390 IO, 500 IO) and a hetero- inverse opal structure (termed as 390-500 IOH). The microstructure (Fig. 5a-c)

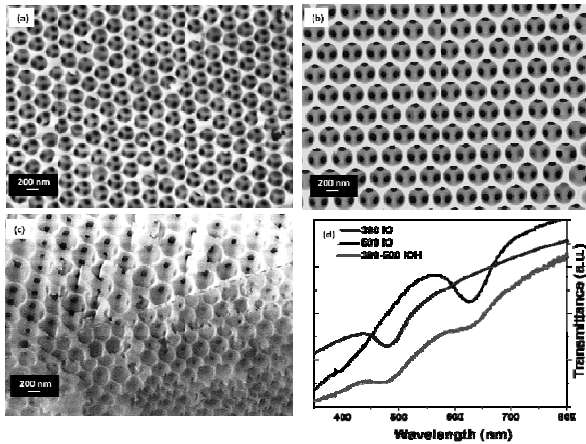


Fig. 5. Field emission scanning electron microscope (FESEM) images: top view of (a) 390 IO (b) 500 IO and (c) cross section view of 390-500 IOH samples; and (d) transmittance spectra of 390IO, 500 IO and 390-500 IOH measured at incident angle of 20°

shows the pore separation (center to center distance) of air spheres in 390 IO and 500IO are observed to be ~ 273 and 358 nm. Further, The photonic stop band (PSB)

positions of are found to be 484 and 610 nm 390IO and 500IO, respectively measured at $\theta=20^\circ$. Notice that in case of 390-500 IOH, there are two PSB positions in each, close to those found in the individual inverse opal. The photoluminescence spectra of 390IO, 500IO, and 390-500 IOH are presented (Fig. 6a-c) along with that of reference ($\text{SiO}_2:\text{Tb}^{3+}$ gel powder) in each as recorded with a detector held at 20° from the sample normal. It is clear that 390-500 IOH shows the suppression of

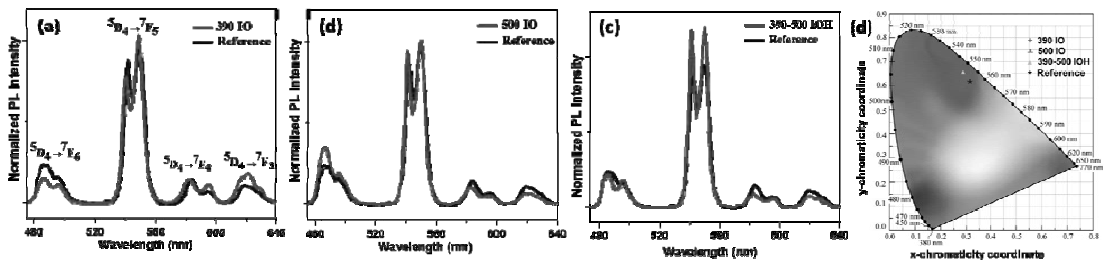


Fig. 6. Photoluminescence spectra of $\text{SiO}_2:\text{Tb}^{3+}$ inverse opal structures along with reference: (a) 390 IO, (b) 500 IO, and (c) 390-500 IOH; and (d) CIE coordinates of Tb^{3+} emission in all the sample. Excitation wavelength 230 nm, emission spectra measured at $\theta=20^\circ$

blue ($^5\text{D}_4 \rightarrow ^7\text{F}_6$), orange ($^5\text{D}_4 \rightarrow ^7\text{F}_4$), and red ($^5\text{D}_4 \rightarrow ^7\text{F}_3$) emission bands with an enhancement of green ($^5\text{D}_4 \rightarrow ^7\text{F}_5$) emission band of Tb^{3+} ion with respect to the reference sample which is the resultant effect of the single inverse opals (390IO and 500IO). Suppression of these emission bands occurred due to their overlapping with the photonic band gaps of hetero-structure; while the enhancement of green emission is observed due to its matching with the pass band of hetero-structure. Overall effect produces the purified green emission of Tb^{3+} ions in 390-500 IOH vis-à-vis reference and single inverse opals.

Conclusions

Lanthanide-doped oxide nanomaterials with various morphologies and crystal structure have been prepared for light emitting and biological applications. Ln^{3+} ions

have been successfully doped in MgO despite of their bigger size and aliovalency using sol-gel route. The doped samples are less stable and phase segregate at lower annealing temperature. In contrast, doping of Eu^{3+} ions in LaVO_4 enhances the stability of zircon type tetragonal phase due to its lesser size. In addition, the polymer capsules encapsulating lanthanide ion doped LnVO_4 ($\text{Ln}=\text{La, Gd, Y}$) are found to be internalized and biocompatible with various cells e.g. HeLa, A498, H460, MCF-7, L929, IC-21 and Schwann cells showing the applicability in different types of cells. Nano-needle, cuboidal and rugby ball morphologies of $\text{NaLa}_{1-x}\text{Eu}_x(\text{WO}_4)_2$ were prepared using chloride, nitrate, sulfate, and acetate salts of lanthanides, respectively. The prepared morphologies produce bright white light emission upon excitation with 270 nm light. We observed localized bright upconverting green fluorescence from Er^{3+} ion ($\lambda_{\text{ex}} = 980 \text{ nm}$) present inside cells suggesting their potential use as targeted bioimaging agents. In addition, Tb^{3+} infiltrated inverse opal heterostructure (390-500 IOH) fabricated by convective self-assembly method via polystyrene spheres (diameter 280, 390 and 500 nm) shows the two photonic stop bands appearing at 484 nm and 610 nm suppressing blue, orange and red emission of Tb^{3+} ion bands with enhancement of green emission. The CIE chromaticity coordinates of modified emission of 390-500 IOH deduced as $x=0.2936$, $y=0.6512$ are closest to those of green color (545 nm).

References

- [1] S. V. Eliseeva, J.-C. G. Bunzli, *Chem. Soc. Rev.*, **2010**, 39, 189-227.
- [2] G. Wang, Q. Peng, Y. Li, *Acc. Chem. Res.*, **2011**, 44, 322-332.
- [3] C. K. Rastogi, S. Saha, S. Sivakumar, R. G. S. Pala, J. Kumar, *Phys. Chem. Chem. Phys.*, **2015**, 17, 4600-4608.
- [4] M. Yu, J. Lin, J. Fang, *Chem. Mater.*, **2005**, 17, 1783-1791.
- [5] S. Singh, A. Tripathi, C. K. Rastogi, S. Sivakumar, *RSC Adv.*, **2012**, 2, 12231-12236.
- [6] V. P. Shrivastava, S. Sivakumar, J. Kumar, *ACS Appl. Mater. Interf.*, **2015**, 7, 11890-11899.
- [7] H. M. Sami, A. Kumar, S. Sivakumar, *PLoS ONE*, **2012**, 7, e36195.



Dr. Sri Sivakumar, PhD (University of Victoria, BC, Canada, 2006)

Dept. of Chemical Engineering, Indian Institute of Technology Kanpur, Kanpur, Uttar Pradesh, India, PIN 208016.

Area of Interest: Drug delivery, bioimaging, photoelectrochemical water splitting, lanthanide-doped nanomaterials, polymer capsules

Academic Curriculum/Professional Affiliation: 2006-Associate Professor, Dept. Chemical Engineering, IIT Kanpur, Kanpur, India

Material Science Programme, IIT Kanpur, Kanpur, India

Awards and Honors

2012 Class of 1979 Research Fellowship

2015 Prof. CNR Rao award for best research contribution

Anderson Localization Random Lasers

Sushil Mujumdar, A K Tiwari, R Uppu, K S Alee and Randhir Kumar

*Department of Nuclear and Atomic Physics, TATA Institute of Fundamental Research
Mumbai - 400 005.*

E-mail: sumujumdar@gmail.com

Light propagation through disordered media has revealed a number of puzzling and exciting optical phenomena. When a pulse of light is incident onto an ensemble of scatterers, the multiple scattering underwent by the light forces its propagation to assume a diffusive character. In other words, the light propagates via a random walk of photons, similar to particle diffusion. The evolution of specific intensity of light follows the diffusion equation within the disordered volume. Interestingly, this is analogous to the propagation of electric current through a conductor, wherein the electrons are multiply scattered off various scattering centres in course of their propagation. Indeed, several aspects of photon propagation in random media have analogues in the electron propagation domain. The most exotic of these analogies happens to be Anderson localization of light [1]. In the domain of condensed matter physics, it was envisaged that a conductor can transit into an insulator phase purely on the basis of disorder; essentially, the disorder is so strong that the electrons continually remain scattering off the sites ad infinitum, and electron flow is inhibited. This situation, proposed by Phil Anderson, is known as the Anderson localization of light. The phenomenon happens due to the self-interference of light waves in a manner that constructive interference happens only in certain isolated regions of space, creating an island of high intensity surrounded by dark regions of destructive interference. Anderson localization in three dimensional samples is an extremely elusive phenomenon, as it requires a critical degree of disorder to manifest. This requirement implies samples with particle sizes and refractive indices that are not easily implementable. However, in lower dimensions, localization is within reach. A feature that is uniquely applicable to light and not to electrons (due to their fermionic nature) is amplification. Light can be amplified by using a suitable material that can be provided energy, which is then channelled into an optical wave propagating through the medium. These materials are precisely what are used in lasers. A few years ago, it was realized that the combination of amplification and multiple scattering can realize very interesting characteristics in the optical emission, giving rise to the materials called random lasers [2]. Random lasers are essentially structurally disordered amplifying materials, in which an incident light wave propagates through scattering, and simultaneously experiences amplification. It was shown theoretically that such materials can emulate laser behaviour, giving an evidence of a threshold of lasing at the right excitation energy. These calculations were carried out in the diffusive domain, where the disorder is not strong enough to localize light. Subsequently, it was envisaged that if gain can be provided to a strongly disordered medium, then the localized states

can lase, providing coherent emission exactly similar to lasers. However, the difficulty of obtaining localization, that too with gain, has kept this domain fairly out of reach and conclusive results thereof are yet to be obtained.

In this regard, we have recently created an optical system that successfully obtains lasing from localized states. This was achieved by realizing a PARS state, a periodic - on - average random system. An array of monodisperse microdroplets was created from a solution of Rhodamine dye in methanol. The array was excited by a frequency - doubled NdYAG laser ($\lambda = 532$ nm), upon which the array fluoresced in the yellow-orange wavelengths. The light travelling in the axial direction (along the array) experienced a multilayer, comprising a dielectric layer of the alcohol separated by air. On virtue of the monodispersity of the microdroplets, the array assumes a strong periodicity. One can further overwrite on this periodicity a certain degree of randomness by tweaking the process of generation of the microdroplets. Thus, a periodic-on-average random system with gain is realized. We measured the lasing modes from this system, and analysed the frequency distribution of the modes. Transfer matrix computations revealed that these modes originate from the gap states of the PARS system [3]. A periodic system sustains photonic bands and forbidden bandgaps. When randomness is added to this periodic system, new states are realized in the bandgap called the gap states. Interestingly, these gap states have several qualities that were known theoretically but not experimentally demonstrated. The achievement of the PARS system has enabled us to experimentally verify the properties of gap states. For example, we have shown that extreme frequency control in random lasers can be achieved using gap states [4]. We have also shown the counter-intuitive result that weakly random systems can sustain higher-quality factors than even the periodic systems [5]. Finally, it is known theoretically that gap states have a small localization length, implying a higher propensity of localization. Indeed, we have recently achieved the measurement of Anderson localization random lasing in this system, thus proposing what we believe is the first conclusive demonstration of lasing over Anderson localized states [6].

References:

- [1] P. W. Anderson, *Phys. Rev.*, **1958**, *109*, 1492.
- [2] N. M. Lawandy, R. M. Balachandran, A. S. L. Gomes and E. Sauvain, *Nature*, **1994**, *368*, 436.
- [3] A. K. Tiwari and S. Mujumdar, *Phys. Rev. Lett.*, **2013**, *111*, 233903.
- [4] A. K. Tiwari, K. S. Alee, R. Uppu and S. Mujumdar, *Appl. Phys. Lett.*, **2014**, *104*, 131112.
- [5] K. S. Alee, R. ir Kumar and S. Mujumdar, *Phys. Rev. A*, **2015**, *91*, 053818.
- [6] "Anderson localization random lasers", In preparation.



Sushil Mujumdar, completed his PhD in 2001 from Raman Research Institute, Bangalore in the field of light propagation in passive and active random media. He followed up with postdoctoral research in coherent random lasing and near-field optics in LENS, Florence, University of Alberta, Canada, and ETH, Zurich. He is currently an associate professor at Department of Nuclear and Atomic Physics, TIFR, Mumbai.

Optical Materials for Spectroscopy Applications

Dinesh V. Udupa

Atomic & Molecular Physics Division, Bhabha Atomic Research Centre Mumbai.

E-mail: dudupa@barc.gov.in

Introduction

Optical spectroscopy is an important tool for investigating properties of materials in material analysis and material science research. In the recent years, advancements in optical spectroscopic devices, lasers, photonic devices, optical waveguides and optical fiber based devices have all been mainly due to the recent advances in optical material developments rather than due to new optical phenomena implementation itself. The materials being employed for broad optical applications in general and spectroscopic applications in particular require certain optical and mechanical properties which define their utilizations. Recent advances in optical glass, optical polymers and optical crystals, have opened up possibilities of robust optical devices and instruments for various applications ranging from consumer optics, display devices, light sources, and high end optics such as for space and defense applications. The presentation will be giving a flavor of the various optical and spectroscopic devices. It will deal with different aspects of the optical materials with a focus on their key properties that are innovatively used for achieving desired performance in optical and spectroscopic domains.

Optical Spectroscopy

Optical spectroscopy can be broadly classified into three types, namely, emission spectroscopy, absorption spectroscopy and fluorescence spectroscopy. An optical Spectrometer is the heart of these techniques. Spectrometers consist of three main portions optically, which are collection optics, wavelength dispersing element and focusing optics. Collection optics collect the radiation from the source or sample, the dispersing element separates the light into constituent wavelength and focusing optics converge the dispersed light on to a detector. Spectrometers can be classified as being of two kinds, which are monochromators and spectrographs. While monochromators are for filtering out one constituent wavelength light in the source (Fig. 1), spectrographs are for detecting a range of wavelengths (wavelength band) simultaneously (Fig. 2). Other classes of spectrometers are interference spectrometers such as Fourier transform spectrometers and Fabry-perot etalons.

Optical glasses

Traditionally optical components and devices have been made of optical glasses such as silicates and borosilicates, with various dopants such as barium, lanthanum, lead, antimony, zinc, tantalum, niobium, etc. Typically glasses transmit light in the range of 360-2000 nm covering visible and near IR. Pure fused silica has good transmission in the range

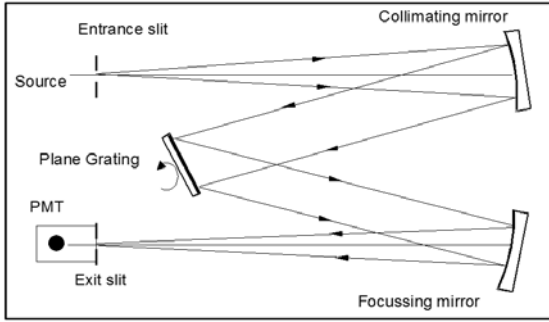


Fig. 1. Monochromator optical layout

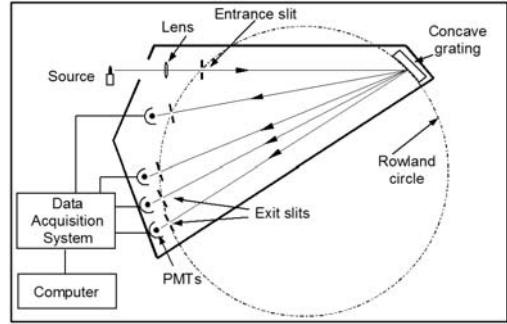


Fig. 2. Spectrograph optical layout

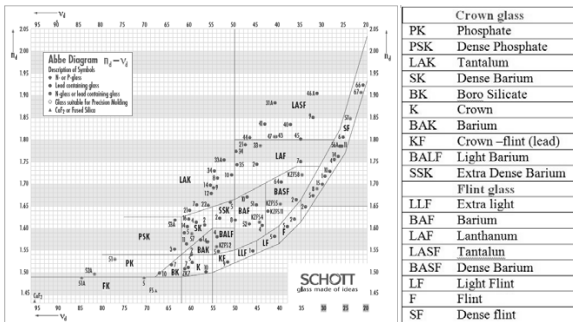


Fig. 3. Index-Dispersion plots of SCHOTT optical glasses

of 190-2000 nm covering UV region. Glass optics offers various advantages such as excellent light transmission, high manufacturing precision and diverse choices in refractive index offering good flexibility in optical design. Chemically, glasses are quite stable and can withstand harsh environments with higher thermal stability which is a merit for high optical power applications. Important optical properties of glass besides transmission are refractive index, dispersion, the

combinations of which are used for optical lens designing where optical aberrations are corrected. Generally optical glasses have refractive index values in the range of 1.4-1.9. The dispersion measured by Abbe number (v_d) defined as $v_d = \frac{n_d - 1}{n_F - n_C}$ where n is the refractive index and the suffixes d, F and C denotes wavelengths 587.56nm, 486.13nm and 656.27nm respectively, is in the range of 20-80. Glasses with Abbe number more than 50 are called crown glasses while glasses with Abbe number less than 50 are called Flint glasses Fig.3 shows the Abbe diagram plot for various optical glasses.

Optical crystals

Single crystal optical materials are used for many applications such as optical windows and lenses where transmissions in the wavelength ranges in the UV or IR regions are required. A common window used in UV region is Sapphire (Al_2O_3) and some fluoride windows such as CaF_2 , MgF_2 , LiF and BaF_2 . For the IR regions, halide crystal windows such as KBr, KCl, NaI and NaCl are used. While halide windows

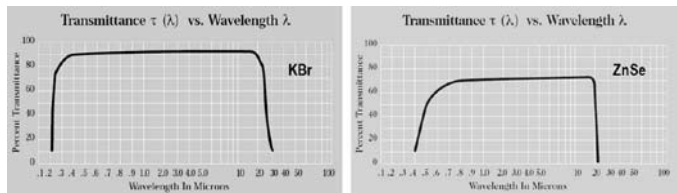


Fig. 4. Transmission curves of KBr and ZnSe crystals

have excellent transmission in wavelength regions of 0.3 – 20 μm , they are nevertheless hygroscopic and require frequent polishing to remove fogging. Other IR transmitting crystals such as Zinc selenide, Zinc sulphide, Zinc telluride, Cadmium selenide, Cadmium sulphide, Cadmium telluride, Thallium bromoiodide (KRS-5), Germanium arsenide, Germanium and Silicon are non hygroscopic, but they have lower transmittance and also smaller bandwidth compared to halide crystals in general (Fig. 4).

Other optical crystals include laser crystals used for solid state laser applications such as Neodymium doped Yttrium Aluminum Garnet (Nd:YAG), Neodymium doped Gadolinium Gallium Garnet (Nd:GGG), Neodymium doped yttrium orthovanadate (Nd:YVO₄) and Ti:Sapphire - Ti:Al₂O₃. Yet another group of optical crystals are scintillator materials such as Sodium iodide activated by thallium (NaI:Tl), Yttrium aluminum garnet activated by cerium (YAG:Ce), Calcium fluoride activated by Europium (CaF:Eu), Cesium Iodide activated by thallium (CsI:Tl) and intrinsic scintillator Bismuth germinate (BGO).

Optical polymers

Several optical polymer materials have been developed in the recent years and are increasingly being used as optical materials resulting in many advantages such as lower cost, ease of manufacturing and assembly compared to glass optics. In several applications, polymers offer additional merits such as lower weight and resistance to breakages as compared to glass. Polymers also offer advantages such as possibility of integrated manufacturing of oddly shaped parts. The only demerits currently are their limited types for design choices offering generally low refractive index and the presence of undesirable optical birefringence. The birefringence is more due to residual stresses in the material and is currently being reduced by better process controls. Most common kinds of optical polymers are Polycarbonates (PC), Acrylics (polymethylmethacrylate or PMMA) and Polystyrene (PS). Optical grade PCs have good transparency and are strong and tough materials. A major application of polycarbonates is in optical storage devices such as CDs, DVDs and Blu-Ray Discs[1]. PMMA has good clarity and higher transmittance in the visible light, but is not as mechanically tough as polycarbonates but are cheaper[2]. PS is similar to polycarbonate and has high impact strength and good performance over broad temperatures of up to 120 °C but also has better water resistance and is non hygroscopic[3] allowing greater stability of index and dispersion characteristics. Styrene

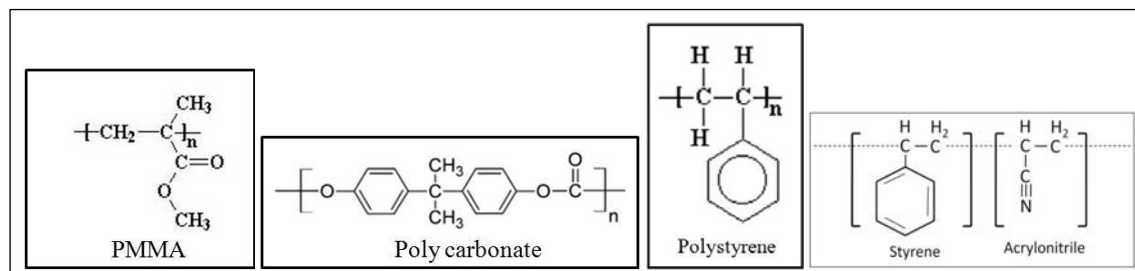


Fig. 5. Chemical structure of some optical polymer materials

Table 1. Index and dispersion of some optical polymers

Dispersion characteristics	PMMA	PS	PC	<u>Zeonex</u> E48R	<u>Optorez</u> 1330	SAN	BK-7 glass
<u>nd</u>	1.4914	1.5917	1.5849	1.5309	1.5094	1.5667	1.5168
<u>v_d</u>	59.2	30.5	29.1	56.5	52.5	35.4	64.17

acrylonitrile (SAN), which is a copolymer plastic consisting of styrene and acrylonitrile is an optical material having greater thermal resistance compared to PC. Recently developed Cyclo Olefin Copolymer (COC) (also called Zeonex) feature much lower birefringence and extremely low moisture absorption, relating directly to the stability of the index of refraction.[4,5] In recent developments, Polyetheramides (PEI) are also now available in optical grades. These plastics having higher refractive index exhibit higher transmission quality than previously possible in the near-IR and withstand operating temperatures⁴ from below zero to above 210 °C.

Non-linear optical materials

Non-linear optical effects arise in those materials that have high non linear polarizability of the molecule in response to large electric fields in intense light. Some of the non-linear optical effects give rise to phenomena such as frequency doubling, phase conjugation based on second order susceptibility ($\chi^{(2)}$) and optical Kerr effect based on third order susceptibility ($\chi^{(3)}$). Many anisotropic crystals having non centro-symmetric structure are used as non-linear optical materials. Lithium niobate (LiNbO_3), lithium tantalate (LiTaO_3) and Potassium niobate (KNbO_3) having a strong nonlinearity are used for nonlinear frequency conversion and for electro-optic modulators. Potassium di-hydrogen phosphate (KH_2PO_4) has a high damage threshold, but is hygroscopic and has a low nonlinearity. Borates, such as lithium triborate (LiB_3O_5 or LBO), cesium lithium borate ($\text{CsLiB}_6\text{O}_{10}$ or CLBO), β -barium borate ($\beta\text{-BaB}_2\text{O}_4$ or BBO), (strongly hygroscopic), bismuth triborate ($\text{BiB}_3\text{O}_6 = \text{BIBO}$), and cesium borate (CSB_3O_5 or CBO) are other crystals typically used for blue or green wavelengths. Yttrium calcium oxyborate (YCOB) and $\text{YAl}_3(\text{BO}_3)_4$ (YAB) are also available in rare-earth-doped form for use as a laser gain medium.

In the recent years, polymers have found increasing applications in Non Linear Optical (NLO) devices as active components. In polymer-based NLO materials, an NLO chromophore is incorporated into a polymer matrix either as a guest (in a host-guest-system), or as an integral component covalently grafted to polymer chain, or even co-polymerized into the polymer backbone itself. Covalent incorporation in the system can markedly improve stability of the NLO chromophores in applications[6]. The active chromophores in the polymer have to be ordered in a specific direction to get the NLO property either by applying a DC electric field or by specific thin film fabrication methods designed to yield order at the molecular level.

Fiber optics materials

An optical fiber consists of optically transparent cylindrical core and cladding structure. Cladding has a lower refractive index than core which results in light being transmitted from one end of the fiber to the other due to total internal reflection (see Fig. 6). Optical fibers allow for flexibility in arrangements of spectroscopic setups where light from one part (sample or a source) has to be transported to other part (spectrometer or detector). Materials used in the optical fibers can be all glass fibers where the core and the cladding are made of glass; all plastic fibers where core and cladding are of plastic or plastic-clad fibers where glass core is clad with plastic cladding. Glass used in fibers is ultra pure fused silica with dopants such as boron or fluorine to decrease refractive index (in cladding); germanium or phosphorous to increase the refractive index (in core). Plastic fibers cores are generally made of optical grade polymers of PMMA, PS and PC, while the cladding is of fluorinated or perfluorinated polymers. While glass fibers have merits of low attenuation due to high transmission for a higher bandwidth, plastic fibers have advantages of lower cost, greater flexibility and are less brittle than glass fibers. Glass fibers also have a limitation of lower core diameters (100-200 microns) compared to plastic fibers which can have cores of millimetre sizes. Light coupling in glass fibers is more demanding and sensitive due to lower core sizes. Plastic fibers however tend to suffer from optical birefringence limiting their use over short distances. However plastic fiber core designs have the flexibility of large number of dopants to choose from allowing diverse applications such as optical fiber-photonic devices, fiber sensors, fiber optical amplifiers and fiber lasers.

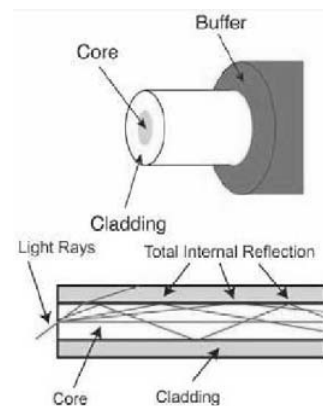


Fig. 6. Optical fiber structure

References

- [1] S. Volker, "Polycarbonates" in Ullmann's Encyclopedia of Industrial Chemistry, Wiley-VCH, Weinheim, **2000**. doi:10.1002/14356007.a21_207
- [2] W. F. Smith, J. Hashemi, "Foundations of Materials Science and Engineering" (4th ed.) McGraw-Hill, **2006**.
- [3] V. Doushkina, *Photon. Spectra*, **2010**, 4, 54-58.
- [4] P. Tolley, *Photon. Spectra*, **2003**, 10, 76-79.
- [5] US Patent no. US 20110244249 A1.
- [6] P. Prasad, D. Williams, Introduction to Nonlinear Optical Effects in Molecules & Polymers, Jon Wiley & Sons, **1991**.



Dr. Dinesh V Udupa completed his M Sc in physics at IIT Bombay in 1992 and M. Tech in Applied optics at IIT Delhi in 1993. He joined the first batch OCEP (Orientation Course for Engineering Post-graduates) course of the Training School of Bhabha Atomic Research Centre (BARC). After the completion of the training, he joined Spectroscopy Division of BARC and has been working in the field of Optical design, instrumentation, optical testing, optical interferometry and laser holography primarily for spectroscopic research and analytical applications. He got his PhD in Physics from University of Mumbai with the thesis entitled "Techniques in refractive index measurement and the testing of optical components". He has designed and developed several spectroscopic instruments such as Czerny -Turner monochromators, 22 channel polychromator, Micro-Raman spectrograph, 6.65 meter Vacuum ultraviolet scanning spectrometer for synchrotron beamline and 0.25 m echelle spectrograph for spectroscopic applications. He has also designed and developed a 6 meter optical periscope for visual inspection in the core of the nuclear Fast Breeder Test Reactor, Kalpakkam and a 10 m optical periscope for the Prototype Fast Breeder Reactor. He was conferred the "Scientific and Technical Excellence Award" for the year 2009 by the Department of Atomic Energy for his special contributions to the R&D program of the Department. He is a fellow member of the Optical society of India and is presently leading the Optics & Analytical Spectroscopy Section of the Atomic & Molecular Division, BARC.

Optical Materials for Laser Applications

K. S. Bartwal

*Laser Materials Development and Devices Division, Raja Ramanna Centre for
Advanced Technology, RRCAT, Indore- 452013*

E-mail: bartwal@rrcat.gov.in

1. Introduction

Materials have played an important role in our civilization, embedding our political history and culture. The history of materials science, including the engineering, production and testing stages of development, reveals a great deal about how much we depend on materials today. Manufactured materials can be found in nearly every aspect of modern life, from the metals and alloys found in our cars, to the plastics, ceramics and composites in our households. Materials can be found or synthesized in different forms e.g. crystalline, amorphous, glass etc. Humans are fascinated by glittering pieces of crystals (Gem stones) since the evolution of civilization. These gem crystals found in nature are known as natural crystals. In the twentieth century the science of synthetic crystals was evolved. The science of crystal growth and their important role in modern technologies is now well established.

The materials which alter or control electromagnetic radiation in the ultraviolet, visible, or infrared spectral regions are known as optical materials. Optical materials are mostly glass, crystals, or polymers. These optical materials are fabricated into optical elements such as lenses, mirrors, windows, prisms, polarizers, detectors, and modulators. The optical elements serve to refract, reflect, transmit, disperse, polarize, detect, and transform light. At the microscopic level, atoms and their electronic configurations in the material interact with the electromagnetic radiation (photons) to determine the material's macroscopic optical properties such as transmission and refraction. The optical properties are functions of the wavelength of the incident light, the temperature of the material, the applied pressure on the material, and in certain instances the external electric and magnetic fields applied to the material. Understanding of the interaction between light and matter is vital. The incident light is either reflected, absorbed, or transmitted when pass through any materials medium.

$$I_O = I_T + I_A + I_R$$

In metals, the fine succession of energy states causes absorption and reflection. On the other hand in non-metals, it may have full ($E_{gap} < 1.8\text{eV}$), no ($E_{gap} > 3.1\text{eV}$), or partial absorption ($1.8\text{eV} < E_{gap} = 3.1\text{eV}$). Color is determined by light wavelengths that are transmitted or re-emitted from electron transitions. Color may be changed by adding impurities which change the band gap magnitude. The transmitted light distorts electron clouds. The light is slower in a material medium compared to vacuum. Adding

large, heavy ions (e.g., lead) can decrease the speed of light. Intensity of transmitted light decreases with distance traveled. In this lecture, I will give brief description of optical materials, their synthesis, particularly, single crystals for laser host and NLO applications.

2. Optical Materials

Optical materials are mostly glass, crystals, and polymers. Crystals with wide band gaps are transparent from the ultraviolet through the visible region; crystals with a narrower band gap may appear opaque but are transparent in the infrared region. Crystal symmetry plays a critical role in the selection of material for optical applications. Optically isotropic crystals are used most frequently for windows and lenses although a uniaxial single crystal (such as sapphire) precisely oriented along the optical axis can be used as a window material. Anisotropic single crystals are widely used for other specific optical applications such as the polarizers, optical wave plates, and wedges. In nonlinear frequency conversion, all the optical materials used at present must not only be crystalline but also highly anisotropic and noncentrosymmetric. Several crystals are used as laser host materials to fabricate lasers.

Glasses are being used for optical applications since long. Optical glasses are characterized and designated by their refractive index and dispersion. The most common measure is the refractive index at the wavelength of the He d line (587.6 nm) or the Na D line (589.3 nm). There are more than 200 types of optical glasses. Optical glasses cover a general range of refractive indices $n_d = 1.4$ to 2.0 and reciprocal dispersion $v_d = 20$ to 90.

Among the large number of known polymers, several exhibit useful optical properties. Optical plastics transmit well in the visible and near infrared, but absorb strongly in the ultraviolet (fluoropolymers are an exception) and throughout the infrared. Most plastics degrade somewhat both in physical and optical properties when exposed to ultraviolet radiation. Being carbon-based materials, the index of refraction and dispersion of polymers differ significantly from those of glasses and crystals.

In some cases metals are used in optical systems as reflective optical components, optical thin films, structural elements, and mirror substrates. For these optical applications only a limited number of metals are useful. The materials and properties are therefore necessarily selective, depending upon the application, various physical, optical, mechanical, and thermal properties are of interest.

3. Single Crystals

A material having 3-dimensional periodic arrangement of atoms/molecules extending up to infinity is called single crystal. The periodicity of the building blocks decides the nature of the material whether it is crystalline, polycrystalline, amorphous or glass. There are two aspects to this arrangement of atoms; periodicity and the symmetry. The preservation of form and configuration across a point, line or a plane is called symmetry. The best example to understand the effect of crystalline structure is the three allotrops

of carbon ${}^6C^{12}$; Amorphous (normal carbon), Hexagonal (Graphite) and the Cubic (Diamond). Growth of single crystal is involved with the control of a phase change. This is basically an isothermic, isobaric, reversible process. Three main growth mechanisms are:

- Solid growth : Solid to solid (S-S) phase transition
 Melt growth : Liquid to solid (L-S) phase transition
 Vapour growth : Vapour to solid (V-S) phase transition

A) Solution Growth

Class of materials, which are water-soluble/soluble in any organic solvent, can be grown by solution growth technique. Saturated solution is made and the crystal grows with slow evaporation/cooling. Fig. 1 (a) shows the crystallizer used for solution growth of crystals. The KDP, DKDP and most of the alkali halide crystals are grown by this technique.

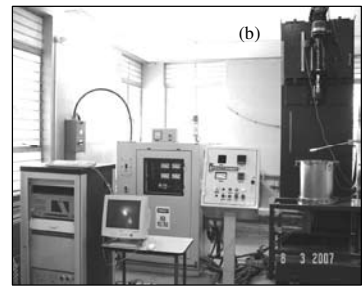
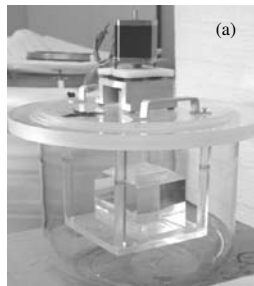


Fig. 1 (a) Crystallizer for Solution growth (b) Czochralski crystal puller

B) Melt Growth

Class of materials, which melt congruently and have the melting point which is easily achievable are grown by melt technique. It is named on its inventor, as Czochralski technique. In this technique material is melted in a suitable crucible and a rotating seed crystal is dipped into it and then slowly pulled from the melt, during the withdrawal process, melt is attached to the seed and forms a crystal. Most of the laser host crystals are grown by this technique. Fig. 1 (b) shows the Czochralski set up.

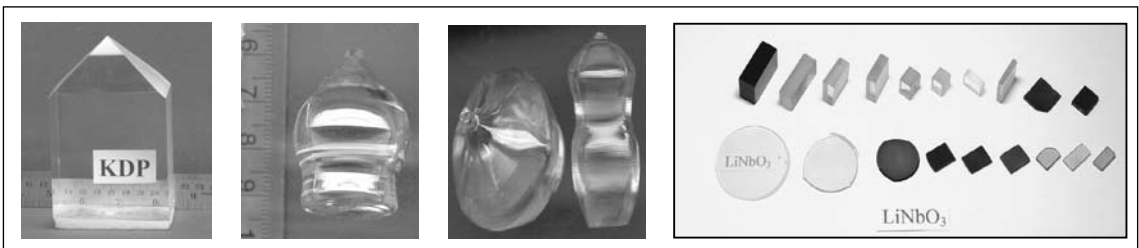


Fig. 2 Some of the crystals grown in our Laboratory at RRCAT

Some of the important crystals used for solid state laser host applications are: Rare earth doped Yttrium Aluminum Garnet (YAG), Transition metal ion doped Sapphire (Al_2O_3). Most common host crystals are $Nd:Y_3Al_5O_{12}$, $Er:Y_3Al_5O_{12}$, $Cr:Al_2O_3$, $Ti:Al_2O_3$. Some of the

important crystals used for non-linear optical (NLO) applications are: KDP, KD*P, ADP, LiNbO₃, BBO, LBO, LTB, KTP, KNbO₃, etc.

It is must to characterize the grown crystals for their structural and optical quality before using them for any device application. The grown crystals were analyzed by XRD, high resolution XRD and transmission electron microscopy for their phase and crystallinity. The optical homogeneity of the grown crystal is very crucial for its device application. The Li/Nb ratio is governing factor in optical parameters as well. The physical properties sensitive to Li/Nb ratio are: extraordinary index of refraction, transparency in UV, absorption edge (UV), phase matching temperature (T_m), Curie temperature (T_c) and Raman scattering. The optical homogeneity of the crystal measured using birefringence interferometry technique.

4. NLO Applications

For selecting a suitable crystals for a particular application a balance has to made between physical limitations of the crystal and the demand of the device. The important crystal parameters to be taken care for NLO application are: Damage threshold, Phase matching angle (type I and II), Acceptance angle, Walk off angle, Spectral transmission range, Absorption, Birefringence, Temperature range, SHG conversion efficiency, Photo refractive damage threshold and crystal size.

5. Lasers

Laser is a devices generating visible or invisible light, based on stimulated emission of light. "Laser" is an acronym for "Light Amplification by Stimulated Emission of Radiation", coined in 1957 by the laser pioneer Gordon Gould. The first laser device was a pulsed ruby laser, demonstrated by Theodore Maiman in 1960. In the same year, the first gas laser (a helium-neon laser) and the first laser diode were made. A laser device usually comprises an optical resonator (laser resonator, laser cavity) in which light can circulate (e.g. between two mirrors), and within this resonator a gain medium (e.g. a laser crystal), which serves to amplify the light. The gain medium amplify the circulating light, thus compensating the losses if the gain is high enough. The gain medium requires some external supply of energy - it needs to be "pumped", e.g. by injecting light (optical pumping) or an electric current (electrical pumping → semiconductor lasers). The principle of laser amplification is stimulated emission.

Types of Laser:

- | | |
|------------------------|------------------------|
| * Gas lasers | * Chemical lasers |
| * Solid-state lasers | * Fiber lasers |
| * Bio laser | * Exotic laser media |
| * Free electron lasers | * Semiconductor lasers |
| * Excimer lasers | * Dye lasers |

6. Applications of Lasers

Manufacturing: Cutting, drilling, welding, cladding, soldering, hardening, ablating, surface treatment, engraving, micromachining, pulsed laser deposition, lithography, alignment, etc.

Medical Applications: Eye surgery and vision correction (LASIK), dentistry, dermatology (e.g. photodynamic therapy of cancer), various kinds of cosmetic treatment.

Metrology: Optical metrology e.g. for extremely precise position measurements and optical surface profiling with interferometers, for long-distance range finding and navigation.

Data Storage: Optical data storage e.g. in compact disks (CDs), DVDs, Blu-ray Discs and magneto-optical disks,

Communications: Optical fiber communication, extensively used particularly for long-distance optical data transmission, mostly relies on laser light in optical glass fibers.

Displays: Laser projection displays containing RGB sources can be used for cinemas, home videos, flight simulators, etc., and are often superior to other displays

Spectroscopy: Atmospheric physics and pollution monitoring profits from trace gas sensing with differential absorption LIDAR technology, medicine (e.g. cancer detection), biology, and various types of fundamental research

Microscopy: Laser microscopes and setups for optical coherence tomography (OCT) provide images of, e.g., biological samples with very high resolution, often in three dimensions. It is also possible to realize functional imaging.

Various Scientific Applications: Laser cooling makes it possible to bring clouds of atoms or ions to extremely low temperatures. Optical tweezers can be used for trapping and manipulating small particles, such as bacteria or parts of living cells. Laser guide stars are used in astronomical observatories.

Energy Technology: High-power laser systems might play a role in electricity generation, Laser-induced nuclear fusion, isotope separation.

Military Applications: Lasers are used as weapons; the “laser sword” has become popular in movies, but not in practice, high power lasers as directed energy weapons on the battle field, or for destroying missiles, projectiles and mines., blind soldiers temporarily or permanently with laser beams

LIDAR: Stands for light detection and ranging. LIDAR is an optical remote sensing technology that can measure the distance to, or other properties of, targets by illuminating the target with laser light and analyzing the back scattered light.

References

- [1] J.W. Mullin, "Crystallization", Butterworth-Heinemann Ltd. Oxford, 3rd Ed., **1993**.
- [2] R.V.A. Murthy, K.S. Bartwal, Krishan Lal, *Mat. Sci. & Engg.*, **1993**, B18, L4-L6.
- [3] R. K. Choubey, P. Sen, S. Kar, G. Bhagavannarayana, K.S. Bartwal, *Solid State Commun.*, **2006**, 140, 120-124.
- [4] S. Kar, H. Ryu, K.S. Bartwal, *Open Crystallogr. J.*, **2008**, 1, 1-5.
- [5] N. Kaithwas, M. Dave, S. Kar, K.S. Bartwal, *Physica E*, **2012**, 44, 1486-1489.
- [6] N. Kaithwas, M. Dave, S. Kar, K.S. Bartwal, *Open J. Modern Phys.*, **2014**, 1, 29-33.
- [7] C. Debnath, S. Kar, S. Verma, K.S. Bartwal, *J. Nanosci. Nanotech.*, **2014**, 14, 1-7.
- [8] S. Kar, C. Debnath, S. Verma, V.P. Dhamgaye, G.S. Lodha, K.S. Bartwal, *Physica B*, **2015**, 456, 1-4.



Dr. Bartwal, Ph. D. in Physics, Banaras Hindu University, Varanasi, 1991.

Dr. Bartwal, Scientist, National Physical Laboratory (NPL), New Delhi, 1990-1993.

Dr. Bartwal, Scientist, RRCAT, Dept. of Atomic Energy since 1993-.

Area of research:

- *Solid State Physics and Condensed Matter Physics*
- *Laser Science & Technology*
- *Nano Materials*
- *X-ray and Electron diffraction techniques*

Membership of the Scientific Societies:

- *Life member, Indian Laser Association.*
- *Life member, Indian Physics Association.*
- *Vice President, Indian Association for Crystal Growth.*
- *ice President, Indian Physics Association Indore chapter.*

Editorial Board Member, International Journals:

- *Editorial Board Member, Open Crystallography Journal, Bentham Science Pub. USA.*
- *Editorial Board Member, Advances in Materials, Science Publishing Group, USA.*
- *Editorial Board Member, Universal J of Materials Science, Horizon Research Pub. USA.*
- *Editorial Board Member, Open Journal of Modern Physics, Science Online Pub. USA.*
- *Editorial Board Member, Journal of Applied Physics, ISST, India.*

Deputed Abroad:

- *Anhui Institute of Optics and Fine Mechanics, Hefei, China*
- *Hong Kong National University*
- *Korea Research Institute of Chemical Technology, Daejeon, South Korea*

Research Publications:

More than 250 papers in International Journals & Seminar Proceedings.

Non-linear Optical Studies on Some Specific Glasses and Glass Ceramics

N. Veeraiiah

Department of Physics, Acharya Nagarjuna University, Nagarjuna Nagar- 522 510, Guntur, Andhra Pradesh.

E-mail: nvr8@rediffmail.com

Abstract

Studies on non-linear optical (NLO) properties of the materials help in examining the suitability of them for potential applications in non-linear optical devices such as optical switchers, limiters etc., broad band optical amplifiers and in a number of solid state ionic devices. So far such studies are mainly focussed on crystalline materials. In this talk we propose to present some of the highlights of the non-linear optical properties of glass materials. Some of the experimental techniques being adopted (viz., two photon absorption method, second harmonic generation and z-scan technique) for measuring higher order non-linear susceptibilities and birefringence of the materials will be discussed. Later we present some of the results of NLO properties related to heavy metal oxide based glasses and glass ceramics viz., Sb_2O_3 , Bi_2O_3 , TeO_2 , Nb_2O_5 . The analysis of the results obtained and their correlation with the structural changes taking place in the studied material will be presented in detail. Some light will also be thrown on the non-linear optical efficiency and its connection with the chemical composition of these materials. Finally, the possible applications of these materials in NLO devices will be discussed.

Brief introduction On Non-linear optical in glasses and glass ceramics

When some heavy metal oxide (Sb_2O_3 , Bi_2O_3 etc.,) glass or glass ceramic is placed in an electric field and each constituent molecule acts as a dipole, with a dipole moment P_i . The dipole moment vector per unit volume P is given by

$$P = \sum_i P_i = \chi E \quad (1)$$

The orienting effect of the external field on the molecular dipoles depends both on the properties of the medium and on the field strength. In the Eq. (1), χ is called polarizability or dielectric susceptibility of the medium. When the material is subjected to high intensity laser radiation, the Eq.(1). does not hold good and is to be generalized as

$$\vec{P}_i = \vec{P}_i^L + \vec{P}_i^{NL} = \alpha_{ij} E_j^{(\omega)} + \beta_{ijk} E_j^{(\omega)} E_k^{(\omega)} + \gamma_{ijkl} E_j^{(\omega)} E_k^{(\omega)} E_l^{(\omega)} + \dots \quad (2)$$

where α_{ij} , β_{ijk} , γ_{ijkl} etc., are microscopic susceptibilities in microscopic case (hyper polarizabilities) which are related with macroscopic susceptibility χ_{ijk} by Eqs.

$$\chi_{ij}^{(\omega)} = L_i^{(\omega)} L_j^{(\omega)} \alpha_{ij}; \quad \chi_{ijk}^{(\omega)} = L_i^{(\omega)} L_j^{(\omega)} L_k^{(\omega)} \beta_{ijk}; \quad \chi_{ijkl}^{(\omega)} = L_i^{(\omega)} L_j^{(\omega)} L_k^{(\omega)} L_l^{(\omega)} \gamma_{ijkl} \quad (3)$$

In these Eqs., χ_{ij} , χ_{ijk} , χ_{ijkl} represent first, second and third order susceptibilities, respectively, and $L_{i,j,k}$ representing Lorenz field factors. χ_{ijk} and χ_{ijkl} define the degree of nonlinearity and are known as nonlinear susceptibilities. A polarization, oscillating at frequency 2ω , radiates an electromagnetic wave of the same frequency. The wave thus produced has the same characteristics of directionality and the monochromaticity as the incident wave and emitted in same direction. This phenomenon is known as second harmonic generation (SHG). This polarization is represented by

$$P_i^{(2)} = \sum_{j,k} \chi_{ijk}^{(2)} E_j E_k \quad (4)$$

For amorphous material as such this χ_{ijk} is zero and it is non-zero when exposed to high intense laser beam. The development of Q-switched laser made possible to generate third harmonic represented by

$$P_i^{(3)} = \sum_{j,k} \chi_{ijk}^{(3)} E_j E_k E_l \quad (5)$$

even in amorphous materials by optical poling. But the energy conversion efficiency in such cases is very low. In case of the optical poling, the IR induced non-centro symmetry of the photo-induced vibrations begins to play a dominant role and it is necessary to consider a process of interaction of at least two photons and three phonons. Interactions of the one or two photons with one or two phonons do not give contribution to the non-zero polarization of the medium (Fig. 1).

For getting birefringence, anharmonic electron-phonon interactions with at least three phonons as shown in Fig. 3 are required. Otherwise, we shall have harmonic electronic-phonon interactions which would not give non-centro symmetry as shown in Fig. 3.

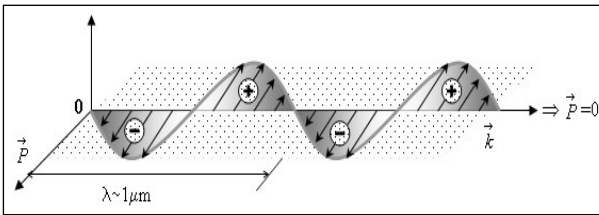


Fig. 1 General scheme of the medium polarization for the pure electronic contribution

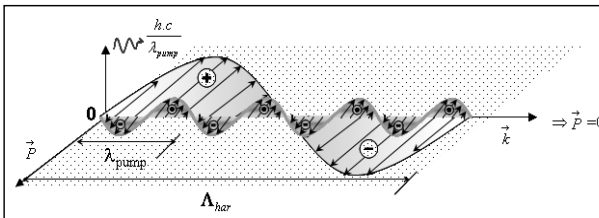


Fig. 2 Scheme Electronic + harmonic electron-phonon contribution

As an example for such studies we can consider antimony/bismuth oxide based glass ceramics mixed with some transition metal oxides. Sb_2O_3/Bi_2O_3 participates in the glass network with SbO_3/Bi_2O_3 structural units and can be viewed as tetrahedrons with the oxygen situated at three corners and the lone pair of electrons of Sb^{3+}/Bi^{3+} at the fourth corner localized in the third equatorial direction of Sb/Bi atom (Fig. 4). The deformability of this pair probably favor different optically

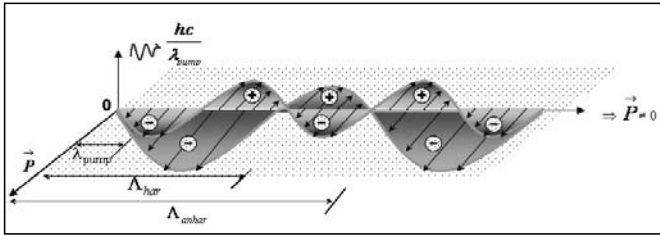


Fig. 3. Electronic + harmonic electron-phonon + anharmonic electron-phonon contribution

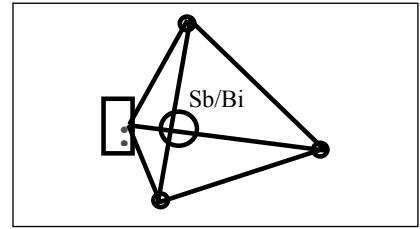


Fig. 4 SbO₃/Bi₂O₃ structural unit with the lone pair of electrons

polarized effects and make these glass ceramics to exhibit non-linear optical susceptibility described by third rank polar tensors.

Experimental Setup

The photo-induced birefringence (PIB) of the glass ceramics was measured using standard nano-second (ns) photo-induced technique (Fig. 5). A Nd:YAG laser operated at 10 Hz with the pulse duration of 10 ns was used as a fundamental laser light source.

The fundamental laser beam was split into two beams by a beam splitter with the intensity ratio 8:1. The strong beam acts as the pump one and the weak one as the probe.

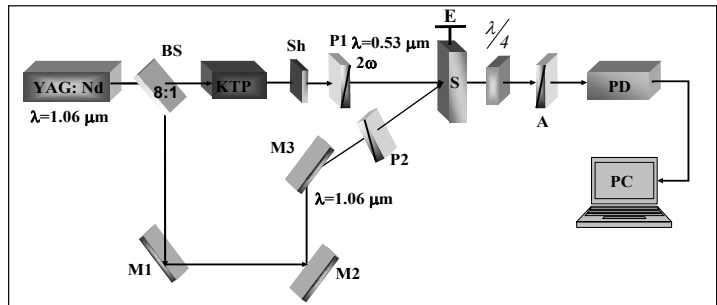


Fig. 5. Principal experimental set-up used for measuring photo induced birefringence (PIB).

Two beams were adjusted to be almost parallel and then focused by a convex lens to overlap spatially inside the glass sample. After transmitting through the specimen, the pump beam was blocked by chopper, while the probe beam passed through a polarizer and phase inverter plate which is an element of Senarmont schema. After the rotation of the output signal, polarization was determined to evaluate the photo-induced birefringence.

The photo-inducing 7 ns 1064 nm Nd:YAG laser was incident on the sample at angle about 5-7 degree with respect to the surface normal. The photo-inducing UV laser beam and the probing laser beams were temporary synchronized. Varying successively an intensity of the photo-inducing beam power density, we have operated by pumping power density.

Results and Discussion

Fig. 6 (a) and 6 (b) represent the PIB results of TiO₂ doped Sb₂O₃ based glass ceramics. These figures indicate that with the enhancement of the photo-inducing power, there is a substantial increase of the output PIB. The maximum is observed for the perpendicular

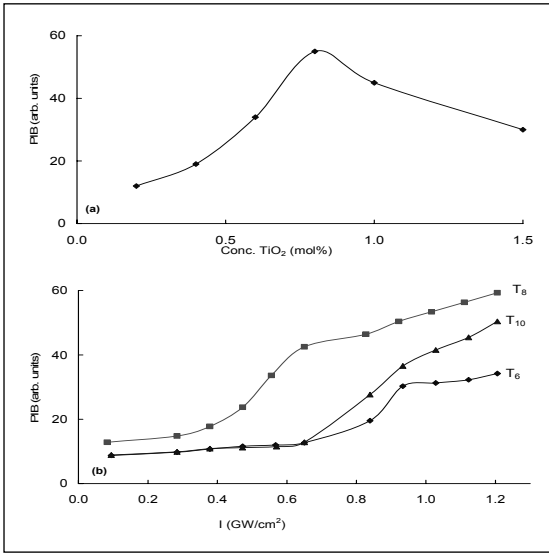


Fig. 6 (a) Photo-induced birefringence with the concentration of Sb_2O_3 based glass ceramic with the concentration of TiO_2 measured with the power density 1.2 GW/cm^2 ($\lambda = 1064 \text{ nm}$). (b) Photo-induced birefringence versus the power density of the pumping power for some of the samples.

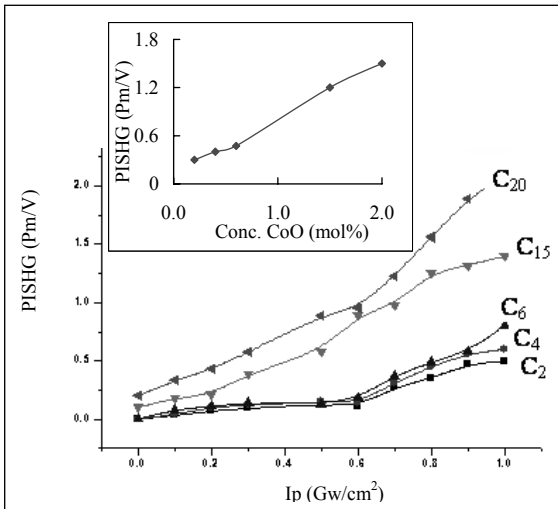


Fig. 7. Variation of photo induced birefringence with the photo-inducing power for $\text{PbO-Sb}_2\text{O}_3\text{-B}_2\text{O}_3$ glass ceramics crystallized with different concentrations of CoO. Inset shows the variation of photo-induced birefringence with the concentration of the crystallizing agent measured with the pump power density, 0.8 GW/cm^2 ($\lambda = 1064 \text{ nm}$).

polarization of the photo-inducing and probing beams. After achieving of the pumping power density equal to about 1.2 GW/cm^2 , there occurs irreversible changes which destroy the effect. One can see that maximal PIB signal is observed for the glass doped with 0.8 mol% of TiO_2 .

From these figures it is clear that with the enhancement of the photo-inducing power, we observe substantial increase of the output PIB. This maximum is observed for the perpendicular polarization of the photo-inducing and probing beams. After achieving of the pumping power density equal to about 1.2 GW/cm^2 there occurs irreversible changes which destroy the effect. One can see that maximal PIB signal is observed for the glass mixed with 0.8 mol% of TiO_2 . This is very principal result of the current investigation because it allows to conclude that Ti ion surrounding ligands play principal role in the observed PIB.

Results on CoO doped glass ceramics

In the Fig. 7 shown below, we have presented the results of PIB measurements for $\text{PbO-Sb}_2\text{O}_3\text{-B}_2\text{O}_3\text{:CoO}$ glass ceramics. We have observed substantial increase of the PIB output with the increase of the pumping power for all the samples. In the inset of Fig. 5, we have presented photo-induced birefringence with the concentration of the CoO measured with the pump power density, 0.8 GW/cm^2 ($\lambda = 1064 \text{ nm}$); the figure indicates a slow raise of PIB intensity up to 0.6 mol% concentration of nucleating agent and for further increase of CoO content, a rapid increase could be observed. This observation allowed us to conclude that the surrounding ligands of octahedrally positioned cobalt ions play principal role in the observed PIB.

Overall analysis of PIB the results coupled with a variety of other experimental results indicated that with the optimal levels of crystallizing agents (TiO_2 and CoO) the Sb_2O_3 based glass ceramics are suitable materials for the applications in non-linear optical devices.

Some results obtained on Bi_2O_3 , TeO_2 , Nb_2O_5 based glasses will also be presented and discussed in detail.



Prof Nalluri Veeraiah did his M. Sc in Physics from Osmania University and Ph.D in Solid state physics from Indian Institute of Physics, Kharagpur. Currently he is working as Professor in Physics at Acharya Nagarjuna University, A.P. Prof Veeraiah has got 31 years of teaching experience and 35 years of research experience. His research interests include dielectric and, spectroscopic properties of glass materials. He was honoured with the Best Teacher Award by the Govt. A.P., in 2015, A.P Scientist award by the Govt. A.P in 2010. Under his guidance so far 39 students have obtained their Ph.D degrees and 50 students have got their M. Phil. He has published nearly 250 research articles in reputed International journals with h-index 32 and citations 3500. Delivered more than 100 invited talks at various National and International conferences. He has handled several major research projects funded by UGC, DST, DAE-BRNS, DRDO, CSIR etc. He is currently working as Visiting Professor at Jan Dlugosz University, Poland. He has visited several Universities in various countries namely Poland, Japan, Romania, Portugal, Czech Republic, Italy, Croatia, Germany and delivered Invited talks on glass materials. He has organized two national and two international conferences on glass materials.

Use of Eu (III) ion as a PL Probe to Understand the Radiation Induced Changes in Borosilicate Glass Matrices

M. Mohapatra

Radiochemistry Division, Bhabha Atomic Research Centre, Mumbai

E-mail: manojm@barc.gov.in

1. Introduction

In view of the green house effect, global warming and limited resources of fossil fuel, nuclear energy is one of the cleanest options to meet the growing energy demands of developing countries. However, during the course of the nuclear fuel cycle a lot of radioactive waste is generated whose handling poses a serious challenge to nuclear engineers and scientists. Most of the radioactivity of the entire nuclear fuel cycle is concentrated in the so-called high level radioactive liquid waste (HLW). The accepted approach for HLW management today is to concentrate and fix the waste in suitable matrices like glasses, tailor made synthetic ceramics (Synroc) and naturally occurring minerals like zircon etc. [1]. Borosilicate based glass formulations have been adopted worldwide as a suitable matrix for immobilizing the HLW [2]. These glasses possess desirable properties like high chemical, mechanical, thermal and radiation stability for HLW storage. Also, the amorphous nature of the glass helps to accommodate the waste containing a variety of elements easily. However, the glass composition varies with the composition of the HLW, which in turn depends on the type of reactor, burn up, off reactor cooling of spent nuclear fuel and nature of reprocessing flow sheets etc. Although the basic network is of silicon and boron oxides, other modifiers are necessary to take into account site specific variations in HLW composition.

As it is already said the HLW is expected to contain almost all the elements of the periodic table including minor actinides (Am, Cm and Np), rare earths (RE) or lanthanides (mostly as fission products) and short lived fission products (^{137}Cs and ^{90}Sr etc.). Because of the decay of these radioactive components present in the waste, the borosilicate glass experiences radiation damage. The sources of radiation are the alpha (α), beta (β), gamma (γ) and neutrons emanating from the residual actinides, fission and activation products. Due to the impingement of the radiation, the glass structure and consequently their long term integrity can be severely affected [3].

A comprehensive review by Weber et al in this aspect is worth mentioning [4]. Several other reports are also available in literature where irradiated glasses have undergone changes in their structure, caused mostly by ionization and ballistic interaction of high-energy radiations with the solid constituents of the glass matrix that introduce disorders in the original structure causing formation of defect centers accompanied with volume changes, phase separation or gas accumulation in the irradiated glasses [5-6]. It is essential to study these changes so as to predict the long term integrity of the vitrified waste

product. Trivalent RE elements are considered as possible surrogates for the trivalent minor actinides. These can mimic minor actinides viz. Am and Cm. Moreover, one of them i.e. Eu^{3+} can mimic trivalent plutonium Pu(III) in glassy matrices, which was found to be more soluble in borosilicate glasses than the usual Pu(IV) [7].

Photoluminescence (PL) technique is a non-invasive and reliable method for studying the radiation induced changes in these glass matrices. By the virtue of its triple resolving power (namely excitation, emission and temporal), it provides a non destructive as well as sensitive tool to study the local environment and oxidation states of various ions especially rare earths in the glass matrix. On the other hand, many RE ions and especially Eu(III), due to its electronic arrangement (and of course special nature of 'f-f' transition), can act as suitable structural PL probe to study these radiation induced changes.

2. Case study with Eu(III) ion

The electronic structure of the lanthanide elements, with minor exceptions is $[\text{Xe}] 6s^2 4f^n$. The chemistry of the lanthanides is dominated by the +3 oxidation state and in Ln (III) compounds the 6s electrons and (usually) one 4f electron are lost and the ions have the configuration $[\text{Xe}] 4f^n$. All the lanthanide elements exhibit the oxidation state +3. In addition Ce^{3+} can lose its single f electron to form Ce^{4+} with the stable electronic configuration of xenon. Similarly, Eu^{3+} can gain an electron to form Eu^{2+} with the f^7 configuration which has the extra stability of a half-filled shell. Other than Ce(IV) and Eu(II), none of the lanthanides are stable in oxidation states other than +3 in aqueous solution.

In terms of reduction potentials, the Ln0/3+ couples are nearly the same for all lanthanides, ranging from -1.99 (for Eu) to -2.35 V (for Pr). Thus, these metals are highly reducing, with reducing power similar to alkaline earth metals such as Mg (-2.36 V).

2.1 The Asymmetric Ratio (A)

Fig. 1 shows the emission spectrum of the Eu incorporated in borosilicate glass matrix before and after gamma irradiation with 2, 50 and 900 kGy (J/kg) dose and 395

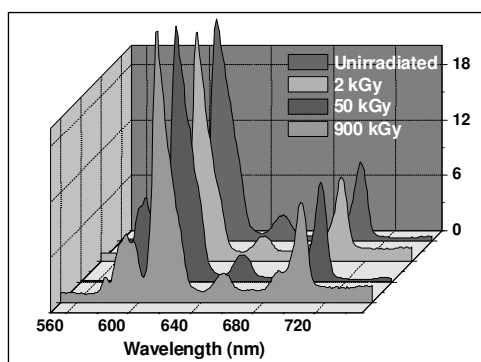


Fig. 1: Emission spectrum of the glass samples before and after gamma irradiation

nm excitation (corresponding to the ${}^7\text{F}_0 \rightarrow {}^5\text{L}_6$ transition). The assignment of the different emission peaks observed is given in Fig. 2.

As it is evident from the figures, upon irradiation, no significant changes in the line position or intensity of the peaks were observable. However, one noteworthy observation here was the change in the asymmetric ratio ('A') for the Eu^{3+} ion which is defined as the ratio of the intensity of the ${}^5\text{D}_0 \rightarrow {}^7\text{F}_2$ and the ${}^5\text{D}_0 \rightarrow {}^7\text{F}_1$ transitions (I_{611}/I_{591}). The electric dipole transition (${}^5\text{D}_0 \rightarrow {}^7\text{F}_2$) is

hypersensitive in nature than the magnetic dipole transition (${}^5D_0 \rightarrow {}^7F_1$). Thus the value of 'A' indicates the symmetry and the covalence of the rare earth ion. Its value increases with increasing covalence of the ligands or decreasing site symmetry. The 'A' values obtained for the borosilicate glasses obtained before and after irradiation is presented in table-1. It can be seen that upon irradiation, the values increased indicating a decrease in the site symmetry of the rare earth ion in the glass after irradiation [8].

Table 1: Comparison of the Asymmetric ratios and FWHM of the ${}^5D_0 \rightarrow {}^7F_0$ transition of Eu^{3+} species in glasses before and after gamma irradiation

Sample	Unirradiated	5 k Gy irradiated	50 kGy irradiated	900 kGy irradiated
Asymmetric ratio ($A = I_{611}/I_{591}$)	2.91	2.95	2.96	3.05
FWHM data of the ${}^5D_0 \rightarrow {}^7F_0$ emission band (cm^{-1})	120	122	140	168

2.2 Stark Splitting in the spectrum

The local site symmetry of the Eu ion can also be characterized by the line position and the full width at half-maximum (FWHM) data of the ${}^5D_0 \rightarrow {}^7F_0$ emission band. This transition becomes allowed only cases where the site symmetry of the metal ion is C_{nv} or lower, due to the presence of a linear term in the Hamiltonian of the respective crystal field, and gains strength from mixing of J values in one or both of the levels described earlier [9]. In the present case, the band is centered at 578 nm with FWHM of 120 cm^{-1} . This value is close to that of Eu^{3+} in sodium borosilicate glasses as reported by Pucker et al [10]. As shown by Ollier et al, a lower value of the FWHM infers a smaller site distribution of the RE ions [11]. Here in case of the barium borosilicate glass, the FWHM is fairly large indicating a fairly large site distribution for the RE ion. Furthermore, the site symmetry of the Eu ion can also be determined from the number of Stark components observed as described below. For every J level, the maximum numbers of Stark components that one might expect are $(2J + 1)$. In general, with decrease in the symmetry of the electric field, the number of Stark components into which a band is split increases. Here in this case, for the F_1 transition, at least 3 components at 587, 591 and 596 nm are observed. Similarly for the F_2 transition, components at 610, 619 and 626 nm are observed. For the F_4 transition, 2 components at 689 and 704 nm are seen. The presence of multiple components can be either due to the presence of Eu-ion in lower symmetry or due to the presence of 2 types of Eu-species in higher symmetries. However, the presence of a single component for the F_0 transition, suggests that, there is only one type of Eu-ion in a lower symmetry. Brecher et al have given a detailed account of the relationship of the symmetry of the Eu ion and the number of observed components in the emission spectrum that is presented

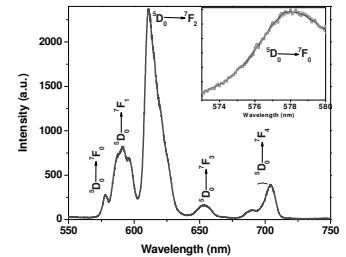


Fig. 2: Emission spectrum of the glass samples after gamma irradiation (900 kGy) with transitions

in table-2 [12]. Based on this, it can be argued that, the rare earth metal ion must be in symmetry equal to C_2 .

Table-2: Selection rules for Eu^{3+} transition in various coordination structures

Spatial Configuration	Site Symmetry	Active Representations		
		${}^5\text{D}_0 \rightarrow {}^7\text{F}_2$	${}^5\text{D}_0 \rightarrow {}^7\text{F}_1$	${}^5\text{D}_0 \rightarrow {}^7\text{F}_0$
Face-centered isosceles prism	C_{2v}	4 components (A_1, A_1, B_1, B_2)	3 components (A_2, B_1, B_2)	1 component (A_1)
	C_2	5 components (A, A, A, B, B)	3 components (A, B, B)	1 component (A)
Archimedean antiprism	D_{4d}	None	2 components (A_2, E_3)	None
	D_4	1 component (E)	2 components (A, E)	None
	D_2	3 components (B_1, B_2, B_3)	3 components (B_1, B_2, B_3)	None
Tetragonal dodecahedron	D_{2d}	2 components (B_2, E)	2 components (A_2, E)	None
	S_4	3 components (B, B, E)	2 components (A, E)	None
	D_2	3 components (B_1, B_2, B_3)	3 components (B_1, B_2, B_3)	None
Ninefold antiprism adduct	C_{4v}	2 components (A_1, E)	2 components (A_2, E)	1 component (A_1)
	C_4	2 components (A, E)	2 components (A, E)	1 component (A)
	C_2	5 components (A, A, A, B, B)	3 components (A, B, B)	1 component (A)

2.3. The PL Decay Time (τ)

The PL decay time of life time of a particular species is defined as the time taken for the excited state population to become $1/e$ of its original value. For all practical purposes it is taken as the $1/3^{\text{rd}}$ of the intensity. The decay time being unique to particular species can be used as a finger print to identify multiple species present simultaneously in a system.

Before irradiation, the glass samples had shown a single exponential decay curve of 2.7 ms and after gamma irradiation the sample showed bi-exponential decay curves with two life time values viz. ~ 2.7 and 1.3 ms. One interesting thing observed here was that the relative percentage of the short lived component (1.3 ms) kept on increasing with radiation dose which suggested that the RE ion upon irradiation is going preferentially

to a site with lower symmetry. The decay time values of the glass samples as a function of the gamma dose is represented in table -3.

Table 3: Comparison of the decay time values of the Eu^{3+} ion in borosilicate glass before and after irradiation. The figures in bracket indicate the relative percentages

Sample	Unirradiated	5 kGy	50kGy	900kGy
$\tau_1(\text{ms})$	2.7 ± 0.1 (100)	2.78 ± 0.1 (90)	2.81 ± 0.1 (85)	2.80 ± 0.1 (80)
$\tau_2(\text{ms})$	---	1.3 ± 0.1 (10)	1.3 ± 0.1 (15)	1.3 ± 0.1 (20)

2.4. Inference from Judd-Ofelt (JO) Parameters

The J-O analysis of the emission spectrum is a powerful tool for calculating the parity-forbidden electric-dipole radiative transition rates between the various levels of a rare earth ion [13-14]. For all these calculations, the corrected spectra (with respect to source and detector response) have to be taken into consideration. Through these analyses, the local environment around the metal ion and the M-L bond covalency can be interpreted. Apart from this, the radiative transition rate (A_R), radiative lifetimes (τ_R) and luminescence branching ratios (β_R) can also be computed. It is possible to determine the J-O intensity parameters Ω_J (where $J = 2, 4, 6$ etc.) based on the emission spectral data as shown by various authors [15-16].

The J-O intensity parameters (Ω_J) of the Eu^{3+} ion in the glass matrix reveal information regarding the covalence and surrounding of the metal ion. Jorgensen and Reisfeld have discussed the physical meaning of these parameters in one of their papers [17]. The parameter Ω_2 is related to the covalency and structural changes in the vicinity of the Eu^{3+} ion (short range effect) and Ω_4 is related to the long-range effects. A larger value of Ω_2 is an indication of a high covalence of the metal-ligand bonds and more distortion of the symmetry of the Eu^{3+} sites in that matrix compared to a matrix where the Ω_2 value is smaller. Large values for Ω_4 can be expected for organic ligands, because of low rigidity of these matrices.

Table 4: Comparison of the J-O intensity parameters of Eu^{3+} species obtained in glasses after gamma irradiation

	Unirradiated		5 kGy		50 kGy		900 kGy	
	Ω_2	Ω_4	Ω_2	Ω_4	Ω_2	Ω_4	Ω_2	Ω_4
Ω_J in 10^{-20} cm^2								
Long lived species	6.57	1.81	6.55	1.83	6.58	1.85	6.57	1.88
Short lived species	-	-	6.59	2.2	6.56	2.38	6.58	2.48

A comparison of the JO parameters for the un-irradiated and gamma irradiated samples are shown in table-4. After irradiation of the glasses by gamma radiation, though there is no change in the symmetry and short range ordering in the glasses, as indicated from the trend observed for Ω_2 , the long range ordering gets modified (as indicated from the Ω_4 values).

3. Conclusion

From the above discussion it is clear that with a single dopant ion e.g. Eu^{3+} and with a simple technique e.g. PL, much deeper information can be extracted regarding the changes taking place in the vicinity of the central metal ion.

References

- [1] E. Y. Vernaz, Summary of an International Workshop, National Academy Press E 26 (1996).
- [2] C. P. Kaushik, R. K. Mishra, P. Sengupta, A. Kumar, D. Das, G. B. Kale, K. Raj, *J. Nucl. Mater.*, **2006**, 358, 129.
- [3] D. R. Cousens, S. Myhra, *J. Non-Cryst. Solids*, **1983**, 54, 345.
- [4] W. J. Weber, R. C. Ewing, C. A. Angell, G. W. Arnold, A. N. Cormack, J. M. Delaye, D. L. Griscom, L. W. Hobbs, A. Navrotsky, D. L. Price, A. M. Stoneham, M. C. Weinberg, *J. Mater. Res.*, 1997, 12, 1946.
- [5] W. J. Weber, *Nucl. Instrum. Methods B*, **1988**, 32, 471.
- [6] R. C. Ewing, W. J. Weber, F. W. Clinard, *Prog. Nucl. Energy*, **1995**, 29, 63.
- [7] X. Feng, H. Li, L. L. Davis, L. Li, J. G. Darab, M. J. Schweiger, J. D. Vienna, B. C. Bunker, P. G. Allen, J. J. Bucher, I. M. Craig, N. M. Edelstein, D. K. Shuh, R. C. Ewing, L. M. Wang and E. R. Vance, *Ceram. Trans.*, **1999**, 93, 409.
- [8] J. de Bonfils, G. Panczer, D. de Ligny, S. Peugeot and B. Champagnon, *J. Nucl. Mater.*, **2007**, 362, 480.
- [9] R. Reisfeld, E. Greenberg, R. N. Brown, M.-G. Drexhage and C. K. Jorgensen, *Chem. Phys. Lett.*, **1983**, 95, 91.
- [10] G. Pucker, K. Gatterer, H. P. Fritzer, M. Bettinelli, M. Ferrari, *Phys. Rev. B*, **1996**, 53, 6225.
- [11] N. Ollier, G. Panczer, B. Champagnon, G. Boulon and P. Jollivet, *J. Lumin.*, **2001**, 94/95, 197.
- [12] C. Brecher, H. Samelson and A. Lempicki, *J. Chem. Phys.*, **1965**, 42, 1081.
- [13] B. R. Judd, *Phys. Rev.*, **1962**, 127, 750.
- [14] G. S. Ofelt, *J. Chem. Phys.*, **1962**, 37, 511.
- [15] M. Mohapatra, R. K. Mishra, C. P. Kaushik and S. V. Godbole, *Physica B*, **2010**, 405, 4790.
- [16] M. Mohapatra, R. M. Kadam, R. K. Mishra, C. P. Kaushik, B. S. Tomar and S. V. Godbole, *Physica B*, **2011**, 406, 3980-3984.
- [17] C. K. Jorgensen and R. Reisfeld, *J. Less-Common Met.*, 1983, 93, 107.



Dr. Manoj Mohapatra did his M.Sc. (Inorganic Chemistry) from Utkal University, Bhubaneswar and joined the 46th batch of BARC Training School in Chemistry Discipline. Later he joined Radiochemistry Division of BARC in 2003. His main areas of research are solid state spectroscopic studies using Luminescence and Magnetic Resonance techniques and chemical quality control of nuclear materials. He is the recipient of outstanding Radiochemist award for the year 2010; "DAE Group Achievement Award" for the year 2012 and "DAE-Young Scientist Award" for the year 2014. Till date he has authored 60 journal papers and 2 book chapters which have resulted in about 800 citations.

Tailoring light-matter Interactions Using 3D Photonic Crystals

Rajesh V. Nair

Laboratory for Nano-scale Optics and Meta-materials (LaNOM), Department of Physics, Indian Institute of Technology Ropar, 140 001 India

E-mail: rvnair@iitrpr.ac.in

Controlling and manipulating the spontaneous emission of light sources embedded in nanophotonic structures is a contemporary topic of research due its potential applications in photonics. Photonic band gap structures constitute a class of meta-materials characterized with a periodically altered refractive index along three orthogonal directions [1]. They exhibit photonic stop gaps or even band gap for light wherein the photon density of states vanishes for a range of frequencies irrespective of the directions and polarizations of the incident light.

It is a challenging task to synthesize and measure photonic band gap due to stringent constraints set by the refractive index contrast and crystal symmetry. The most appealing structure is silicon photonic crystals with diamondlike symmetry [2]. It is very difficult to synthesize diamondlike photonic crystals. On the other extreme, low refractive index self-assembled structures with face centered cubic (*fcc*) symmetry is proposed as an alternative candidate for controlling the light emission. Such self-assembled photonic crystals which exhibit only *photonic stop gaps* wherein the light propagation is forbidden only in selected propagation direction.

1. Experimental Details

We use commercially available Polystyrene (PS) and Rhodamine B dye doped PS spheres of sub-micron diameter for the synthesis of photonic crystals. Large area ($\sim 2 \text{ cm}^2$) photonic crystals are synthesized using self-assembling method [3]. This diameter of Rhodamine PS spheres is specifically chosen so as to overlap the Rhodamine B dye emission. We also synthesized a control sample using same dye doped PS spheres of diameter 617 nm. The Rhodamine B dye emission does not overlap with the [111] photonic stop gap for this sphere diameter. Thus, the control sample has the same photonic structure, same packing fraction and the same dye embedded, the only difference being in the stop gap wavelength.

The structural quality of the photonic crystals is investigated using the field emission scanning electron microscope. The stop gap is measured from the reflectivity and transmittance spectra using a PerkinElmer Lambda 950 spectrophotometer. The light source used is a Halogen lamp with beam dimensions of 5 mm \times 5 mm, the light beam being unpolarized. Laser induced emission studies are performed using a frequency-doubled Nd: YAG laser as a pumping source at a wavelength of 532 nm and pulse duration of 6 ns. The light is focused on the sample using a lens of focal length 300 mm

to an illumination spot of ~ 1 mm. The emitted light is focused onto the input slit of a monochromator and detected with a charge coupled device (CCD).

2. Results and Analysis

Field emission scanning electron microscope image of the photonic crystals is given in Fig. 1(a). The well-ordering of spheres on the surface of the crystal is evident. This image represents the (111) plane of the face centered cubic (*fcc*) lattice. We have also measured impressive optical properties exhibited by our 3D photonic crystals in the visible and near-infrared wavelength ranges. Angle-resolved reflectance spectroscopy indicates the coupling between photonic stop gaps originating from different crystalline planes. Through angle-resolved stop gap measurements, well-resolved multiple Bragg peaks with equal diffracted intensity at certain conditions of the incident wave vector is observed; as seen in Fig. 1(b). The Bragg wave coupling regime is extended over more than 18° in the present work. We compare our experimental measurements with dispersion curves at the *K* or *U* points of the *fcc* Brillouin zone and assign the new stop gap, in the coupling regime, to the (-111) crystalline plane [4]. We will also discuss the polarization induced stop gap branching in self-assembled 3D photonic crystals. Our studies on the non-trivial nature of polarization coupling to photonic crystals provide new insight in the light-matter interactions in 3D photonic crystals.

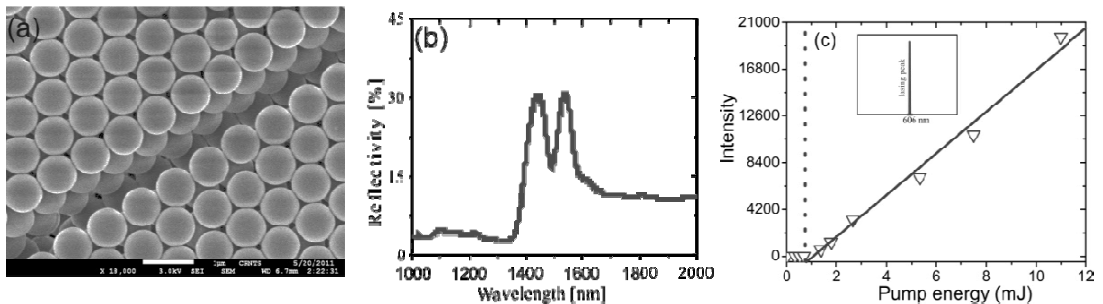


Fig. 1. (a) The microscope image of the self-assembled photonic crystal with impressive ordering on the surface and in the depth. The image indicate the (111) plane of the *fcc* lattice. (b) The stop gap measured at 56° indicates Bragg wave coupling regime with two Bragg peaks with equal intensity and width. (c) The threshold curve suggests the crossover from spontaneous to stimulated emission at 0.7 mJ. The inset shows the emission spectrum above the threshold value.

The laser-induced emission experiments are performed on self-assembled photonic crystals consisting of Rhodamine B dye doped PS spheres. In our crystals the gain medium is attached with every building block of the unit cell, thus avoiding the post-infiltration of the gain medium. We have measured the suppression of spontaneous emission intensity within the stop gap and enhancement in a range of frequencies near the blue side of the stop gap. This is due to the re-distribution of photon density of states. The attenuation in emission intensity at the stop gap is quantified by $\Delta I/I_0$ and is

estimated to be 51%. We have observed the emission intensity is higher near the blue side of the stop gap. This shows more photons are emitted in the blue side when the emission is inhibited within the stop gap. This excess emission is attributed to diffuse scattering of emitted photons in the crystal and can be explained using escape function for the emitted photons [5]. At higher excitation energy, we observe low-frequency photonic-band-edge-induced lasing at a threshold of 0.7 mJ. . The threshold curve is depicted in Fig. 1(c) for the lasing peak at 606 nm. A clear threshold at 0.7 mJ is observed wherein the stimulated emission overcomes the spontaneous emission. The inset shows the emission intensity above threshold. We explain the origin of band-edge lasing is due to the enhancement of density of states and light field distribution at the band edge frequencies [6].

3. Conclusions

We have studied the structural and optical characteristics of 3D ordered self-assembled photonic crystals in the visible and near-IR wavelength ranges. The phenomenon of Bragg wave coupling is discussed through angle-resolved measurements of stop gaps. We have also discussed the laser-induced emission studies on all-solid photonic crystals consisting of Rhodamine B dye doped PS spheres. Inhibition in emission intensity at the stop gap wavelength region is observed. At higher excitation energies, we have demonstrated the signature of band-edge-induced lasing characteristics. The origin of lasing is explained as due to the enhanced density of photon states and field distribution at the band edge frequencies.

References

- [1] E. Yablonovitch, *Phys. Rev. Lett.*, 1987, 58, 2059-2062.
- [2] S. R. Huisman, R. V. Nair, L. A. Woldering, M. D. Leistikow, A. P. Mosk, and W. L. Vos, *Phys. Rev. B*, **2011**, 83, 205313-1-7.
- [3] C. Lopez, *Adv. Mat.*, **2003**, 15, 1679-1704.
- [4] R. V. Nair and B. N. Jagatap, *Phys. Rev. A*, **2012**, 85, 013829-1-10.
- [5] I. S. Nikolaev, P. Lodahl, and W. L. Vos, *Phys. Rev. A*, **2005**, 71, 053813-1-10.
- [6] R. V. Nair, A. K Tiwari, S. Mujumdar, and B. N. Jagatap, *Phys. Rev. A*, **2012**, 85, 023844-1-7.



Dr. Rajesh V. Nair

PhD (Indian Institute of Technology, Mumbai)

Research Interests: Light-matter interactions in nano-scale structures, meta-materials, photonic micro-cavities, light sensitive materials

Biography:

Dr. Nair has earned his PhD degree from Indian Institute of Technology (IIT), Mumbai in 2008. He carried out his post-doctoral research during the period 2008-2010 in Complex Photonic Systems (COPS), University of Twente, The Netherlands. He worked as Dr. K. S. Krishnan Research Fellow in Bhabha Atomic Research Centre, Mumbai for the period 2010-2012 and later as Scientific Officer D till 2013. Starting November 2013, Dr. Nair has joined as Assistant Professor in the Department of Physics at IIT Ropar Punjab. He has made notable contributions in the field of nano-optics such as the observation of sub-Bragg diffraction of waves in crystals, the first-ever signature of three-dimensional photonic band gap, and lasing from nano-scale photonic structures. He has published his scientific findings in high-impact journals and is highlighted in international scientific magazines.

Awards and Honors:

- *Indian National Science Academy (INSA) young scientist prize in Physical Sciences for the year 2015.*
- *Member, National Academy of Sciences in India (2015-onwards)*
- *Treasurer, Photonic Detection Technical Group of Optical Society of America (OSA)*
- *National Academy of Sciences in India (NASI)-Young Scientist Platinum Jubilee Award in Physical Sciences for the year 2012.*
- *Young Scientist Award in Physical Sciences from Indian Science Congress Association (ISCA) for the year 2011-2012.*

List of Publications: > 21 Journal publications in the area of nanophotonics (includes Physical Review Letters)

Thermoluminescent Materials

N. S. Rawat and D. R. Mishra

Radiological Physics and Advisory Division, Bhabha Atomic Research Center, Mumbai
E-mail: naru@barc.gov.in

1. Introduction

Thermoluminescence (TL) is the emission of light from an insulator or semiconductor when it is heated. This is not to be confused with the light spontaneously emitted from a substance when it is heated to incandescence. At higher temperatures (say in excess of 200°C) a solid emits (infra) red radiation of which the intensity increases with increasing temperature. This is thermal or black body radiation. TL is the thermally stimulated emission of light following the previous absorption of energy from radiation.

There are three essential ingredients necessary for the production of TL. Firstly, the material must be an insulator or a semiconductor as metals do not exhibit luminescent properties. Secondly, the material must have at some time absorbed energy during exposure to ionizing radiation. Thirdly, the luminescence emission is triggered by heating the material. Thus heating releases the stored energy in the form of visible light when the material is heated. Note that TL does not refer to thermal excitation, but to stimulation of luminescence in a sample which was excited in a different way. This means that a TL material cannot emit light again by simply cooling the sample and reheating it another time. The storage capacity of a TL material makes it in principle suitable for dosimetric applications.

TL as an experimental technique finds favour in such diverse scientific disciplines as archaeology, geology, medicine, solid state physics, biology and organic chemistry, nuclear forensics to name just some of the mainstream areas of study. This phenomenon has been known since early times: the first to observe and report it was Sir Robert Boyle, 346 years ago, and was in the 1950's when this technique was first proposed as a dosimetry tool. TL was also reported by Marie Curie in her doctoral thesis (Curie, 1904). The phenomena of TL can be observed in a great variety of materials, and it has been applied to different disciplines: radiation protection of workers exposed to ionizing radiation, radiation protection of patients in medicine, environmental monitoring, archaeological and geological dating, and verification of antiquities, retrospective dosimetry, or food irradiation dosimetry.

The aforementioned successful applications of TL dosimetry stemmed from the search, development, and analysis of properties of materials, which were used in TL detectors of ionizing radiations. Some desirable attributes of TL material as illustrated by McKeever in 1995 are i) wide dynamic dose range for which the luminescence intensity is linear with absorbed dose. ii) High sensitivity (a high TL signal per unit absorbed dose) is important for use in personal and medical dosimetry, as well as in environmental radiation monitoring. iii) Effective atomic number (Z_{eff}) should be close or equivalent to

that of tissue (7.4) as it implies low dependence of the TL response on the energy of the incident radiation that mimics with biological effects on tissue. However, for non tissue equivalent material, the energy dependence can be partially compensated by metallic filters. iv) Low fading, i.e., the ability to store dosimetric information for a long time. v) Simple TL curve (with one isolated peak). If several peaks are present, the dosimeter heating protocol is complicated. vi) Luminescence spectrum should match the maximum spectral sensitivity of the photomultiplier. vii) The TL dosimetric material should be mechanically strong, chemically inert, and radiation resistant.

Generally, all these requirements should be fulfilled in a high quality TL dosimeter. As is often the case, not all requirements can be fulfilled, especially the condition of small fading. This report presents a brief overview of the properties of TL dosimetric materials. More detailed information can be found in the cited reviews and books. The main emphasis is on new trends in the research and use of these materials.

2. Basic concepts of thermoluminescence

It is believed that the impurities in the TL material give rise to localised energy levels within the forbidden energy band gap and that these are crucial to the TL process. TL is used as a means of detecting the presence of these defect levels. Townsend and Kelly estimate that the technique is capable of detecting as few as 10^9 defects levels in a specimen. To put this number into perspective one should realize that detectable chemical 'purity' in a sample is six orders of magnitude higher. The high sensitivity, on the one hand, allows the determination of very low radiation doses. On the other hand, it hampers us in investigation into the relation between the luminescence and the defects involved in this process. It also causes the TL properties to be highly sensitive to many parameters.

2.1. The one trap-one centre model

An explanation of the observed TL properties can be obtained from the energy band theory of solids. In an ideal crystalline semiconductor or insulator most of the electrons reside in the valence band. The next highest band that the electrons can occupy is the conduction band, separated from the valence band by the so-called forbidden band gap. The energy difference between the delocalised bands is E_g . However, whenever structural defects occur in a crystal, or if there are impurities within the lattice, there is a possibility for electrons to possess energies which are forbidden in the perfect crystal. In a simple TL model two levels are assumed, one situated below the bottom of the conduction band and the other situated above the top of the valence band (see Fig. 1). The highest level indicated by T is situated above the equilibrium Fermi level (E_f) and thus empty in the equilibrium state, i.e. before the exposure to radiation and the creation of electrons and holes. It is therefore a potential electron trap. The other level (indicated by R) is a potential hole trap and can function as a recombination centre. The absorption of radiant energy with $h\nu > E_g$ results in ionization of valence electrons, producing energetic electrons and holes which will, after thermalization, produce free electrons in the conduction band

and free holes in the valence band (transition a). The free charge carriers recombine with each other or become trapped. In the case of direct recombination an amount of energy will be released which may excite a luminescent centre (which may coincide with the recombination centre). The luminescent centre relaxes (returns to the ground state) under the emission of light. The phenomenon of direct ($<10^{-8}$ s) recombination of free electrons and holes under emission of light is called radioluminescence. However, in semiconductors and insulators a certain percentage of the charge carriers is trapped: the electrons at T and the holes at R (transition b). The probability per unit time of release of an electron from the trap is assumed to be described by the Arrhenius equation,

$$p = s \exp\left(-\frac{E}{kT}\right) \quad \dots(1)$$

where p is the probability per unit time. The term 's' is called the frequency factor or attempt-to-escape factor. In the simple model s is considered as a constant (not temperature dependent) with a value in the order of the lattice vibration frequency ($\sim 10^{12} - 10^{14} \text{ s}^{-1}$). E is called the trap depth or activation energy, the energy needed to release an electron

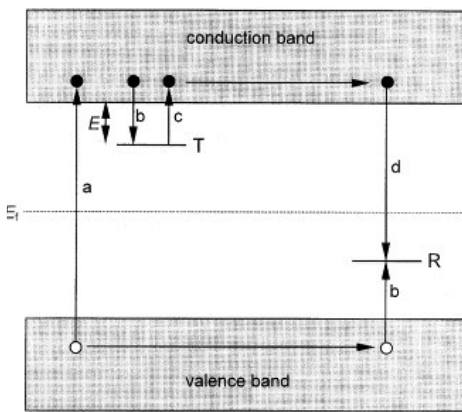


Fig. 1. Energy band model showing the electronic transitions in a TL material (a) generation of electrons and holes; (b) electron and hole trapping; (c) electron release due to thermal stimulation; (d) recombination. Solid circles are electrons, open circles are holes. Level T is a electron trap, level R is a recombination centre, E_f is Fermi level.

from the trap into the conduction band (Fig. 1). The other symbols have their usual meaning: k =Boltzmann's constant= 8.617×10^{-5} eV/K, and T the absolute temperature. If the trap depth $E \gg kT_0$, with T_0 the temperature at irradiation, then any electron that becomes trapped will remain so for a long period of time, so that even after radiation exposure there exists a substantial population of trapped electrons. Furthermore, because the free electrons and holes are created and annihilated in pairs, there must be an equal population of trapped holes at level R. Because the normal equilibrium Fermi level E_f is situated below level T and above level R, these populations of trapped electrons and holes represent a non-equilibrium state. The reaction path for return to equilibrium is always open, but because the perturbation from equilibrium (during exposure to ionizing radiation) was performed at low temperature (compared to E/k), the relaxation rate as determined by Eq. (1) is slow. Thus, the non-equilibrium state is metastable

and will exist for an indefinite period, governed by the rate parameters E and s.

The return to equilibrium can be speeded up by raising the temperature of the TL material above T_0 . This will increase the probability of detrapping and the electrons will now be released from the trap into the conduction band. The charge carrier migrates through the conduction band of the crystal until it undergoes recombination at recombination

centre R. In the simple model this recombination centre is a luminescent centre where the recombination of the electron and hole leaves the centre in one of the higher excited states. Return to the ground state is coupled with the emission of light quanta, i.e. TL. The intensity of TL, $I(t)$ in photons per second at any time t during heating is proportional to the rate of recombination of holes and electrons at R. If m (m^{-3}) is the concentration of holes trapped at R the TL intensity can be written as

$$I(t) = -\frac{dm}{dt} \quad (2)$$

Here we assume that each recombination produces a photon and that all produced photons are detected. The rate of recombination will be proportional to the concentration of free electrons in the conduction band n_c and the concentration of holes m ,

$$I(t) = -\frac{dm}{dt} = n_c mA \quad (3a)$$

Where A is the probability of recombination in volume per unit time and is assumed to be temperature independent. The rate of change of the concentration of trapped electrons n is equal to the rate of thermal release minus the rate of retrapping,

$$-\frac{dn}{dt} = np - n_c(N - n)A_r \quad (3b)$$

Where, N is concentration of electron traps and A_r the probability of retrapping (m^3/s). Similarly the rate concentration of free electrons is expressed as

$$-\frac{dn_c}{dt} = np - n_c(N - n)A_r - n_c mA \quad (3c)$$

Equations (3a)- (3c) described the charge carrier traffic in the case of release of a trapped electron from a single-electron trap and recombination in a single centre. For TL produced by the release of holes the rate equations are similar to equations (3a) - (3c). These equations form the basis of many analyses of TL phenomena. There is no general analytical solution. To develop an analytical expression some simplifying assumptions must be made. An important assumption is that at any time

$$\left| \frac{dn_c}{dt} \right| \ll \left| \frac{dn}{dt} \right|, \left| \frac{dn_c}{dt} \right| \ll \left| \frac{dm}{dt} \right| \quad (4)$$

This is referred as quasiequilibrium assumption (ref.) since it

requires that the free electron concentration in the conduction band is quasistationary. The trapped electrons and holes are produced in pairs during the irradiation. Charge neutrality therefore demands

$$n_c + n = m, \text{ which for } n_c \approx 0 \text{ means that } n \approx m \text{ and } I(t) = -\frac{dm}{dt} \approx -\frac{dn}{dt}$$

Also since $\frac{dn_c}{dt} \approx 0$ we obtain

$$I(t) = \frac{m A n s \exp\left\{-\frac{E}{kT}\right\}}{(N-n)A_r + mA} \quad (5)$$

2.2 First Order Kinetics

Equation (5) cannot be solved analytically without additional simplifying assumptions.

Randall and Wilkins {reference} assumed negligible retrapping (first order kinetic) during the heating stage, i.e. they assumed $mA \gg (N-n)A_r$. Under this assumption Eq. (5) can be written as

$$I(t) = -\frac{dn}{dt} = sn \exp\left\{-\frac{E}{kT}\right\} \quad (6)$$

This equation describes the charge transport in the lattice as a first order process and the TL glow peaks calculated from this equation are called as first-order glow peaks. The solution of above equation for a linear heating rate $T(t) = T_0 + \beta t$ (with β constant heating rate and T_0 the temperature at $t=0$) yields

$$I(T) = -\frac{dn}{dt} = n_0 s \exp\left\{-\frac{E}{kT}\right\} \exp\left\{-\frac{s}{\beta} \int_{T_0}^T \exp\left(\frac{E}{kT'}\right) dT'\right\} \quad (7)$$

It is a well known Randall-Wilkins first-order expression of a single glow peak. The peak has a characteristic asymmetric shape being wider on the low temperature side than on the high temperature side. On the low temperature side, i.e. in the initial rise of the glow peak, the intensity is dominated by the first exponential ($\exp(-E/kT)$). Thus, if I is plotted as function of $1/T$, a straight line is expected in the initial rise temperature range, with the slope of $-E/k$, from which the activation energy E is readily found. The behavior of first order TL glow peak as represented by equations (6) or (7) is simulated and shown in Fig. 2.

2.3 General Order Kinetics

The rate equation for second order TL Kinetics, i.e. $b = 2$ was proposed by Garlik and Gibson and is given by

$$I_{TL} = -\frac{dn}{dt} = \frac{n^2}{N} s \exp(-E/kT) \quad (8)$$

The solution of (8) yields

$$I(T) = n_0^2 \frac{s}{N} \exp\left(-\frac{E}{kT}\right) \left[1 + \frac{n_0 s}{\beta N} \int_{T_0}^T \exp\left(-\frac{E}{kT'}\right) dT'\right]^{-2} \quad (9)$$

Similarly May-Partidge suggested the following TL equations for general order kinetic

$$I_{TL} = -\frac{dn}{dt} = \frac{n^b}{N^{b-1}} s \exp(-E/kT) \quad (10)$$

The solution of which yields

$$I(T) = \frac{n_0^b}{N^{b-1}} s \exp\left(-\frac{E}{kT}\right) \left[1 + \frac{s(b-1)(n_0/N)^{(b-1)}}{\beta} \int_{T_0}^T \exp\left(-\frac{E}{kT'}\right) dT'\right]^{-\frac{b}{b-1}} \quad (11)$$

Fig. 3 shows effect of order of kinetics on the shape of TL glow curve.

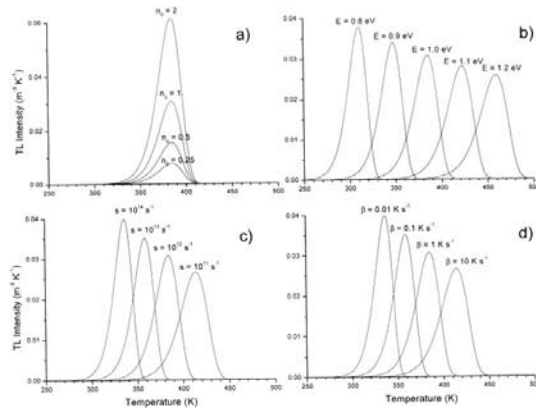


Fig. 2. Properties of the R-W first-order TL equation, showing: (a) variation with n_0 , the concentration of trapped charge carriers after irradiation; (b) the variation with E , the activation energy; (c) the variation with s , the escape frequency; (d) the variation with β , the heating rate. Parameter values chosen are $n_0 = 1 \text{ m}^{-3}$; $E = 1 \text{ eV}$; $s = 10^{12} \text{ s}^{-1}$, $\beta = 1 \text{ K/s}$ of which one parameter is varied while the others are kept constant.

3. Widely practiced Phosphors in TL dosimetry

Table 1 enlists important characteristics of certain materials that are frequently encountered in TL dosimetry including $\text{Al}_2\text{O}_3:\text{C}$. The information furnished in this table amply endorses the reputation of TL as a popular mode of readout which stems from its celebrated capability of detection of very low levels of radiation which in turn is intimately linked to the presence of defects and arises from the extremely efficient detection of the luminescence signal emitted by these defects by photomultiplier tubes.

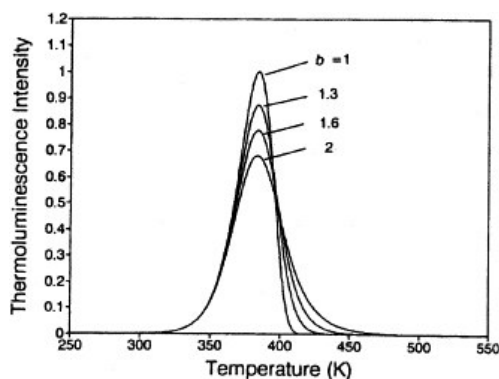


Fig. 3. Comparison of first-order ($b=1$), second-order ($b=2$) and intermediate-order ($b=1.3$ and 1.6) TL peaks, with $E=1$ eV, $s = 10^{12}$ s⁻¹, $n_0 = N = n = 1\text{m}^{-3}$ and $\beta = 1\text{K/s}$.

Table 1. General Characteristics of Some Commercially Available TLDs

TLD type	Effective atomic no. (Z_{eff})	Main TL peak (°C)	Emission max. (nm)	Relative sensitivity	Fading ^b (at 25 °C)	Dose range
LiF:Ti,Mg (TLD-100)	8.2	200	400	1	5%/year	10 μGy -10 Gy
LiF:Mg,Cu,P (TLD-100H)	8.2	210	400	25	5%/year	0.2 μGy -10 Gy
$\text{Li}_2\text{B}_4\text{O}_7:\text{Mn}$	7.4	220	605	0.20	4%/month	0.1 mGy-3 Gy
$\text{Li}_2\text{B}_4\text{O}_7:\text{Cu}$	7.4	205	368	2	10%/2 months	10 μGy - 10^3 Gy
$\text{MgB}_4\text{O}_7:\text{Dy}$	8.4	190	490	10	4%/month	5 μGy -50 Gy
BeO	7.1	190	200-400	0.20	8%/2 months	0.1 mGy-0.5 Gy
$\text{Mg}_2\text{SiO}_4:\text{Tb}$	11	200	380-400	40	very slight	10 μGy -1 Gy
$\text{CaSO}_4:\text{Dy}$	15.3	220	480-570	30	1%/2 months	2 μGy -10 Gy
$\text{CaSO}_4:\text{Tm}$	15.3	220	452	30	2%/2 months	2 μGy -10 Gy
$\text{CaF}_2:\text{Mn}$ (TLD-400)	16.3	260	500	5	16%/2 weeks	10 μGy -10 Gy

Natural CaF ₂	16.3	260	380	23	very slight	10 μGy-50 Gy
CaF ₂ :Dy (TLD-200)	16.3	215	480-570	15	8%/2 months	10 μGy-10 Gy
Al ₂ O ₃ :C (TLD-500)	10.2	190	420	60	3%/year	0.1 μGy-10 Gy

^c Heating rate 4 °C/s, ^b Fading in the dark

Commercial TL dosimeters have been designed using LiF, CaF₂ and Al₂O₃. Historically, the first basic TL material is LiF:Ti, Mg (TLD-100), whose properties are still extensively studied. Interest in this material arises from its tissue equivalence ($Z_{\text{eff}} = 8.04$), which is an important factor for personal dosimetry.

Table 1 shows that dosimeters with a greater sensitivity (LiF:Mg, Cu, P) and a high sensitivity (CaF₂:Dy, CaF₂:Mn, Al₂O₃:C) may be distinguished with respect to the basic TLD-100 dosimeter. The majority of the commercial TL dosimeters have small fading (not over 5% annually), except CaF₂ dosimeters whose monthly fading may be as high as 25%. Spectra of commercial luminescent dosimeters exhibit an emission maximum at 380–480 nm, which corresponds to the spectral range of common photomultipliers. The dosimetric luminescence peak is maximum at 180–260 °C, making it easy to read. It is also possible to design LiF-based dosimeters sensitive to neutrons by enriching them in the ⁶Li isotope.

From the simple band model of luminescence, it follows that fading is small if the electron traps, which produce luminescence excitation centers, have sufficiently large activation energy or trap depth. The temperature of glow peak maximum (180–260 °C) corresponds to the relatively deep centers (0.9–1.3 eV). So, the requirement of small fading leads us to look for TL dosimetric materials among wide band gap dielectrics.

The requirement to detect small doses makes it necessary to evaluate the intrinsic efficiency of TL materials. The intrinsic efficiency η_i characterizes the conversion of energy absorbed under irradiation to visible light. Ultimately, it determines the luminescence yield Y , i.e., the number of photons emitted after exposure to irradiation.

The intrinsic efficiency η_i is defined as the product of the efficiency factors for the individual processes. Recombination of some charge carriers is non-radiative. The experimental determination of η_i and Y is a complex problem involving careful calculations of emitted quanta and the absorbed dose. The intrinsic efficiency η_i changes from $1.7 \times 10^{-2}\%$ in LiF:Mg, Ti to $84 \times 10^{-2}\%$ in Al₂O₃:C.

It is necessary to analyze the mechanisms responsible for the high light yield in sensitive TL materials. Without going into details, it suffices to mention that the anion lattice of many efficient materials of TL dosimetry contains defects, which produce F-centers. The role of the F-centers in the optical and luminescence properties of halides of alkali

and alkali-earth metals has been discussed extensively in the literature, including their role in dosimetric materials. Carbon doped aluminum oxide was ranked as the most sensitive material in TL dosimetry that was developed initially by the Urals Polytechnical Institute, Russia. The extreme sensitivity of the material to radiation made this material very attractive for use as a radiation dosimeter. The high sensitivity is due to the creation of a large concentration of oxygen vacancy centers in the material during the crystal growth process. The oxygen vacancy centers (F- and F⁺ - centers) act as a recombination sites yielding a bright emission. The trapping sites are not known. A potential difficulty with the material was its sensitivity to visible light, giving rise to light-induced fading of the TL signal. By taking advantage of this apparent disadvantage, however, the material could be made into an efficient OSL dosimeter by using light rather than heat to stimulate the radiation induced luminescence signal. Since then, Al₂O₃:C has gone on to become the foremost OSL dosimetry material, seeing use in a multitude of dosimetry applications.

4. Current trends in research and application of TL materials

Well-established and new materials for TL dosimetry are extensively studied by means of optical absorption, luminescent spectroscopy, electron paramagnetic resonance, and others in combination with Monte-Carlo calculations and computer-aided deconvolution of glow curves. This is accompanied by analysis of various regular features related to preparation of samples, including selection of optimal concentrations of dopants.

The search for materials with a high TL yield is ongoing. Studies into the TL properties of the AlN ceramic, which represents a new class of compounds, are of relevance. At equal doses, the TL yield of this ceramic is dozens of times larger than the TL yield of the most sensitive Al₂O₃:C dosimeter. However, so far, an extremely high fading prevents the development of AlN-based dosimeters suitable for practical applications.

Unfortunately, a brief review cannot cover the entire wide range of TL materials whose properties are relevant for dosimetry. The efficient X-ray phosphors BaFBr:Eu³⁺; RbBr:Eu³⁺ are available and the wide-gap oxides SiO₂:Cu; BeO:Li have interesting TL properties as well. However, it is not always possible to evaluate the applicability of materials for TL dosimetry because TL properties (spectrum, shape of the glow curve) are often described omitting information about fading, energy response, and dose dependence of the TL yield.

TL materials have been traditionally used for the detection of X-ray, gamma and beta radiations. In recent years, the dosimetric properties of these materials have been studied extensively with respect to measurements of high-energy particles (alpha particles, protons, charged ions, and fast neutrons). The interest in these properties is explained by the advancement of space research and the use of beams of charged particles in medicine. In this connection, characteristics of TL materials such as the linear energy transfer (LET) response, which characterizes the stopping power of materials to high-energy particles, is gaining in importance. The TL yield of materials decreases considerably with increasing LET during detection of high-energy particles.

Attempts to use commercial TL dosimeters for detection of fast neutron fluxes have been less successful. The TL yield of LiF:Ti,Mg; LiF:Mg,Cu,P and $\text{Al}_2\text{O}_3\text{:C}$ proved to be very low. The relative neutron sensitivity (neutron: gamma) is less than 0.03 at neutron energies of 0.3–3 MeV and grows slowly as the neutron energy increases. A promising method proposed by Milman for the development of dosimeters of mixed $\gamma + n$ field envisages the use of (n, γ) converters. Materials that contain Li or simultaneously Li and B are most sensitive to neutrons. They include, for example, $\text{Li}_2\text{B}_4\text{O}_7\text{:Mn}$ (TLD-800). If these materials are enriched in ^6Li and ^{10}B isotopes, they become sensitive to thermal neutrons (due to $^6\text{Li}(n,\alpha)^3\text{H}$ reaction with a cross-section 940 barn and $^{10}\text{B}(n,\alpha)^7\text{Li}$ with cross section 3400 barn). If the detector material is enriched with the aforementioned isotopes, it may prove to be an efficient dosimeter for mixed $(\gamma+n)$ fields. In this case, fast neutrons are thermalized by the use of hydrogenous materials (polyethylene, teflon, etc.). The dosimetry of mixed $(\gamma+n)$ fields is important at nuclear power plants.

Finally, it is appropriate to point out some opportunities arising in connection with the use of nano sized materials in TL dosimetry. The processes which determine the efficiency of the energy transfer to emission centers and the radiation efficiency are expected to change in nano-crystalline dielectrics. The TL yield and spectrum in nano-crystalline materials are largely affected by their preparation conditions, especially their thermal treatment regime.

5. Conclusions

Thermoluminescence based dosimetry has come to a long way since a glimmering light was first observed by Sir Robert Boyle, and the curious after-glow quenching phenomena observed by Becquerel. Modern applications of TL/OSL are at the forefront of the challenges within dosimetry, namely the dosimetry of energetic-charged particles in space, and the complex, rapidly varying (both in time and location) radiation fields experienced during modern radiotherapy and radio-diagnosis. The overall intent of this short review has been to highlight the need for an understanding, as much as possible, of the TL production mechanisms in potential TLD materials. It was shown how TL dosimetric materials can be used for the detection of mixed fields containing high-energy charged particles and for the monitoring of $(\gamma + n)$ fields. The conceptual possibility of using TL detectors in high-temperature dosimetry has been verified. Studies of basic processes and mechanisms are as important today as they were at the birth of luminescence dosimetry. New applications will undoubtedly follow the accumulation of this fundamental knowledge.

References:

- [1] M.S. Akselrod, V. S. Kortov, D. J. Kravetsky, V. I. Gotlib. *Radiat. Prot. Dosim.*, **1990**, 32, 15-20.
- [2] J. Azorin, C. Furreta, A. Scaco, *Phys. Status Solidi A*, **1993**, 138, 9-46.
- [3] G. A. Klemic, N. Azziz, S. A. Marino, *Radiat. Prot. Dosim.*, **1996**, 65, 221-226.
- [4] B. Meijvogel, B. van der Burg, A. J. J. Bos. *Radiat. Prot. Dosim.*, **1996**, 65, 117-122.

- [5] A. J. J. Bos, *High sensitivity thermoluminescence dosimetry*, **2001**, 184, 3–28.
- [6] S. W. S. Mckeever, *Thermoluminescence of solids*. Cambridge University Press, **1985**.
- [7] M. Martini, F. Meinardi, L. Kovacs, K. Polgar, *Radiat. Prot. Dosim.*, **1996**, 65, 343-346.



Dr. N. S. Rawat is from 48th batch of BARC training school and joined Radiological Physics and Advisory Division of BARC in 2005. Dr. Rawat is working in the field of solid state luminescence dosimetry and has contributed towards the development of ultra sensitive TL/OSL phosphors for various applications. His research work also involves formulation of thermoluminescence (TL) and optically stimulated luminescence (OSL) based advanced techniques to analyze dosimetric performance of various phosphors.

Optically Stimulated Luminescent Materials

M. S. Kulkarni

*Radiation Safety Systems Division, Bhabha Atomic Research Centre, Mumbai 400085,
E-mail: kmukund@barc.gov.in*

Abstract:

During the last two decades optically stimulated luminescence (OSL) technique has become more popular as an alternative option to the conventional thermoluminescence (TL) in the field of passive radiation dosimetry. The principal of OSL technique is to stimulate an X-ray / gamma-ray / beta irradiated sample with light of selected wavelength and to monitor the emission from the sample at a different wavelength. This optical readout process in OSL method does not involve problems of blackbody radiation and thermal quenching that are faced by the TLDs. OSL has many other advantages over the TLD based dosimetry system like fast and multiple readouts, ease in dose estimation and flexibility offered by multitude of possible stimulation protocols. Due to these advantages, OSL is also being used for various applications in radiation dosimetry, such as personnel and environmental monitoring, retrospective / accident dosimetry, medical and space dosimetry, etc.

In addition to high sensitivity to ionizing radiation and negligible post irradiation fading of signal, the OSL phosphor material must have attribute like high concentration of defects (trap and recombination centers), long storage time of trapped carriers at room temperature (fading), stability of traps to radiation (i.e. radiation should not create new trap centers or destroy them), high luminescence efficiency, high photoionization cross section, tissue equivalent atomic number, and stability against environmental conditions (like temperature, humidity).

Both natural and synthetic materials are known to possess OSL response. Natural materials like quartz, feldspar, flint, and unseparated geological materials have shown to possess OSL properties. The OSL sensitivity of quartz (stimulation wavelength band 420-570nm) depends upon the thermal history of the material with annealed samples having an order of magnitude larger signal than unheated samples. In the initial studies of quartz, the use of green light (514.5 nm) from an argon laser operated in CW mode demonstrated that the energy of visible light is sufficient to empty the OSL electron traps directly in this material. Feldspar has wider dose response than quartz. It has complex stimulation spectrum and generally stimulation is in the near infrared region. K-rich feldspar and flint suffer from long term instability, certain feldspars have anomalous fading. Flint has dose-dependent OSL signal for crystalline quartz phase and dose-independent response for amorphous phase. The depth dose profiles in the unseparated material across a brick can be found out by measuring the OSL signals for its use in the retrospective accident dosimetry.

In the early years of discovery of the OSL technique, the popularity of the OSL technique was limited due to limited availability of OSL phosphor materials. OSL investigations on highly sensitive phosphors which are currently used in TL dosimetry like LiF:Mg,Ti, LiF:Mg,Cu,P, CaF₂:Mn, CaSO₄:Dy etc. for different excitation wavelengths revealed a very weak OSL signal which could not compete with their TL signal. However, a lot of developments have taken place during the last two decades and a large number of highly sensitive synthetic OSL phosphor materials are now available for various dosimetric applications as well as basic research. As a result of these recent developments, worldwide there is a paradigm shift in personnel and environmental monitoring from TL based systems to OSL based systems.

Several oxides, sulphides, phosphates, halides, fluoro-silicate based OSL phosphors have been successfully synthesized using different techniques and investigated for their OSL response. Among the oxides, Al₂O₃ was one of the earlier materials studied for its possible application as a radiation dosimeter. Development of single crystal α -Al₂O₃:C by Urals Polytechnical Institute, Russia initially as TL material and later investigation of its suitability for personnel dosimetry using pulsed OSL (POSL) technique boosted the prospects of OSL technique for radiation dosimetry applications. α -Al₂O₃:C due to its ultra high sensitivity and desirable attributes like excellent thermo chemical stability and very low fading, has been widely accepted as reference OSL phosphor. Some of the useful OSL materials synthesised and studied by various researchers are BeO ceramic discs, MgO:Tb, Mg₂SiO₄:Tb, MgS, CaS, SrS and SrSe doped with different rare earth elements (like Ce, Sm, Eu), Al₂O₃:B, NaMgF₃:Eu, Li₂B₄O₇:Cu, LiMgPO₄:Tb,B, LiAlO₂:Cu, BaSO₄:Eu, CaSO₄:Eu, SrSO₄:Eu, LiF:Mg, Cu,P, LiAl₅O₈:Tb, SiO₂:Cu, YAG:C, Li₃PO₄:Cu, LiCaAlF₆:Eu and many more.

Electronic components of mobile phones like resistor, capacitor, display are also found to have shown good OSL response which has opened up a feasibility of dosimetry and dose reconstruction (using the internal components of electronic gadgets of everyday use) in the unforeseen event of radiological accidents.

A large number of techniques have been developed and applied for the synthesis of OSL phosphor materials. These include solid state synthesis, combustion synthesis, coprecipitation, solvent assisted synthesis, sono-chemical, sol-gel, hydro & solvothermal, microwave synthesis, metathesis, ion-exchange, high pressure synthesis, vacuum heat treatment, melt and quench technique, etc. All these techniques have their merits and demerits over one another and can be used based on the need and ease of synthesis of a given phosphor material. History of luminescence reveals that quite often the discovery of phosphor is an accident rather than design. In such cases applications precede the understanding contrary to the sequence of prediction, design and application.

Single crystals of technologically important materials can be grown by the conventional Czochralski growth method. For example α -Al₂O₃:C is grown in the reducing environment of carbon. Growing single crystals from melt is an involved and costly process. Soft chemical methods mentioned earlier are therefore popular techniques

for phosphor preparation. From the innocuous looking chemical formulae of OSL phosphors one fails to anticipate the difficulties in preparing the phosphors. In reality, phosphor synthesis is very tricky for the reason of presence of unintentional impurities. In BARC development of OSL phosphors started in 2002 onwards and a large number of sensitive OSL phosphors were developed during the last decade. Few to list are $\alpha\text{-Al}_2\text{O}_3\text{:C}$, $\text{Li}_2\text{B}_4\text{O}_7\text{:Cu,Ag}$, YAG:C , $\text{Al}_2\text{O}_3\text{:Si,Ti}$, $\text{LiMgPO}_4\text{:Tb,B}$, $\text{LiAlO}_2\text{:Mn/Ce/Tb}$, $\text{SiO}_2\text{:Ag}$, $\text{LiAl}_5\text{O}_8\text{:Tb}$, $\alpha\text{-Al}_2\text{O}_3\text{:B}$, M_2SiF_6 ($\text{M}=\text{Li,NaK}$), $\text{CaSO}_4\text{:Eu}$. Out of which $\alpha\text{-Al}_2\text{O}_3\text{:C}$ was prepared by three different methods owing to its importance as most promising material for applications in radiation dosimetry.

Understanding the basic luminescence mechanism in the OSL phosphor materials and the kinetics is very important from academic point of view. Therefore, beside the TL - OSL characteristics of these materials, several spectroscopic techniques like photoluminescence (PL), optical absorption (OA) and electron paramagnetic resonance (EPR), positron annihilation spectroscopy (PAS) and nuclear magnetic resonance (NMR) are used to understand the luminescence mechanisms in the given phosphor material. Significant advances have been made in the recent years to understand the material and improve their performance for OSL dosimetry. A brief review of the popular OSL phosphors, their characteristics and applications will be presented in the talk.



Dr. M.S.Kulkarni joined the Division of Radiological Protection after graduation from 31st batch of BARC Training School. Dr. Kulkarni has been working on the development of indigenous instruments and detectors for personnel monitoring of radiation workers. He received his Ph.D degree in Physics from Mumbai University in 2007 for his work on thermoluminescence (TL) and optically stimulated luminescence (OSL) reader systems and development of OSL phosphor materials. Dr. Kulkarni has over 100 publications in various national and international journals. Dr. Kulkarni is a Member of the International Solid State Dosimetry Organization (ISSDO) and Fellow, Maharashtra Academy of Sciences. He is a recognized Ph.D. guide of Homi Bhabha National Institute (HBNI). Dr. Kulkarni is presently Head, Radiation Radiation Standards Section of Radiation Safety Systems Division, BARC.

Lanthanide-doped Luminescent Nanocrystals: Synthesis, Properties and Applications

Venkataramanan Mahalingam

Indian Institute of Science Education and Research (IISER) Kolkata, Mohanpur, Nadia,
West Bengal 714246

E-mail: mvenkat@iiserkol.ac.in

Introduction

There is a growing research interests towards developing optical materials based on lanthanides.[1] This interest stems from their unique optical properties arising from the intra $4f-4f$ transitions which find ubiquitous applications such as in the development of laser crystals, phosphors for light emitting diodes (LEDs), authentication, probes for bio imaging, etc.[2] This lengthens their excited state lifetimes which are typically in the range of milli seconds to micro seconds. In addition, the intra $4f$ transitions are less influenced by the ligand environment as they are covered by outer $5s$ and $5p$ orbitals. [3] This led to sharp emission peaks possessing a full width at half maximum (FWHM) about 5 nm. By choosing appropriate lanthanide (Ln^{3+}) ions, one can get emissions over a wide spectral regions, say from ultraviolet to near infrared (NIR). The luminescence from the Ln^{3+} ions are typically Stokes shifted i.e. they energy of the emission is lower than the excitation energy. Most of the Ln^{3+} ions are excited in the near UV region (~ 300 to 400 nm) and the emission peaks cover almost the entire visible and some of the NIR regions.[4] Additionally, some Ln^{3+} ions like, Er^{3+} , Tm^{3+} and Ho^{3+} are able to convert low energy radiations (NIR) into high energy visible emissions. This nonlinear process is known as upconversion or anti-Stokes emission.[5] A schematic of the Stokes and anti-Stokes emissions are shown in Fig. 1. The upconversion process sometimes occurs through energy transfer via a sensitizer such as Yb^{3+} ions which possess high absorption coefficient compared to other Ln^{3+} ions and having one excited energy level matches with Er^{3+} , Tm^{3+} and Ho^{3+} ions.

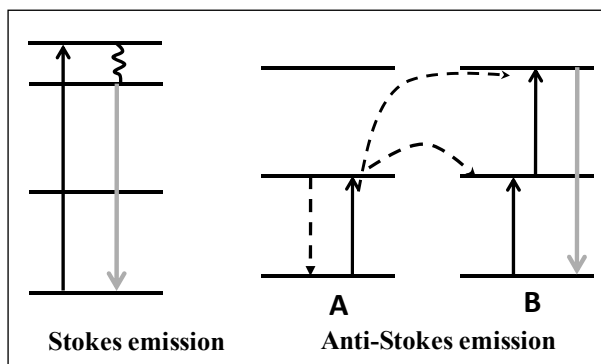


Fig. 1. Schematic illustration of mechanisms of Stokes and upconversion emission processes.

The rich optical properties of the Ln^{3+} ions can be envisioned only when they are doped in a suitable host matrix.[6] Among the various host matrices, fluorides are interesting as they possess low phonon (vibrational) energy typically about ~ 350 to 400 cm^{-1} . This is advantageous as they reduce the non radiative relaxations which otherwise can decrease the luminescent quantum efficiency. In addition, they are several

synthetic routes to make a wide range of fluorides hosts particularly in the dispersible forms.[7] Some of the extensively studied fluorides hosts are NaYF_4 , LaF_3 , BaYF_5 , LiYF_4 , etc.[8]

Single band blue emission from colloidal $\text{Ce}^{3+}/\text{Tm}^{3+}$ -doped NaYF_4 nanocrystals:

Our objective in this work is to develop dispersible nanocrystals (NCs) which emit strong single band blue emission. Our idea is to use Ce^{3+} and Tm^{3+} combination where Ce^{3+} is used as sensitizer as it possess $4f5d$ band in the UV region and Tm^{3+} has a characteristic emission in the blue region. The $4f$ to $4f5d$ band excitation has higher absorption coefficient due to the allowed nature of the transition compared to weak intra $4f-4f$ transitions. Moreover, the excited level of the Tm^{3+} ions ($^1\text{D}_2$) is close in energy with the $4f5d$ band of the Ce^{3+} ions, a good energy transfer possibility is expected. We chose NaYF_4 as the host matrix as it is one of the superior hosts for the Ln^{3+} ions.

We have synthesized citric acid-coated $\text{NaYF}_4:\text{Ce}^{3+}(15\%)/\text{Tm}^{3+}(0.5)$ NCs *via* microwave assisted method. Briefly, stoichiometric amounts of Y_2O_3 and Tm_2O_3 were converted into their corresponding nitrates by heating in 1(M) HNO_3 . $\text{Ce}(\text{NO}_3)_3 \cdot 6\text{H}_2\text{O}$ was then added to it and this nitrate mixture was dissolved in 5 ml of distilled water in a 50 ml round bottom flask (RBF). Then 4 mmol of NaF dissolved in 5 ml of distilled water separately and 15 ml ethylene of glycol were added to the above solution in RBF. The entire mixture was stirred for 15 minutes followed by the addition of 4 mmol of citric acid (CA) and stirred for 30 minutes. Subsequently the above colloidal solution was transferred to a 30 ml vial used for microwave synthesis and placed in the microwave reactor (Anton Paar Monowave 300). The vial was tightly sealed with Teflon cap and heated at 150°C for 10 minutes. Finally the white color product appear as a precipitate collected by centrifugation and washed three times with absolute ethanol, followed by deionized water to remove impurities.

The XRD pattern of the $\text{Ce}^{3+}(15\%)/\text{Tm}^{3+}(0.5\%)$ -doped NaYF_4 NCs along with that of the standard pattern of cubic phase NaYF_4 crystals are shown in Fig. 1A. The observed diffraction peaks match well with the standard pattern confirming the formation of cubic

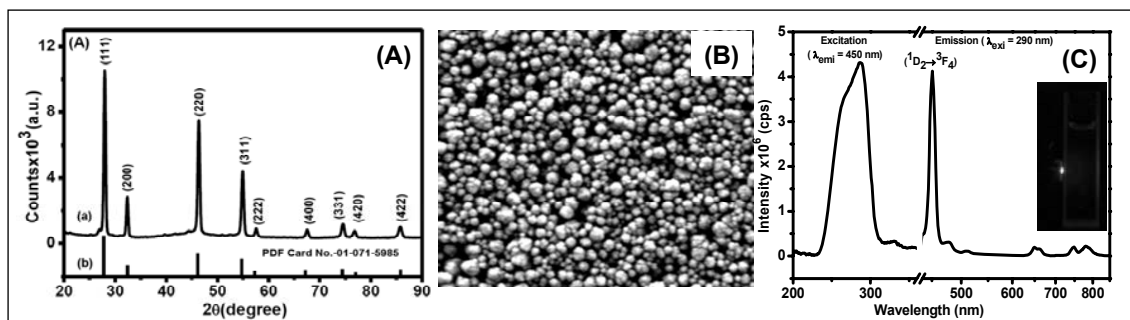


Fig. 1. Experimental and standard (vertical lines) XRD patterns (A) and SEM image (B) of $\text{NaYF}_4:\text{Ce}^{3+}/\text{Tm}^{3+}$ nanocrystals. (C) excitation and emission spectra collected from the nanocrystals. The inset shows the digital image of the blue emission when excited with a commercial UV LED.

phase material. The sharp diffraction peaks in the XRD patterns indicate good crystallinity in the as synthesized NCs. Scanning electron microscopy (SEM) image shown in Fig. 1B indicates that the NCs are spherical in shape and the average size of the NCs is ~ 100 nm. The binding of CA molecules to the surface of $\text{NaYF}_4:\text{Ce}^{3+}/\text{Tm}^{3+}$ NCs is confirmed by FTIR and TGA analyses. FTIR results confirm the binding of citric acid molecules to the nanocrystals via the carboxylate ion (COO^{-1}) as the spectrum shows a shift in the $\text{C}=\text{O}$ stretching from 1726 cm^{-1} to 1600 cm^{-1} upon binding. Similarly, for the TGA analysis of the CA capped NaYF_4 NCs, the onset of decomposition is shifted to higher temperature ($200\text{-}350^\circ\text{C}$) compared to free citric acid molecule (results not shown).[9]

The photoluminescence (PL) and excitation spectra of $\text{NaYF}_4:\text{Ce}^{3+}(15\%)/\text{Tm}^{3+}(0.5\%)$ nanocrystals are shown in Fig. 1C. Upon excitation at 290 nm , a strong emission is observed at 450 nm , which corresponds to the transition $^1\text{D}_2 \rightarrow ^3\text{F}_4$ levels of Tm^{3+} ions. The other very weak emissions observed near 480 nm , 650 nm and 800 nm are characteristics of the Tm^{3+} emissions. We strongly believe that the intense blue emission from Tm^{3+} ions is achieved through Ce^{3+} ion sensitization. This is supported by the observation of a broad peak in the excitation spectrum with maxima at 290 nm ($\lambda_{\text{emi}} = 450\text{ nm}$). This broad excitation band is characteristic of Ce^{3+} ions, which is assigned to $4f^1-4f^05d^1$ level. Furthermore, direct excitation of Tm^{3+} ions at 357 nm resulted in a very weak 450 nm emission. The blue emission intensity of Tm^{3+} ions is almost 12 times higher in case of 290 nm excitation compared to 357 nm . The digital image of the blue emission upon exciting with a commercial UV LED is shown in the inset of Fig. 1C. Additional support for the occurrence of energy transfer between Ce^{3+} and Tm^{3+} comes from the lifetime measurements.

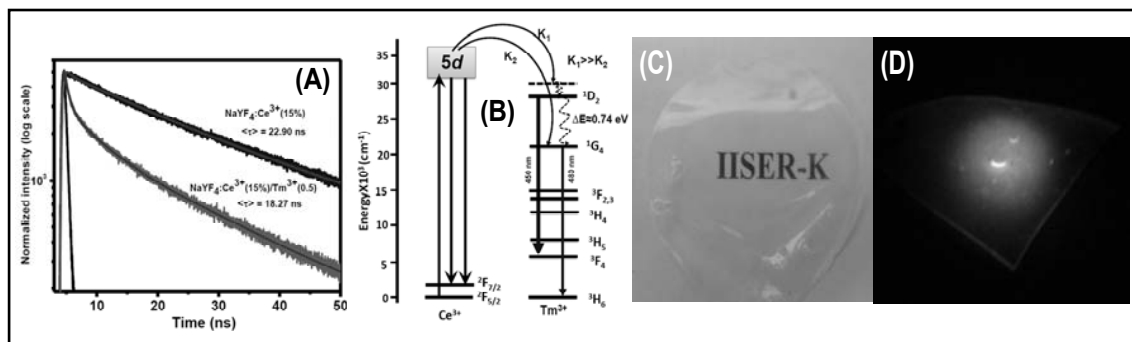


Fig. 2. (A) Luminescence lifetimes decay curves of Ce^{3+} -doped and $\text{Ce}^{3+}/\text{Tm}^{3+}$ -doped NaYF_4 NCs. (B) Proposed energy transfer mechanism between Ce^{3+} and Tm^{3+} ions. (C) The digital images of the nanocomposites showing the transparency and (D) the same after excited with the UV light.

The calculated average lifetimes are $79\ \mu\text{s}$ and $50\ \mu\text{s}$ for 290 nm and 357 nm excitation, respectively. The semi log plot of the decay curve implies a multiexponential decay. The energy transfer (ET) efficiency between donor (Ce^{3+}) and acceptor (Tm^{3+}) ions is evaluated using the equation $\eta = 1 - \tau_{\text{d}'} / \tau_{\text{d}0}$. The terms $\tau_{\text{d}'}$ and $\tau_{\text{d}0}$ are denoted for the excited state lifetimes of the sensitizer in the presence and absence of the activator, respectively.

For the calculation of energy transfer efficiency, we measured the time resolved PL decay of sensitizer Ce^{3+} ions in the presence and absence of the activator, respectively. For the calculation of energy transfer efficiency, we measured the time resolved PL decay of sensitizer Ce^{3+} ions in the presence and absence of emitter (i.e. Tm^{3+} ions). The lifetime values of Ce^{3+} ions in $\text{NaYF}_4:\text{Ce}^{3+}(15\%)$ and $\text{NaYF}_4:\text{Ce}^{3+}(15\%)/\text{Tm}^{3+}(0.5\%)$ NCs are found to be 22.9 ns and 18.27 ns, respectively. The time resolved PL decay curves are shown in Fig. 2A. The calculated energy transfer efficiency is close to 20%. A schematic of the energy level diagram for Ce^{3+} and Tm^{3+} ions and the proposed ET mechanism is shown in Fig. 2B. Briefly, exciting the nanocrystals at 290 nm the Ce^{3+} ions are excited from $4f^05d^1 \rightarrow 4f^1$ level. Subsequent energy transfer from Ce^{3+} to Tm^{3+} ions populates the upper excited level (1D_2). Radiative decay between $^1D_2 \rightarrow ^3F_4$ levels results in the strong blue emission at 450 nm. The probability of the ET from $5d$ level of Ce^{3+} ions to 1D_2 level of Tm^{3+} ions is more than that of 1G_4 level i.e. $K_1 \gg K_2$ (see Fig. 2B). The energy difference, i.e the energy gap (ΔE) between 1D_2 and 1G_4 levels is approximately 0.74 eV. According to inverse energy gap law, rate of non-radiative process is inversely proportional to ΔE . The number of effective phonons required for de-excitation is calculated using the simple formula $\Delta E / \Omega$, where Ω is the phonon energy of the host matrix (for NaYF_4 , Ω is $\sim 360 \text{ cm}^{-1}$ i.e. 0.044 eV). In our case it requires more than 15 phonons to non-radiatively populate the 1G_4 level, which is less probable. Thus the radiative transition is favored from 1D_2 to 3F_4 level which gives single band emission at 450 nm and very weak emission at 480 nm, due to less population of 1G_4 level.

To extend the scope of these NCs towards device fabrication we have prepared a transparent nanocomposite film using the $\text{NaYF}_4:\text{Ce}^{3+}/\text{Tm}^{3+}$ NCs and poly (vinyl alcohol) (PVA). The reason for choosing polymer is because polymeric systems possess several advantages like less optical damage, ease of integration into photonic devices and low processing cost. Poly(vinyl alcohol) (PVA) has been widely used as a host for the fabrication of polymer composites due to the unique physical and chemical properties. Briefly, 1 wt% dispersion of the NCs was added to the 5 wt% PVA solution and the resulting mixture was heated at 70°C . The mixture was concentrated and casted on a glass disc and dried in a vacuum chamber. The resulting nanocomposite is very transparent (Fig. 2C) and exhibits strong blue light upon UV irradiation (Fig. 2D). Furthermore, the film when deposited over the UV LED shows strong blue emission upon application of voltage.

3,5-dinitro benzoic acid (DNB)-capped NaYF_4 nanocrystals for melamine sensing:

Melamine, an organic base and a trimer of cyanamide, with a 1,3,5-triazine skeleton is an important industrial material which had wide application in plastic engineering and agriculture as fertilizer in the early 50s.[1] However, the high nonprotein nitrogen content of melamine led to illegal use in infant formula, wheat gluten, pet foods, etc., to increase the apparent protein content.[2] Standard tests such as the Kjeldahl and Dumas tests used to estimate protein levels in food products by measuring the nitrogen content, can easily be misled by adding nitrogen-rich compounds such as melamine. In 2007, several

pet food brands have been recalled in U.S. by Food and Drug Administration (FDA) because of an outbreak melamine induced illness. The UN food standard commission set the new guidance and safety limit of melamine in food and infant formula as 2.5 and 1 parts-per-million (ppm), respectively. Our aim was to develop upconversion based detection of melamine. Our strategy is to functionalize NaYF_4 nanocrystals (NCs) with electron deficient molecule such as 3,5-dinitro benzoic acid as melamine is electron rich. The strong interactions between them is expected to be reflected in the upconversion properties.[10]

Water dispersible DNB-coated $\text{Yb}^{3+}/\text{Er}^{3+}$ -doped NaYF_4 nanocrystals were successfully synthesized using microwave procedure. Briefly, the nitrate precursors of the lanthanide salts were mixed with NaF and stirred for 15 minutes. This is followed by the addition of DNB and again stirred for 15 minutes. Subsequently, the colloidal solution was transferred to a 30 ml vial used for microwave synthesis. The powder X-ray diffraction (PXRD) measurement confirms the formation of pure cubic phase NCs. The average size of the nanocrystals is ~ 8 nm as evident from TEM image shown in Fig. 1B. This is also supported by the DLS data where the average hydrodynamic size of the nanocrystals is close to 10 nm. The attachment of DNB molecules onto the surface of the nanocrystals is confirmed by the appearance of strong carbonyl stretching near 1645 cm^{-1} in the FTIR spectrum (see Fig. 2C). This frequency is much lower than that observed for the free DNB molecules. The DNB binding makes the nanocrystals surface hydrophilic thus render them water dispersible.

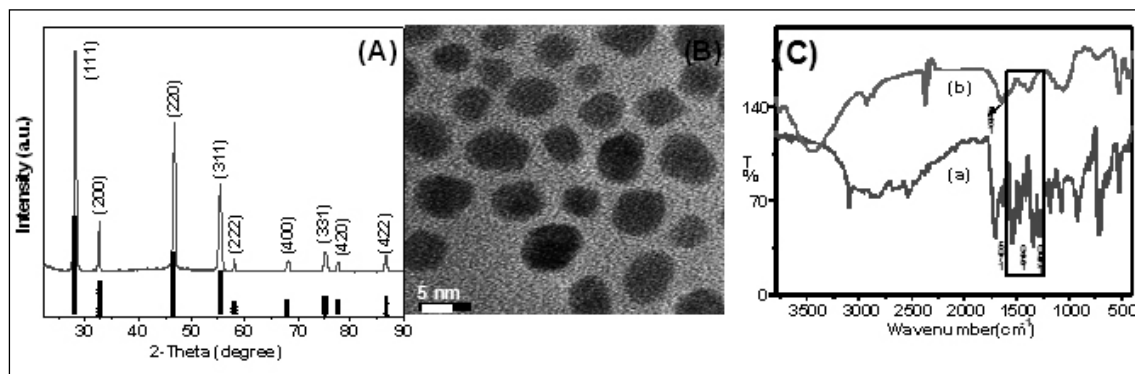


Fig. 2. Experimental and standard XRD patterns (vertical lines) (A) and TEM images of $\text{Yb}^{3+}/\text{Er}^{3+}$ -doped NaYF_4 nanocrystals (B). (C) FTIR spectra of pure (a) and DNB-capped nanocrystals (b).

Fig. 3A shows the upconversion (UC) emission spectrum of DNB coated $\text{NaYF}_4:\text{Yb}^{3+}/\text{Er}^{3+}$ NCs obtained by exciting them at 980 nm using a diode laser. Strong green and red emissions are observed near 550 and 650 nm, respectively. These emissions are ascribed to the ${}^2\text{H}_{11/2}$, ${}^4\text{S}_{3/2} \rightarrow {}^4\text{I}_{15/2}$ and ${}^4\text{F}_{9/2} \rightarrow {}^4\text{I}_{15/2}$ transitions, respectively. The digital image of the colloidal NCs shows yellow color due to the combination of green and red color emissions. (inset of Fig. 3A). The origin of these emissions is from the excited energy levels of Er^{3+} ions, which are predominantly populated by multiple energy transfers from

excited Yb^{3+} ions. The Yb^{3+} ions act as sensitizer for the Er^{3+} ions due to its high absorption coefficient (see Fig. 3B). The number of photons involved in the energy transfer process is understood by doing the power dependent studies as the laser power, $P \propto I^n$, where I is the intensity of the UC emission and n is the number of photons involved in producing the UC emission. The value of n is obtained from the graph of log plot of the laser power against the emission intensity. The values of n are 1.73 and 1.70, respectively for the green and red emission suggesting the involvement of two photons.

To investigate the sensing ability of the $\text{Er}^{3+}/\text{Yb}^{3+}$ -doped NaYF_4 nanocrystals towards melamine solution, aqueous solution of melamine was added to the nanocrystals dispersion. The emission spectra shown in Fig. 3C clearly indicate that upon addition of melamine solution, the Er^{3+} emission intensity of the nanocrystals decreases dramatically. To verify the selectivity, $\text{Er}^{3+}/\text{Yb}^{3+}$ -doped NaYF_4 NCs were exposed to the distinct aqueous solution of other similar analytes such as tyrosine, cytosine, thiamine, uracil, tryptophan and vitamin C. The UC emission spectra shown in Fig. 3 clearly indicate that hardly any change in the emission intensity upon addition of these analytes. The bar diagram in the inset shows the selective quenching of Er^{3+} luminescence intensity occurs only with the addition of melamine. The high selectivity of $\text{Er}^{3+}/\text{Yb}^{3+}$ -doped NaYF_4 nanocrystals towards melamine is verified by measuring the Er^{3+} luminescence from the $\text{Er}^{3+}/\text{Yb}^{3+}$ -doped NCs dispersion containing both melamine and other analytes. The aqueous solution of each foreign analytes was first added to the dispersion followed by the same concentration of melamine.

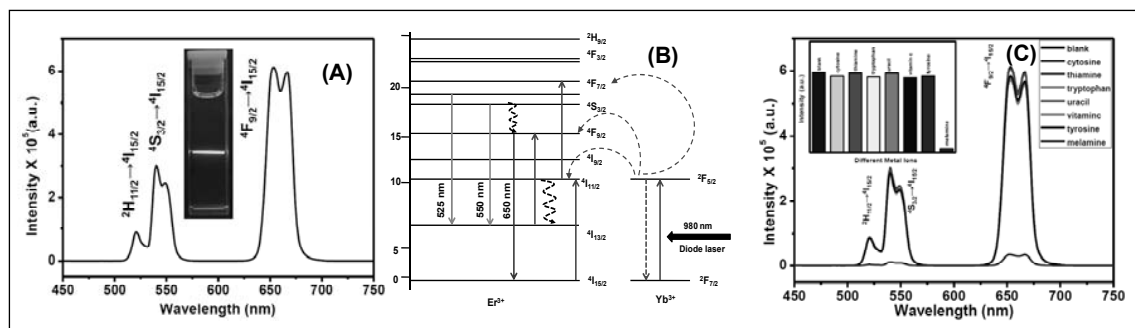


Fig. 3. (A) Emission spectrum via UC of $\text{Er}^{3+}/\text{Yb}^{3+}$ -doped NaYF_4 NCs and the inset shows the digital image of the light from the colloidal dispersion. (B) the UC emission mechanism and (C) the effect of the addition of melamine and other analytes on the emission intensity $\text{Er}^{3+}/\text{Yb}^{3+}$ -doped NaYF_4 NCs.

To understand the nature of the quenching process (dynamic or static) we performed concentration dependence study (i.e. Stern-Volmer plot). The plot of I_0/I against the melamine concentration is almost linear suggesting that the quenching may be either dynamic or static in nature. The dynamic nature is also supported by the decrease in the excited state ($^4\text{S}_{3/2}$ level) of the Er^{3+} ions in DNB-capped $\text{Er}^{3+}/\text{Yb}^{3+}$ -doped NCs from 109 μs to 43.5 μs after the addition of 7 nM melamine. The sensitivity of the $\text{NaYF}_4:\text{Yb}^{3+}/\text{Er}^{3+}$ nanocrystals is evaluated using the formula $3\sigma/k$ and is found to be 2.5 (nM) for the

melamine determination, where σ is the standard deviation of the blank measurements ($n=7$), k is the slope of the linear calibration curve. The detection is found to be reversible with the addition of 0.1 M HCl. Almost 90% of the emission intensity was recovered with the addition of 0.1 M HCl.

We believe that hydrogen bonding or charge transfer interactions between the nitro groups of DNB and amino groups of melamine may cause weakening of nanocrystals-DNB interaction. This might lead to development of some surface defects, thereby the emission intensity of the Er^{3+} ions present near the surface of the NCs is quenched. To verify this hypothesis we prepared a series of NaYF_4 nanocrystals with 0.5, 1 and 2 mol% Er^{3+} concentrations. The luminescence studies of all the samples were performed with the addition of 10 nM melamine to the nanocrystals dispersion. As expected, for the 2 mol% sample the decrease in the emission intensity upon melamine addition is 95% which is greater than 80% and 55% observed for 1 mol% and 0.5 mol% samples, respectively.

We have extended the study to the sensing of Cu^{2+} , Pb^{2+} and Hg^{2+} ions using colloidal $\text{Ce}^{3+}/\text{Tb}^{3+}$ -doped SrF_2 and Eu^{3+} -doped KZnF_3 NCs after capping them with suitable ligands. [11]

References

- [1] G. Blasse, B. C. Grabmaier, *Luminescent Materials*, Springer, Berlin, **1994**; S. V. Eliseeva, J. C. G. Bünzli, *Chem. Soc. Rev.*, **2010**, 39, 189.
- [2] J.-C. G. Bünzli, S. V. Eliseeva, *Chem. Sci.* **2013**, 4, 1939; D. K. Chatterjee, M. K. Gnanasammandhan, Y. Zhang, *Small* **2010**, 6, 2781;
- [3] S. Hübner, *Optical Spectra of Transparent Rare Earth Compounds*, Academic Press, New York, **1978**; S. Singh, A. Tripathi, C. K. Rastogi and S. Sivakumar, *RSC Adv*, **2012**, 2, 12231.
- [4] C. Dong, F. C. J. M. van Veggel, *ACS Nano* **2009**, 3, 123; M. Pedroni, F. Piccinelli, T. Passuello, M. Giarola, G. Mariotto, S. Polizzi, M. Bettinelli and A. Speghini, *Nanoscale*, **2011**, 3, 1456
- [5] Auzel, *Chem. Rev.*, **2004**, 104, 139; b) M. Haase, H. Schafer, *Angew. Chem. Int. Ed.* **2011**, 50, 5808; Sri Sivakumar, F. C. J. M. van Veggel, P. S. May, *J. Am. Chem. Soc.*, **2005**, 127, 12464;
- [6] V. Mahalingam, F. Vetrone, R. Naccache, A. Speghini, J. A. Capobianco, *J. Mater. Chem.*, **2009**, 19, 3149; F. Wang, Y. Han, C. S. Lim, Y. Lu, J. Wang, J. Xu, H. Chen, C. Zhang, M. Hong, X. Liu, *Nature*, **2010**, 463, 1061; N. Bogdan, F. Vetrone, G. A. Ozin, J. A. Capobianco, *Nano Lett.*, **2011**, 11, 835.
- [7] B. Meesaragandla, S. Sarkar, C. Hazra and V. Mahalingam, *ChemPlusChem*, **2013**, 78, 1338.
- [8] S. Sarkar, B. Meesaragandla, C. Hazra, V. Mahalingam, *Adv. Mater.*, **2013**, 25, 856; S. Sarkar, Venkata N. K. B. Adusumalli, V. Mahalingam and J. A. Capobianco, *PhysChemChemPhys.*, **2015**, 17, 17577
- [9] Venkata N. K. B. Adusumalli, S. Sarkar and V. Mahalingam, *ChemPhysChem.*, **2015**, 16, 2312
- [10] C. Hazra, Venkata N. K. B. Adusumalli and V. Mahalingam, *ACS Appl. Mater. & Interfaces* **2014**, 6, 7833.
- [11] M. Chatti, S. Sarkar, and V. Mahalingam, *Microchim. Acta*, **2015** (accepted); S. Sarkar, M. Chatti and V. Mahalingam, *Chem. Eu. J.*, **2014**, 20, 3311.



Dr. Venkataramanan Mahalingam, Associate Professor, Department of Chemical Sciences, IISER Kolkata

Academic Profile:

MSc: *merican College (1996)*

PhD: *Indian Institute of Technology, Madras (2001)*

Post Doc: *University of Twente, Netherlands (2001-2003)*

University of Victoria and Concordia University (2004-2009)

Assistant professor: *IISER Kolkata (from 2009 to 2013)*

Research Interests: *Lanthanide-doped luminescent nanomaterials and their applications in sensing, photocatalysis, imaging, etc. Layered nanostructures for near Infrared photocatalysis and supercapacitor applications*

Ph.D. Students: *Graduated: 2; Current: 8*

BS-MS Students: *Graduated: 5; Current: 1*

Total Publications: 51

Patent: 1

electronic level and then reach to the ground level by emitting light of different wavelengths.

There are some advantages using RE doped materials instead of conventional organic dyes and semiconductors for biolabelling, drug delivery, and in two photon confocal microscope imaging. [4-6] Due to the photoinstability and chemical degradation, organic dyes can't attach with cell for long period. Besides this, organic dyes have narrow excitation band and broad emission spectra with a long tail at red wavelength region where as RE doped materials show narrow emission band due to localized f-f electronic transition.

The efficiency of RE doped nanoparticle depends upon the dynamics of RE ions and their interaction with the host matrix. Host matrix is to be chosen in such a way that it has high refractive index, lower phonon energy and high chemical stability. Beside this, the efficiency also depends upon dopant concentration, energy migration between the active ions, the statistical distribution of active ions and site symmetry of the active ions in the host matrix.⁷ So by tuning crystal phase, shape, size, dopant concentration and the local structure any one can tune the excitation dynamics of RE³⁺ doped nanoparticles. Generally, the luminescence lifetime can be written as

$$\tau = 1 / W_{\text{RAD}} + W_{\text{NR}} + W_{\text{ET}} \quad (1)$$

where W_{RAD} is the radiative (photon) emission rate and W_{NR} is the nonradiative (multi-phonon) emission rate. The term W_{ET} is the energy transfer rate between neighboring RE ions and for a dipole-dipole interaction it scales with the inverse of the sixth power of the inter-atomic distance between the donor and the acceptor. The contribution due to W_{ET} is considered for high concentration of ions. The term W_{RAD} depends basically on the lattice morphology and symmetry while the term W_{NR} depends basically on the host phonon spectrum (cut-off phonon energy). It is well-known that the modification of phonon spectrum, *i.e.* non-radiative relaxation mechanism (W_{NR}) occurs in the different size of nanoparticles. However, local symmetry change, *i.e.* the modification of radiative relaxation mechanism (W_{RAD}) occurs in different crystal phases of the sample. It is well established that, in the luminescence of RE ions, the highest phonon frequencies of the host lattice are responsible for nonradiative relaxations. In accordance with energy law, the presence of a large gap between emitting and terminal levels reduces the probability of nonradiative decay. Lower host phonon energy has a greater number of phonons connecting the emitting level with the next lower level. The more phonons needed to gap the energy will decrease the nonradiative relaxation probability and increase the quantum yield of luminescence. To overcome the phonon decay problem, it is necessary to choose a lattice that has much lower phonon energy. Multiphonon relaxation is related to the number of phonons:

$$W_{\text{NR}} = A \exp(-Bp) \quad (2)$$

Where A and B are constants, and p is the number of phonons and can be calculated using the equation given below:

$$p = \Delta E / \hbar \omega \quad (3)$$

where ΔE is the energy gap between the concerned energy levels, and $\hbar \omega$ is the energy of the phonons (expressed in wavenumbers) of the crystal host. With an increasing number of phonons p , W_{NR} decreases, and, as a result, the lifetime increases. Different shape and size also have prominent effect upon luminescence property. [7] Recently, core-shell particles have been attracting a great deal of interest to improve the luminescence efficiency by reducing the surface defects of the nanocrystals. [8-9] Also, it is reported that interlayer or bound water has a positive effect upon the luminescence property of RE ion. [10]

Photoluminescence properties of the RE ions are studied extensively, as RE ion doped materials has various application in photonics and biophotonics. Eu^{3+} ion is one of the important members of lanthanide family and Fig. 2 shows a schematic energy diagram of Eu^{3+} ion. RE ion doped nanocrystal can be activated through either by directly exciting the $4f^n$ energy levels or by exciting the charge transfer (CT) band. The opposite-parity excited state of the RE ion (charge transfer of $f^{n-1}d$) and same parity excited state of the RE ion (direct transition of $4f^n$) appeared to be important factors for tuning the efficiency of the materials. During charge-transfer excitation of Eu^{3+} ions, a fast radiationless process, *i.e.* the transition occurs from the charge-transfer state to the excited levels of the ${}^5\text{D}_0$ then the ${}^5\text{D}_0$ level can decay radiatively to the ${}^7\text{F}_j$ levels. However, in direct excitation, the emission occurs from the excited levels of the ${}^5\text{D}_0$ level to ${}^7\text{F}_j$ levels as seen in the Fig. 2. In europium, the ${}^5\text{D}_0 \rightarrow {}^7\text{F}_1$ transition is magnetically allowed (a magnetic-dipole transition), while ${}^5\text{D}_0 \rightarrow {}^7\text{F}_2$ is a hypersensitive forced electric-dipole transition being allowed only at low symmetries with no inversion center. Thus, the intensity ratio $I({}^5\text{D}_0 \rightarrow {}^7\text{F}_2)/I({}^5\text{D}_0 \rightarrow {}^7\text{F}_1)$ serves as an effective spectroscopic probe of the site symmetry in which europium

is situated, that is, the higher the ratio, the lower the site symmetry.

Upconversion emission

The process of photon up-conversion is a way to convert long-wavelength excitation radiation into shorter wavelength output radiation. Up-conversion (UPC) was discovered independently by Auzel and Ovsyankin and Feofilov in mid -1960s. [11-13] Up-conversion is one of the most studied nonlinear optical processes after second harmonic generation and two-photon absorption. The up-conversion is based on the existence of at least two real, metastable emitting states, which is the basic difference from second harmonic generation and two-photon absorption. A number of different mechanisms have been recognized to be involved in up-conversion either alone or in combination (Fig. 3).

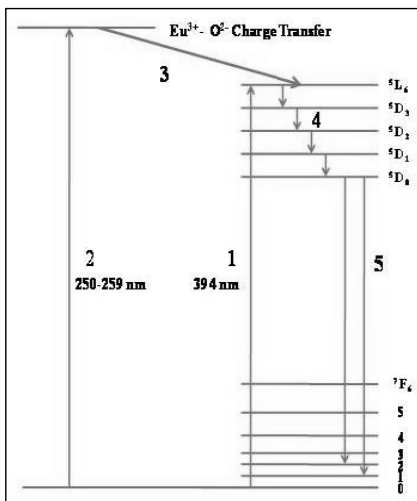


Fig. 2. Schematic energy level diagram and corresponding transition of Eu^{3+} ions.

- Excited State Absorption (ESA)
- Energy Transfer Up-conversion (ETU)
- Co-operative Up-conversion
- Photon Avalanche effect
- EMU (Energy migration mediated upconversion)

Excited State Absorption (ESA) process is sequential absorption of two photons by the same ions. ETU process is defined a process where transfer of excitation occurs from one ion to another that is already in the excited state. ETU process is also synonymed as by Auzel APTE effect (for addition de photon par transferts d'energie). This process is distinguished from a third process named as cooperative upconversion which occurs between two ions or between a pair of ions and a third one. Though some aspects of its theoretical behavior are rather analogous with upconversion by energy transfers, its efficiency is usually much weaker. This is because it involves quasi-virtual pair levels between which transitions have to be described in a higher order of perturbation due to their double-operator nature. The fourth process, photon avalanche effect is based on sequential energy transfers but this is of down-conversion type (usually called cross-relaxation), whereas the up-conversion step itself is due to ESA. In both of ESA and ETU, a simple cw diode laser can be used for the upconversion process, in contrast to expensive mode locked lasers used in two-photon upconversion in organic fluorophore. Another type of up conversion known as EMU was proposed by Wang *et.al.* to occur in $\text{NaGdF}_4:\text{Yb}^{3+}, \text{Tm}^{3+}$ or $\text{NaGdF}_4:\text{Ln}^{3+}$ ($\text{Ln}=\text{Tb}, \text{Eu}, \text{Dy}$ and Sm). [14] This novel UPC process was understood through the use of four types of RE ions located in different layers of the materials serving as the sensitizer, accumulator, migrator and activator. The sensitizer ion (Yb^{3+}) allows pumping photons and promotes a neighboring accumulator ion (Tm^{3+}) to the excited state. Subsequently a migrator ion (Gd^{3+}) receives the energy from the high lying energy levels of the accumulator and then allows for energy migration through the material until energy transfer and subsequent emission from the activator ions occurs.

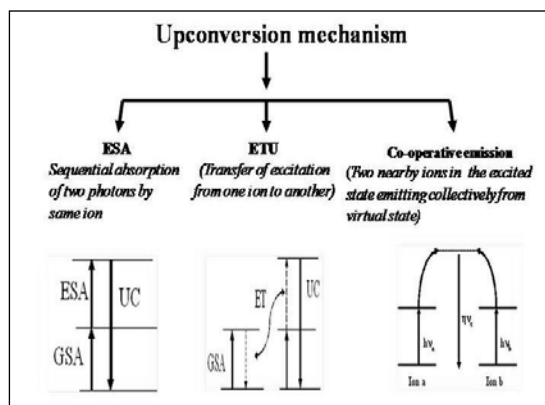


Fig. 3. Mechanism for UPC emission.

Quantum cutting down conversion

Recently, a challenge in the field of luminescence of lanthanide ions is the research in the vacuum ultraviolet (VUV) ($\lambda < 200$ nm) spectral region. This field has become important because of the need for phosphors for VUV excitation. [15] For example, Hg free fluorescent lamps can be made by replacing Hg with a noble gas, such as Xe, as the discharge medium. A Xe discharge offers the advantage of immediate start-up: There is no delay in the

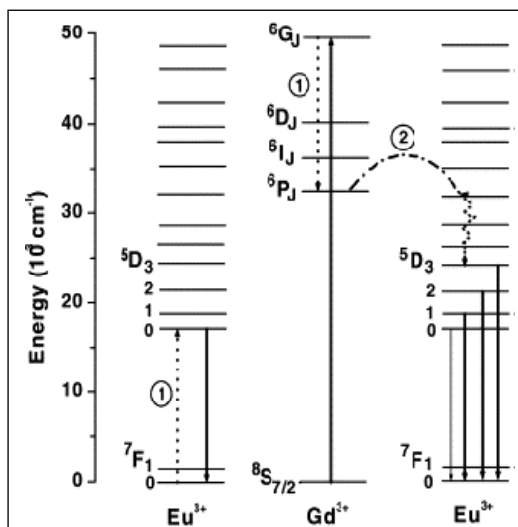


Fig. 4. Mechanism for quantum cutting down conversion for $\text{NaGdF}_4:\text{Eu}^{3+}$ system. [15]

emission of light. (as is the case in conventional fluorescent lamps, where Hg must first evaporate). Immediate start-up is important in special applications (for example, for lamps in facsimile and copying machines and for car brake lights). In plasma display panels, a Xe discharge is also used to generate VUV radiation. In each pixel, the VUV radiation is converted to blue, green, or red light by a phosphor. To get the better efficiency, combinations of two lanthanides ions are used. Through partial energy transfer between the ions, high quantum efficiency (close to 200%) can be obtained.¹⁵This process is the opposite of the process that is known as “Addition de Photons par Transfert d’Energie” (APTE) [which was discovered by Auzel in 1966] and also known as upconversion. Because of this

analogy, this is called as the quantum cutting through energy transfer “downconversion.” Down conversion is a process in which incident high energy photons are transformed by a material into two or more lower energy photons.

RE doped materials are now-a-days extensively used in different applications especially in photonic and biophotonic. For photonic applications, synthesis of white light emitting materials; energy efficient but environmentally benign lighting devoid of Hg are important thrust areas of modern research. To the researcher, it is now a challenge how to make RE doped materials more effective to increase solar cell efficiencies. Similarly on the biophotonic side, Förster Resonance Energy Transfer (FRET) is used along with other biological detection techniques. Likewise, there are need to explore more in the areas of photodynamic therapy and imaging (both in vivo and in vitro).

Dr. Ghosh thanks UGC-Start Up Grant for financial support to attend this workshop.

References:

- [1] N. G. Connelly, T. Damhus, *Nomenclature of Inorganic Chemistry: IUPAC Recommendation*, 2005.
- [2] “1787-1987” *Two hundred Years of Rare-Earth*, Rare-Earth International Center, IPRT, 1987, North Holland.
- [3] R. Reisfeld, C. K. Jørgensen, *Lasers and Excited States of Rare-Earths*, Springer-Verlag, New York, 1977.
- [4] M. Jr. Bruchez, M. Moronne, P. Gin, S. Weiss, A. P. Alivisatos, *Science*, 1998, 281, 2013.
- [5] W.C.W. Chan, S. Nie, *Science*, 1998, 281, 2016.
- [6] 6.I. L. Medintz, H. T. Uyeda, E. R. Goldman, H. Mattoussi, *Nat.Mater.*, 2005, 4, 435.

- [7] R. K.Sharma, A-V. Mudring and P. Ghosh, *RSC Advances*, (submitted).
- [8] P. Ghosh, J.Olivia, E.De.La Rosa, K.K.Halder, D.Solis, A. Patra, *J. Phys. Chem. C.*, **2008**, *112*, 9650.
- [9] P. Ghosh, K. Priolkar, A. Patra, *J. Phys. Chem. C.*, **2007**, *111*, 571.
- [10] P. Ghosh, A. Patra, *J. Phys. Chem. C.*, **2008**, *112*, 3223.
- [11] F. Auzel, *F.C. R Acad.Sci.(Paris)* **1966**, 263B,819.
- [12] V. Ovsyankin, P.P.Feofilov, *Jetp.Lett.*, **1966**, 3, 317.
- [13] 13.V. Ovsyankin, P.P.Feofilov, *Jetp.Lett.*, **1966**, 3, 322.
- [14] 14. F. Wang, R. Deng, J. Wang, Q. Wang, Y. Han, H. Zhu, X. Chen and X. Liu, *Nat. Mater.*, 2011, **10**, 968-973.
- [15] 15. P. Ghosh, S. Tang and A-V. Mudring, *J. Mater.Chem.*, 2011, **21**, 8640-8644



Dr. Pushpal Ghosh has done Ph.D at Indian Association for the Cultivation of Science, Kolkata (Degree given by Jadavpur University), M.Sc. from Presidency College, Kolkata (University of Calcutta) and B.Sc with Honours in Chemistry from Ramkrishna Mission Residential College Narendrapur, Kolkata (University of Calcutta). He is a recipient of prestigious Alexander von Humboldt Fellow (AvH) given by Alexander von Humboldt Foundation, Germany and worked in Ruhr University Bochum, Germany from December 2009 to October 2013. Then he joined as an Assistant Professor in Dr. H.S. Gour Central University Sagar, Madhya Pradesh. Currently he is leading a research group funded by UGC Start-Up grant, DST (Young Scientist) and University itself. His interest is to synthesis new generation optoelectronic nanomaterials using green synthesis. He has published more than 20 research articles in high impact factor journals, book chapters including one German patent

A Review on Rare Earth Based Phosphors

M. Anitha and J. K. Chakravartty

*Rare Earths Development Section, Materials Group, Bhabha Atomic Research Centre,
Mumbai*

E-mail: manitha@barc.gov.in

Luminescent materials are widely used in everyday life, for example, for lighting (energy saving lamps), displays (CRT TV, laptop), liquid crystal display (LCD) TV, plasma TV (PDP), DVD player (laser), diagnosis (X-rays, tomography), lasers etc. In most of the above cases rare earths have greatly contributed in improving the performance of luminescent materials. Rare earths are seventeen elements in the periodic table which include lanthanides, scandium and yttrium. Luminescent properties of rare earths are due to unique spectroscopic properties of rare-earth ions, due to their incomplete 4f shell electrons, led to development of many rare earth phosphors of significant commercial interest. These developments are due to the availability of ultra-high purity individual rare earths in large quantities. La, Y, Ce, Eu and Tb are widely used for lighting devices and displays. Yb and Nd for lasers, Er optical fibres as amplifiers, Gd, Ce, Lu and Tb in medical devices.

A large number of substances, both organic and inorganic, show the property of luminescence. It is an emission of photons which is not due to heat. It is the opposite of incandescence. Some materials, due to their electronic structure, are able to absorb energy after external excitation even at low temperature. If the energy is high enough, an electron can be excited from its fundamental state in an upper electronic layer. The de-excitation to its fundamental level is made either by non-radiative de-excitation or radiative emission by photon corresponding to the emission of photon. The materials involved in this phenomenon can have different names, depending on their composition and their physical properties: phosphors, scintillators, afterglow pigments etc. In all these applications rare earths play a key role. The nature of excitation can be very diverse, leading to sub-categories of luminescent types. As an example, if the excitation source is photonic, the process is known as photoluminescence, electroluminescence (emission by recombination of electrons and holes under the influence of an electric field), chemiluminescence (nonthermal production of light by a chemical reaction), or triboluminescence (emission observed by applying mechanical stress to crystals or by fracture of crystals). High energy excitation always excites the host lattice. Examples are fast electrons, γ rays, X-rays. Direct excitation is only possible with UV and/or visible radiation. The phosphor $Y_2O_3:Eu^{3+}$, for example is excited in the activator itself (the 250 nm band) when applied in a luminescent lamp (254 nm excitation), but in the host lattice when applied as a cathode-ray or X-ray phosphor. Scintillators for tomography and positron emission tomography scan are excited by γ particles. The shape of absorption and emission spectra can be explained using the configurational coordinate diagram.

Fluorescence and phosphorescence are the emission of photons after a sample has been excited by electromagnetic radiation; the distinction between the two is that fluorescence is a spin-allowed process taking 10^{-6} to 10^{-12} seconds whereas phosphorescence involves a change in spin multiplicity and is a slower process, taking from 10^{-6} sec to as much as several seconds.

Phosphor consists of a host lattice in which one or two kinds of foreign ions or ionic groups (centers) are incorporated. These foreign ions called as activator and sensitizer are deliberately added in the optimum proportion during the synthesis of phosphor material. The activator absorbs exciting radiation either through lattice or by itself, gets excited to an excited energy level and come back to lower energy level by emitting light in the visible region. In some phosphors, the activator does not efficiently absorb the exciting radiation and a second impurity ion, sensitizer, absorbs the exciting radiation and transfers this energy to the activator. Some substances like tungstates, titanates, vanadates and molybdates exhibit luminescence even in a pure state when excited by a suitable radiation, which is attributed to a charge transfer process. Rare earth based host lattice with rare earth activators have many favorable features which are: (i) charge compensation problems do not arise (ii) close lattice matching due to similarity in ionic size, leading to minimum lattice distortion (iii) similarity in crystal structure of host cations and that of the activator (iv) there are advantages arising out of identical chemical properties, for material synthesis (v) non-interference of the host emission with activator emission, since the host cation is optically inert (vi) easier incorporation of the activator in large quantities in the host matrix, which is one of the important reasons for improved saturation behaviour of the rare earth phosphors.

The present talk elaborates on how to synthesize solid luminescent materials, phosphors, which are useful for photoluminescence, X-ray and thermo luminescence applications. The evaluation of these phosphors for their characteristics like excitation, emission, quantum efficiency, structural details at higher temperature and thermally stimulated luminescence will be described. Rare earth based phosphors were chosen because of the abundance of rare earth elements found in the mineral monazite sands of India. Monazite is processed for individual rare earths by The Indian Rare Earths Ltd., (IREL) an undertaking of the Department of Atomic Energy, Government of India.

The host of materials YBO_3 , LaBO_3 , $\text{Gd}_2\text{O}_2\text{S}$ and GdVO_4 will be covered in this talk for various applications. The activators and coactivators introduced in these host lattices as well as some non-rare earths ca. Bi. The different techniques for preparation of phosphors like solid state reaction technique, gel combustion route, soft techniques will be covered in this talk. The phosphor samples prepared are characterized by powder XRD. Quantum efficiency (ratio of emitted visible photons by phosphor to incident ultraviolet photons), of the phosphor materials are measured using the instrument indigenously developed in our laboratory.

The optical image can be viewed directly by means of fluoroscopic screens. However, in general radiological practices, the optical images are recorded on films which are

subsequently viewed by radiologist. Without these x-ray intensifying screens, modern radiology would be impossible. For many years, most intensifying screens contained CaWO_4 phosphors. After numerous improvements in CaWO_4 efficiencies and particle shapes, a plateau was reached for the speed of these screens in recording satisfactory radiologic images. In recent years, several new phosphors were discovered which contain rare earth elements and the talk highlights the

In X-ray medical radiography, a uniform flux of x-ray photons passes through an object, a radiologic image is formed of the object parts. In order to be viewed, this radiologic image must be converted into an optical image by means of inorganic crystalline phosphors (blue emitting CaWO_4) which are dispersed in polymeric screens. CaWO_4 has been used for many years. X-ray-to-light conversion efficiency of CaWO_4 is only 6 %. Also its broad band emission (350 nm to 500 nm) is not completely utilized by a blue-sensitive film. All these drawbacks of CaWO_4 led to further research for better phosphors which include $\text{Gd}_2\text{O}_2\text{S:Tb}^{3+}$, LaOBr:Tm^{3+} , BaFCl:Eu^{2+} , etc. The rare earth phosphors $\text{Gd}_2\text{O}_2\text{S:Tb}^{3+}$ and $\text{Gd}_2\text{O}_2\text{S:Tm}^{3+}$ have better energy conversion of 13-18% which can bring down the X-ray dose level by a factor of four. The spectral sensitivity of the photographic film needs to coincide optimally with the spectral energy distribution of the emitted luminescence. The film is surrounded on both sides by the intensifying screen for optimal sensitivity. The smaller the particle size of the crystalline phosphor the closer the packing, thinner the screen layer, and better is the sharpness of the picture. Thus the desired properties of a X-ray phosphor are: (i) high X-ray absorption, (ii) high density, (iii) high efficiency of conversion to light, (iv) a good matching of the film sensitivity to the emission spectra (usually blue or green), (v) high stability and (vi) production cost acceptable for mass applications will be elaborated in the talk.



Dr. M. Anitha, SO/E, joined BARC after completing the 38th Batch of Training School. She obtained her Ph.D from the Mumbai University in 2007. Her research areas include synthesis and characterization of rare earth based phosphors, separation of rare earths by solvent extraction and membrane based techniques, uranium recovery from phosphoric acid and development of analytical methods by ICP-AES. Member of many professional bodies, she has more than 100 papers in various International journals and symposia proceedings including US Patent.



Annual Report -2014

Chemistry Division



Bhabha Atomic Research Centre
Trombay, Mumbai - 400085

PREFACE



It is our great pleasure to present this annual report of Chemistry Division for the calendar year 2014. The report gives glimpses of various scientific and technical activities pursued during the year. The Division has contributed to the scientific programs keeping in mind three basic philosophies- safety in the labs, excellence with ethics, and R & D³ (Research, Development, Demonstration and Deployment). The Division has contributed to both basic and applied research.

The Division is well equipped with sophisticated infrastructural facilities (e.g., powder XRD, High Temperature XRD, Rotating Anode XRD, single crystal XRD, multinuclear NMR (300 and 400 MHz), TG-DTA, SIMS, SEM, AFM, PL, LB trough, IR, Raman, PE Hysteresis facility, AC Impedance Analyzer, ESCA, etc.) to execute our programs in frontier areas of contemporary research. The research activities are supported through the 5-Year Plan projects, namely XI and XII -Plans. There are some collaborative components with other research groups in BARC/ DAE and Universities (both in India and abroad)/ National Institutes through BRNS schemes.

We organized DAE-BRNS 5th Interdisciplinary Symposium on Materials Chemistry (ISMC-2014) during 9-13 December, 2014, at Multipurpose Hall, TSH, Anushaktinagar. The Division extended its support to Human Resource Development activities of the centre and also to the students (M.Sc. and Ph.D.) from different universities working in the Division from few weeks to several months. The service support of instrumental facilities has also been extended, besides within the division, to external users. A large number of scientific papers, Ph.D. theses from different organizations, research proposals submitted to funding agencies, have been reviewed by the scientists of the Division.

Chemistry Division with its scientific, technical and administrative strength of 83 and with additional manpower of doctoral students (17) has been contributing to the above mentioned program. A significant part of our research findings made during the period are published in open literatures, scientific bulletins, BARC News Letter, and has also been presented in several national and international conferences/ symposia. Papers published during 2014 in peer reviewed journals are given at the end of this report. I express my sincere gratitude to all the staff members- scientific, technical and administrative of the Division for their support and cooperation. I take this opportunity to compliment all my colleagues for their sustained excellent performance and look forward in making greater strides in accomplishing our goals.

(Vimal K. Jain)

Head, Chemistry Division, BARC

CONTENTS

1. Nuclear Materials
2. Hydrogen Energy : Generation, Storage and Mitigation
3. Functional Materials
4. Interfacial engineering of nano-structured materials
5. Nanomaterials: Metal Nano-particles, Metal Oxide and Chalcogenides
6. Organometallic Chemistry
7. Catalysis: Homogeneous and Heterogeneous
8. Cluster Chemistry
9. Fuel Cell Materials
10. High Purity Materials
11. Thin Films/ Sensors/ Detectors
12. Development and Maintenance Activities
13. Human Resource Development and other Socio-scientific Activities
14. Miscellaneous
15. Technologies Developed/ transferred during 2014
16. Awards/ recognition during 2014
List of publications (2014)

1. Nuclear Materials

1.1 Ceramics for possible applications in nuclear back end

To overcome the problem of low solubility of minor actinides in glasses and their de-vitrification due to heat generated by stored radioactivity, ceramic matrices have been contemplated as alternate materials. In order to understand the possible incorporation of lanthanide and to simulate for minor actinides in zirconolite based ceramic matrices, phase evolution between $\text{CaZrTi}_2\text{O}_7$ and $\text{Ln}_2\text{Ti}_2\text{O}_7$ ($\text{Ln} = \text{Nd}$ and Sm) has been carried out. The transformation of two-layer monoclinic zirconolite to four-layer monoclinic structure is observed in zirconolite rich regions of both Nd and Sm containing compositions. A broad cubic pyrochlore type phase of composition $\text{Ca}_{1-x}\text{Zr}_{1-x}\text{Sm}_{2x}\text{Ti}_2\text{O}_7$ ($0.40 \leq x \leq 1.00$) has been identified in Sm^{3+} containing compositions. Nearly single phasic four-layer monoclinic zirconolite and perovskite phases identified in phase relations have been prepared separately. A complex oxide, $\text{Ca}_2\text{Zr}_5\text{Ti}_2\text{O}_{16}$ (calzirtite) has been prepared and thermal expansion behavior between RT - 1473 K has been investigated.

The potential of $\text{Gd}_2\text{Zr}_2\text{O}_7$ for uranium incorporation was explored because of its high thermodynamic stability and unique ability to incorporate many radio-nuclides including minor actinides. However, for disposal of long lived minor actinides, it is important to know the effect of minor actinides substitution at Gd-site on thermodynamic stability of the matrix. Uranium is a surrogate for neptunium. The standard molar enthalpy of formation of uranium substituted gadolinium zirconate with general formula $\text{Gd}_{2-x}\text{U}_x\text{Zr}_2\text{O}_{7+\delta}$ ($0.0 \leq x \leq 0.15$) has been determined employing high temperature calorimetry. The enthalpy of formation of $\text{Gd}_{2-x}\text{U}_x\text{Zr}_2\text{O}_{7+\delta}$ ($x = 0.05, 0.1, 0.15$) are found to be -4238.47 ± 0.94 , -4235.7 ± 1.17 , -4210.57 ± 1.32 kJ/mol, respectively. The enthalpy of formation data suggests that the stability of the matrix decreases marginally with increasing substitution of U in place of Gd in $\text{Gd}_2\text{Zr}_2\text{O}_7$.

1.2 Thermodynamic studies on nuclear materials

Barium borosilicate (BBS) glasses have been investigated for incorporation of high level radioactive liquid waste (HLW). The knowledge of thermodynamic stability of these sodium borosilicate glasses used for immobilization of HLW is important for predicting their long term stability. Several BaO substituted sodium borosilicate (NBS) glasses were prepared by melt-quench technique and characterized by XRD, DTA, EPMA and MAS-NMR. The standard molar enthalpies of formation ($\Delta_f H_{298.15}^0$) of NBS glasses with 0, 2, 5 and 8 mole % BaO substitution derived from the measured values of enthalpy of dissolution data are: -952.57 ± 2.96 , -950.65 ± 3.4 , -952.13 ± 2.7 and -953.27 ± 3.9 kJmol⁻¹, respectively. The comparison of thermodynamic stability of International Standard Glass (ISG) and our sodium borosilicate glass, used for nuclear waste disposal, was made by measuring their standard molar enthalpy of formation ($\Delta_f H_{298}^0$) employing a high temperature calorimeter. The enthalpy of formation of our sodium borosilicate glass is 10 kJ mol⁻¹ more negative compared to ISG (In collaboration with WMD, BARC).

Sodium borosilicate glasses containing different amounts of uranium oxides, BaO, CaO, MgO, Al_2O_3 , etc. were investigated for their structural aspects by ²⁹Si and ¹¹B MAS NMR technique. Based

on MAS NMR studies it is confirmed that uranium ions act as network modifier up to 15 wt% and beyond which a separate uranium containing phase, uranium silicate, is formed. For more than 15 wt% uranium oxide incorporation, weaker U-O-U linkages are formed at the expense stronger U-O-Si/B linkages, as suggested by the luminescence measurements. Replacement of Na₂O by MgO, CaO, BaO, etc. do not have any effect on the borosilicate network as revealed by ¹¹B and ²⁹Si MAS NMR studies. ²⁷Al MAS NMR studies on some of the Al₂O₃ containing glasses revealed formation of amorphous alumino-silicate phases during leaching.

Radioactive cesium from high level radioactive nuclear waste by calix crown is being vitrified to make Cs-pencil for industrial and medical applications. There is a great demand to supply Cs-pencils in India and abroad. Estimation of radioactive ¹³⁷Cs loss during the fabrication Cs-pencil is essential. The vapor pressure of volatile Cs₂O over the liquid Cs₂O-containing glass was therefore, measured employing Knudsen effusion mass loss technique. The vapor pressure of Cs₂O over the sodium borosilicate glass measured in the temperature 1050 to 1125K could be expressed by the relation $\ln p(\text{Cs}_2\text{O})/\text{Pa} [\pm 0.03] = -18,888 \pm 35/T + 24.93 \pm 0.03$. Calzirtite (Ca₂Zr₅Ti₂O₁₆) and zirconolite (CaZrTi₂O₇) are potential host matrices for long term disposal of high level radioactive waste (HLW). The standard molar enthalpy of formation of calzirtite (Ca₂Zr₅Ti₂O₁₆, s) and zirconolite (CaZrTi₂O₇, s) have been experimentally determined employing a high temperature Calvet calorimeter. The isobaric heat capacities of the compounds have been derived from the enthalpy increment (H_T-H_{298.15}) data. Thermodynamic functions like standard molar heat capacity, entropy, standard molar enthalpy of formation and standard molar free energy of formation have been generated (In collaboration with WMD, BARC).

Melt densification / incineration of solid wastes such as surgical gloves, postmortem gloves, plastic bottles, polythene sheets, etc. generated in radioactive laboratories/ plants has been investigated. It is necessary to know details of the decomposition steps, the gaseous products evolved and the residue left, in the incineration process. In view of it, TG-DTA and EGA analyses of several representative non-radioactive samples were carried under flowing air with a heating rate 10 °C/min from room temperature to 800 °C. The decomposition temperatures, mass loss steps and the gaseous products formed during the incineration process have been identified. In all these samples, the major gaseous products formed during the heating cycle are found in the order CO₂ > H₂O > CO > CH₄ > H₂. However, in case of surgical and postmortem gloves some gaseous species with mass range 60-105 with intensity 2/3 order less than the major mass peaks have been detected (In collaboration with WMD, BARC).

1.3 Phase evaluation studies of U-10wt% Zr metallic simfuel corroborating to 10 atom% burn up

Extensive studies have been carried out on phase evolution in U-10wt% Zr metallic simfuel (subjected to 10 at % burn up) annealed at 973 and 1273K. A fresh alloy of U-10wt% Zr was simulated step-wise with respect to noble metallic fission products (Ru, Rh, Pd and Mo) and rare earth metals (Ce and Nd) by arc melting under highly purified argon gas. The as-cast alloy was separately annealed at 973K and 1273K under vacuum for 30 days. The microscopic characterization of the alloys has been done. On addition of the noble metals two phases precipitated out at 973K: one

white U-rich and the other dark-grey Zr-rich. Subsequent annealing at high temperature resulted in exsolution of Mo from the white phase and dissolution of Rh and Pd into the white phase. These compositional changes gave rise to needle shaped morphology. The dark grey irregularly shaped low temperature phase gave rise to dark grey circular phase in high temperature annealed sample. On addition of the rare-earths to this partially simulated fuel the lower temperature annealed sample showed the presence of six phases with distinctly different morphologies. These six phases reduced to three (U-rich, Zr & Ru rich, Pd rich) on annealing at 1273K. The present study shows that the total number of fission product phases is decided by the working temperature of the fuel. Across the radial section the high burn-up fuel is expected to contain all the above mentioned phases.

1.4 Studies on fluorides for nuclear applications

Reduction of uranium hexafluoride (UF_6) to stable solid uranium tetrafluoride (UF_4) has several advantages as it has higher stability, lower solubility in water and is safe store. Previously, the reaction process was optimized from X-ray diffraction analyses of the products obtained under different conditions. In continuation of this work, several samples of UF_4 from the downstream of reduction reactor and solid samples of KOH scrub have been analyzed. In scrub samples, the formation UO_2 and oxyfluorides of uranium were observed. The phase purity of UF_4 was evaluated by structural analyses of the reduced samples.

As part of our research for Molten Salt Breeder Reactors (MSBR), several compositions of $KF-ThF_4$ and $KF-UF_4$ have been prepared and characterized. A complex fluoride, K_2ThF_6 , has been prepared by reactive fluorination of ThO_2 and KHF_2 and its thermal stability in air was evaluated by in situ high temperature X-ray diffraction. The K_2ThF_6 is partially converted to ThO_2 above $500^\circ C$ and completely transformed to ThO_2 at $\sim 700^\circ C$. In $KF-UF_4$ system, KU_2F_9 and $K_7U_6F_{31}$ phases are also formed (in collaboration with ChTD, BARC).

2. Hydrogen Energy : Generation, Storage and Mitigation

Hydrogen is projected to be a cleaner energy carrier for the future. It has a high energy density by weight. Various aspects of hydrogen, such as generation, storage, release and mitigation need urgent attention. Chemistry Division has been actively working on these aspects.

2.1 Hydrogen generation

Currently $\sim 90\%$ hydrogen is produced industrially from fossil sources like natural gas, oil or coal by steam reforming. Thermochemical cycles are being developed for large scale production of hydrogen by splitting water. For certain niche applications on a small scale, photo-catalytic methods for hydrogen generation are believed to be quite promising.

2.1.1 Thermo-chemical cycle

There are more than 350 different thermo-chemical cycles which are known for water splitting reaction. Among these, sulfur-iodine (S-I), copper-chlorine (Cu-Cl) and hybrid sulfur cycles

have received much attention. Various aspects of S-I cycle, such as catalyst development, effect of possible reactants on the catalytic activity, iodine speciation during the reaction, etc. have been investigated. A variety of catalysts such as Pt/Al₂O₃ (Commercial), Fe₂O₃/Fe_{1.8}Cr_{0.2}O₃, Fe₂O₃@SiO₂ (hematite phase of Fe₂O₃), etc. with different morphologies have been evaluated for their activities in the decomposition of sulfuric acid, which is the most endothermic reaction in the S-I process. Similarly, a series of Pt/C, Pt/ZrO₂, Pt/TiO₂ and Pt/CeO₂ catalysts have been synthesized and evaluated for their activities in the decomposition of hydroiodic acid, another important reaction in the S-I cycle.

Activities of a series of Fe₂O₃ (x)/SiO₂ (x = 5, 10, 15 and 20 wt.%) oxides were evaluated for sulfuric acid decomposition reaction. Temperature dependent catalytic activity was evaluated in a temperature range of 600-900°C. The SO₂ yield increased with increasing temperature for all the samples. Maximum activity of 92% at 850°C was achieved over the Fe₂O₃ (15%) /SiO₂ (FSO15) sample. To evaluate stability of these catalysts on exposure of sulfuric acid for long duration, the catalytic activity of FSO15 (400 μ size) was evaluated for sulfuric acid decomposition under similar conditions for prolonged durations. There was no deterioration in catalyst activity upto 30 hrs, suggesting that the dispersed catalysts are stable and can withstand harsh environment of sulfuric acid for long durations.

2.1.2 Photo-catalytic methods

Photo-catalytic methods for splitting of water have been explored. Several photo-catalysts have been developed and their catalytic activity for water splitting reaction has been evaluated. Photocatalytic activity of 0.5%PdS/Cd_{0.8}Zn_{0.2}S was investigated in direct sunlight in a reactor of 1L capacity. Na₂S (0.6M) and Na₂SO₃ (0.8M) were used as sacrificial reagents. A hydrogen production rate of 858 ml/h/m² was obtained using this catalyst. Average light intensity measured during the experiment was 71 k lux. Solar to hydrogen energy conversion efficiency for this catalyst is 2.43 %. Under similar conditions, photo-catalytic activity of Pt/Cu_{0.02}Ti_{0.98}O₂ with methanol as sacrificial agent has been assessed. Hydrogen could be generated at a rate of 898 ml/h/m².

2.2 Hydrogen storage

For efficient utilization of hydrogen for energy purpose, suitable strategies need to be developed. Besides pressurization or liquefaction (an energy intensive process), several other hydrogen storage strategies such as metal hydride, chemical hydrides or adsorption on solid support (e.g. activated carbon, nano-structured carbon, MOFs, etc.) are being pursued globally. Chemistry Division has been actively involved for the development of alloys and carbon based materials for hydrogen storage purpose. In this direction hydriding behavior of a wide range of alloys and inter-metallic compounds has been investigated

2.2.1 Hydrogen storage studies on Pd doped CNTs

Hydrogen adsorption studies were carried out on 5% Pd doped carbon nanotubes (CNTs) prepared by wet impregnation route and polyol method. For this system the maximum hydrogen

storage capacities are 0.14, 0.40 and 0.47 wt% at 301, 273 and 269 K, respectively. It has been shown that hydrogen absorption/ desorption process is highly reversible in these samples with negligible hysteresis. Hydrogen storage capacities of the Pd doped CNT samples prepared by polyol method showed better hydrogen storage capacities compared to the one prepared by wet impregnation method. This is due to better dispersion of Pd metals on CNT surface in the sample prepared by polyol method. In both types of Pd doped CNT samples, Pd metal acts as a catalyst to dissociate H₂ molecule to hydrogen atoms. The higher dispersion of Pd metal in Pd-CNT sample prepared by polyol method can more effectively dissociate hydrogen molecule towards hydrogen atoms. The H atoms thus generated can migrate into the carbon nano-tube supports and can get trapped by either physisorption or chemisorption at defect sites, hetero-atom locations, oxygen functionalities etc. The overall mechanism is called spillover mechanism which increases the hydrogen storage capacities of Pd dispersed CNT samples. In addition to Pd doped CNT samples, hydrogen storage studies were also performed on amorphous carbon, meso-porous carbon and inter-metallic alloys based on Zr₂Ni, Ti₂CrV, etc. In general for carbon based material, around 1 wt % hydrogen storage capacity is observed at 123 K and pressures of the order of 50 atm. Unlike this, intermetallic alloys showed more than 2 wt. % hydrogen storage under ambient temperature and pressure. However their desorption temperatures are higher than carbon based samples.

2.2.2 Hydrogen absorption kinetics of Ti_{0.32}Cr_{0.43}V_{0.25} and its composite with TiMn₂

Hydrogen absorption kinetic study of the alloys/composites was carried out after absorption-desorption cycle at room temperature and 20 bar hydrogen pressure. The results showed hydrogen absorption is fast for all the samples. It is evident from the qualitative behavior of the kinetic plots that for a particular alloy/composite, the reaction starts immediately without any incubation time. Reacted fraction, ξ , increases with time and reaches a saturation value after certain time depending on the rate of the hydriding reaction. Ti_{0.32}Cr_{0.43}V_{0.25} reaches 90% of the saturation value [$\xi = 0.90$] within 216 seconds. The results indicate that the overall kinetics of the hydriding reaction decelerate in the presence of the secondary phase.

To understand hydrogen absorption mechanism of the alloy/composites, the kinetics data has been fitted with different equations and the mechanism has been predicted accordingly. The initial part of the hydrogen absorption reaction was fitted successfully with the equation for chemical reaction ($kt = 1-(1-\xi)^4$), where chemical reaction occurs between hydrogen and the composite. The later part can be fitted with the 3-dimensional diffusion mechanism ($kt = 1-2\xi/3-(1-\xi)^{2/3}$), where hydrogen diffuses through the solid matrix. From the rate constant value it can be seen that the chemical reaction occurs at a much faster rate in the composites. Also with increase in the concentration of the secondary phase, the rate constant for the chemical reaction stage increases due to the presence of more interfaces. In composites due to the formation of mixed phase structure the crack formation and initial penetration of hydrogen through the phase boundary is faster so the initial hydrogen adsorption rate increases. In the second stage of hydrogen absorption i.e. in the diffusion stage the rate of the reaction decreases in the composites due to lower hydrogen

diffusion rate in the secondary phase. Hydrogen absorption kinetics of Ti_2CrV alloy and its composite with $\text{ZrFe}_{1.8}\text{V}_{0.2}$ was also evaluated.

2.3 Hydrogen mitigation

Chemistry Division has developed palladium-platinum catalyst supported on SS wire gauze for mitigation of hydrogen generated in nuclear reactor during loss of coolant accident conditions. Catalyst bearing panels (CBPs)(80 Nos) consisting of 240 wire gauze catalysts (16 cm x 12 cm) were supplied to Reactor Safety Division, BARC, for their evaluation at Hydrogen Recombiner Test Facility (HRTF), Tarapur. The catalysts were evaluated for their performance in terms of removal rates, peak catalyst temperatures, etc. under dry and steam-laden conditions. Tests were performed upto 3 % (v/v) H_2 concentration under dry conditions and upto 8 % (v/v) H_2 concentration under steam-inerted conditions. The results indicated that the Passive Catalytic Recombiner Device (PCRD) loaded with the catalyst panels are suitable for fabricating PCRDs (about 1000 in number) required for PHWR Plants. The technology of fabricating the PCRDs will be transferred.

3. Functional materials

3.1 Electro-ceramics

Electro-ceramics represent a category of advanced ceramic materials used primarily for their electrical properties. The properties and applications of electro-ceramics depend on close control of structure, composition, and ceramic texture, dopants distribution. A series of composition with stoichiometry as $\text{SrTi}_{1-2x}\text{Fe}_x\text{Ta}_x\text{O}_3$ ($0.00 \leq x \leq 0.5$) were prepared and their detailed structure and dielectric properties were evaluated. The compositions with $x \leq 0.075$ show single phase cubic perovskite type structure while the compositions with $x \geq 0.33$ show orthorhombically distorted perovskite type structure. The orthorhombic single phase compositions show relaxor like dielectric behavior. Conductivity measurements indicate a possible hopping of ions in the cubic solid solution while hopping of polarons was observed in the orthorhombic solid solutions. In situ high temperature XRD and polarization microscopic (PLM) investigation on single crystal samples of a MPB composition of $[\text{Pb}(\text{Sc}_{1/2}\text{Nb}_{1/2})\text{O}_3]_{0.58} - [\text{PbTiO}_3]_{0.42}$ were carried out to understand the structure and ferroelectric properties. Based on detailed studies, the structural transition sequence could be established in this system. Two olivine type LiFePO_4 and LiMnPO_4 phases were prepared in large quantity by following multistep and optimized reaction conditions and lithium migration was investigated by neutron scattering and molecular dynamics calculations which exhibited the ease of diffusion of lithium along 001 direction. The structure of $\text{Pr}_2\text{Ti}_2\text{O}_7$, a high temperature ferroelectric material was investigated by XRD and Raman spectroscopic studies. The net polarization of $\text{Pr}_2\text{Ti}_2\text{O}_7$ has been assigned to the displacement of the Pr^{3+} ions and rotation and distortion and the total polarization about $6 \mu\text{C}/\text{cm}^2$ has been obtained from the refined structural parameters. Investigation of electrical properties indicates appreciable conductivity above 475°C .

Electrical behavior of rare earth indates has also been explored. The detailed studies were performed on $\text{YIn}_{1-x}\text{Fe}_x\text{O}_3$ ($0.0 \leq x \leq 1.0$) system wherein substitution of a heteroatom at B-site showed interesting dielectric behavior attributed to fine control of BO_5 polyhedra. The dielectric constant drastically increased from 10 for YInO_3 to 1000 for $\text{YIn}_{0.7}\text{Fe}_{0.3}\text{O}_3$ at room temperature. Substitution of Fe into YInO_3 could tune the electrical behavior from a dielectric to relaxor ferroelectric, which is an important observation in context of search for new lead free relaxor materials.

3.2 Multiferroics

In multiferroic materials, two types of ordering of spins and electric dipoles should coexist in the same material and this opens the possibility to make four state memory devices. Thus, the search for these materials is driven by the prospect of controlling charges by applied magnetic fields and spins by applied voltages. Thus a number of multiferroic materials have been prepared and their properties have been evaluated. Scandium and titanium co-doped BiFeO_3 nanostructures synthesized using sonochemical technique exhibited both room temperature ferromagnetism and ferroelectricity. The breaking of spin cycloid due to smaller size and slight structural distortion due to doping is instrumental for enhancement of multiferroic properties. In addition to reduction in the leakage current and increase in polarization values, magnetoelectric coupling was observed in $\text{BiFe}_{0.925}\text{Sc}_{0.05}\text{Ti}_{0.025}\text{O}_3$. Multiferroic Ni-PVDF nanocomposite materials were synthesized by modifying the surface of nickel nanoparticle with hydroxyl groups. The leakage current reduces drastically with concurrent enhancement of electrical polarization. Most importantly, the composite exhibited significantly higher magneto-dielectric coupling. Flexible and self-standing inorganic-organic hybrid films of PVDF incorporated with ZnO nano-rods, graphene oxide (GO) and Fe_3O_4 nanoparticles have been prepared at low temperature by a simple solvent casting method. On incorporating GO and ZnO in Fe_3O_4 -PVDF based films a change in magnetic and dielectric properties has been observed.

3.3 Graphene-like Sn-sheet on Au(111) substrate based on first principles theory

Two dimensional nano-structure materials have immense importance in nano-electronic devices. Since the discovery of graphene, a large number of studies have been carried out to find similar planar sheets of other group IV elements. Motivated by these reports, we have investigated the growth motif and stability of a graphene-like stanene on Au(111) support using first principles theory. For atomic and dimer adsorption, the hollow hcp site of Au(111) substrate is preferred for Sn atom, and the 'in-plane' configuration is preferred for the Sn dimer. Most importantly, the dimer formation of Sn_2 on the substrate is energetically preferred than two Sn atoms adsorbed at a distance. In the Sn/Au(111) heterostructure, significant charge transfer occurs from Sn atoms to the substrate. Stabilization of graphene-like planar stanene on the Au(111) substrate was explored. While free standing stanene showed buckled structure as the lowest energy configuration on Au(111) support the planar graphene-like structure becomes the most stable. This structural transition is attributed to the participation of $\text{Sn-}p_z$ orbitals in bonding with surface Au atoms.

4 Interfacial engineering of nano-structured materials

Interfacial chemistry plays a vital role in developing surface modified materials for drug delivery, catalysis, sensors, etc.

4.1 Interfacial modification of Fe_3O_4 nanoparticles for drug delivery application

Significant progress has been made towards developing multifunctional magnetic nanoparticles for effective treatment of cancer. Biocompatible phosphate anchored Fe_3O_4 nanocarriers (PAMN) were prepared by soft-chemical approach. The surface functionalization of Fe_3O_4 nanoparticles (~10 nm) with bioactive phosphate molecules (sodium hexametaphosphate) was confirmed from infrared spectroscopy, thermogravimetry and light scattering measurements. These nanoparticles show good aqueous colloidal stability, magnetic response and self-heating efficacy under external AC magnetic field (AMF). The bioactive shell not only provides colloidal stability to the particles but also create functionalized exteriors with high densities of negative charges for binding of positively charged drug molecules (In collaboration with RB&HSD).

Folic acid receptors have been explored as specific targeting moieties in anticancer drug delivery. With this objective, bifunctional iron oxide nanoparticles were prepared by tagging folic acid (FA) and fluorescein isothiocyanate (FITC) onto the surface of amine functionalized Fe_3O_4 nanoparticles through well developed conjugation chemistry. XRD and TEM analyses revealed the formation of highly crystalline single-phase Fe_3O_4 nanoparticles of size about 10 nm. FTIR and UV-visible spectroscopy confirmed the conjugations of FA and FITC with nanoparticles. These particles exhibit room temperature super-paramagnetic behavior with a maximum magnetization of 50 emu/g at an applied field of 20 kOe.

Fluorescent magnetic nanohybrids (FMNH) have received a great deal of attention due to their potential biomedical applications. A new class of aqueous stabilized, biocompatible Fe_3O_4 decorated YPO_4 :Eu FMNH has been developed by conjugation of aminosilane functionalized YPO_4 :Eu and carboxyl PEGylated Fe_3O_4 (1:1 wt. ratio) through amide linkage. The surface functionalization of individual nano-particulates as well as their successful conjugation was evident from FTIR, DLS and zeta-potential measurements. XRD analysis revealed the formation of highly crystalline hybrid nanostructures. TEM micrographs showed decoration of 10 nm Fe_3O_4 nanoparticles onto the surface of 150 nm rice grain shaped YPO_4 :Eu nano-structures. These FMNH showed better colloidal stability, good magnetic field responsivity and excellent self-heating capacity under external AC magnetic field (SAR of 122 W/g of Fe at 0.335 kOe field and frequency of 265 kHz). Fluorescence microscopy results indicate excellent optical imaging capability of these FMNH. These multifunctional nanoparticles can simultaneously serve as magnetic resonance contrast agent, hyperthermia agent as well as optical probe.

Mannitol is a well known facilitating agent that can transport drugs across the blood brain barrier (BBB) and increase the uptake of appropriate drugs in brain. In this respect, mannitol functionalized Fe_3O_4 nanoparticles by soft-chemical approach have been prepared. The time-dependent DLS and UV-visible absorbance studies suggest good colloidal stability of these nanoparticles in

water and cell culture medium. Hydrodynamic diameter (*z*-average) of nanoparticles was around 90 nm with have good magnetic field responsivity. Furthermore, mannitol functionalized Fe₃O₄ nanoparticles are resistant to protein adsorption under physiological conditions, and transform from a negatively charged to a positively charged form in acidic environment.

4.2 Microstructure of block copolymer and surfactant assemblies

Microstructure evaluation of self assembled materials comprising of block copolymers, surfactants, novel extraction agents, etc. was carried out to understand the structure-property correlation. Pluronic® are an important family of non-ionic surfactants because of their rich phase behavior and numerous industrial and biomedical applications. F127, an FDA approved Pluronic® is the most prominent member amongst them owing to its potential uses as vehicle for drug delivery and template for fabrication of mesoporous materials. Microstructure and rheological evaluation of *n*-butanol solubilised Pluronic F127 micelles were carried out using techniques like small angle neutron scattering, fluorescence, light scattering and rheology. The studies show that solubilization of *n*-butanol results in a large increase in viscosity of micellar solution at a fixed copolymer concentration, and leads to the formation of stiff gel at F127 concentration as low as 9 wt. %. The observed improvement in gelation characteristics can have important bearing with the application in making mesoporous materials since *n*-butanol is used as co-surfactant to control pore size of such structures formed with F127 gels as a template.

Influence of butyl paraben (BP) on the aggregation characteristics of CTAB has been investigated by DLS, SANS and rheological measurement techniques. Parabens are extensively used as preservatives in cosmetic, pharmaceutical and food products. Our studies show that BP induces a sphere-to-rod growth of CTAB micelles by reducing head group repulsion in the micellar interface. These rod like micellar systems quite interestingly show micellar attraction driven phase separation at the cloud point, which is first of its kind in micellar systems of ionic surfactants.

4.3 Self assembled material for metal separation and decontamination

Mixed micelles have been explored as a viable substrate to remove trace amounts of metals from waste water through cloud point extraction method. The effect of di-(2-ethylhexyl) phosphoric acid (D2EHPA), an organophosphorus ligand used in the extraction of uranium and other heavy metals, on microstructure of non-ionic micelles composed of Triton X-100 was investigated by scattering techniques. Combining dynamic light scattering and small angle neutron scattering (SANS) measurements, it was observed that the effective charge on the surface of the micelles increases with the addition of D2EHPA, while the dimension of the micelles remains same. The increase in repulsive interactions with addition of D2EHPA is also confirmed from an increase in the cloud point of the micellar solutions upon addition of D2EHPA. D2EHPA molecules take part in micellization process through cooperative self assembly leading to mixed micelles. The surface functional groups present on the micelles are conducive for binding of uranyl ions.

Hydrogels have emerged as an attractive material for diverse applications such as chemical separation, cleaning formulations, catalysis and controlled drug delivery systems. Poly vinyl alcohol (PVA) is one of the well known hydrogel forming materials and its rheological properties are dependent on various factors such as pH, temperature, concentration and also on the nature of the additives. With a view to exploit hydrogels as soft coatings for decontamination, rheological properties of PVA hydrogel in the presence of hydrotropes and metal ion complexing agents have been undertaken. The important rheological parameters of the hydrogel, i.e. crossover frequency, storage modulus and loss modulus are obtained in the presence of additives such as sodium salicylate and ethylenediaminetetracetic acid. A dual nozzle sprayer was developed for in-situ cross linking of gels on vertical surfaces. These studies suggest the possibility of using these materials as soft coatings in decontamination.

5. Nanomaterials: Metal Nano-particles, Metal Oxide and Chalcogenides

Nanomaterial research explores unique properties of materials and processes at the nano-scale and probes special properties stemming from their nano-scale dimensions. A variety of nanomaterials based on metal oxides and metal chalcogenides have been synthesized and characterized.

5.1 Metal oxide nanoparticles

One pot synthesis of highly crystalline metal oxide nanoparticles, viz., CoO, Ga₂O₃, NiO and SnO₂ by heating respective metal acetates in oleyl alcohol at temperatures varying between 180-250° C has been developed. Detailed characterization of nanoparticles reveals that highly crystalline and phase pure oxide nanomaterials are formed in each case. Ga₂O₃ nanoparticles (average particle size ~5 nm) exhibit broad photoluminescence bands in visible range and have wide absorption range from ultraviolet to infra red. NiO (average particle size, ~5 nm) nanoparticles exhibit room temperature ferromagnetism. SnO₂ nanocrystals (average particle size, ~10 nm exhibit an absorption edge at ~ 300 nm and photoluminescence bands in both UV and visible region.

TiO₂, Ag-doped TiO₂ and Ag and Fe-doped TiO₂ nanoparticles were prepared by chemical route and characterized by XRD. Antibacterial activity of these nanoparticles has been explored against two representative Gram positive bacteria *Bacillus cereus* and *Staphylococcus* and two Gram negative bacteria *Escherichia coli* and *Klebsiella* by disc diffusion method. The order of activity observed was Fe-Ag-doped TiO₂ > Ag-doped TiO₂ > TiO₂. This is indicative of the synergistic bactericidal effect of Fe over and above Ag by way of generating reactive oxygen species (ROS) (in collaboration with NABTD, BARC).

The potential of α-Ag₂WO₄ nanorods, MnWO₄ and MnMoO₄ nanoparticles, synthesized by sonochemical method, as adsorbents to remove organic pollutants has been explored. MnWO₄ and MnMoO₄ nanoparticles completely remove dyes like Rhodamine B within 2-10 minutes. The α-Ag₂WO₄ nanorods have also been used for adsorption of various cationic dyes (Rhodamine B, Methylene blue, Malachite green) from aqueous solution. The adsorption process is fast and

~100% adsorption of a 20 ppm mixture of all three dyes occurs within 10 min. The influence of initial pH, amount of adsorbent and contact time has been investigated so as to optimize the adsorption conditions. The thermal regeneration of the sorbents is possible and they show similar adsorption efficiency up to ten consecutive cycles.

5.2 Fe₃O₄ nanoparticles for absorption of short lifetime radionuclides

Fe₃O₄ nanoparticles (NP) (10 nm) have been prepared by co-precipitation method. In this, FeSO₄ and FeCl₃ (1:2 molar ratio) were treated with ammonia. The particles were then coated with oleic acids. The particles were dispersed in Na₂CO₃ solution. Radio-labeling studies of the dispersed nanoparticles using ⁶⁸Ga and ¹⁷⁷Lu have been carried out with an aim to develop potential agents for therapy. Besides this, radio-labeling studies of the bare nanoparticles are also being carried out with a host of reactor produced therapeutic radionuclides namely ⁹⁰Y, ¹⁶⁶Ho, ¹⁵³Sm, ¹⁷⁷Lu and ¹⁶⁹Er, having a wide range of energy of β-emission, for their potential use in the treatment of arthritis of different joints of human body.

(In collaboration with IPAD, BARC)

5.3 Improved luminescence from Eu doped ZnO:SnO₂ composite

Nanocomposite of ZnO-SnO₂ finds application in gas sensing and photocatalysis. Eu doped ZnO-SnO₂ nanocomposite have been synthesized and their photoluminescence properties have been evaluated. ¹¹⁹Sn NMR for the undoped samples showed a broad peak ~ -603 ppm suggesting the presence of SnO₂ phase. For Eu-doped samples luminescence measurements were carried out. The emission spectra show intense peaks around 590 nm characteristic of ⁵D₀ → ⁷F₁ magnetic dipole transition, indicating the presence of Eu in the highly symmetric environment. The decay curves corresponding to the ⁵D₀ level of Eu³⁺ ions present in these samples showed a lifetime of ~20 msec. The lifetime values for composite are much higher than that observed for the parent material i.e. Eu doped either ZnO or SnO₂.

5.4 Photoluminescence studies of Eu³⁺ doped ZnS: bulk v nanoparticles

An attempt has been made to understand the photoluminescence behavior of bulk and nanoparticles of Eu-doped ZnS. Samples were characterized by XRD pattern. Luminescence studies were carried out on nanoparticle and bulk samples. Emission spectra show peaks at 590, 615, and 700 nm which are characteristic of ⁵D₀ → ⁷F₁, ⁵D₀ → ⁷F₂, and ⁵D₀ → ⁷F₄ transitions of the Eu³⁺ ions respectively. The ⁵D₀ level of Eu³⁺ ions decay bi-exponentially with a major component around 300 μs. These lifetime values are comparable to those reported for Eu₂O₃. Bulk sample shows different luminescence in comparison to nanoparticle.

5.5 Metal chalcogenide nanomaterials

Single source molecular precursor strategy has been employed for the synthesis of metal chalcogenide materials. Accordingly several precursors have been synthesized. Reactions of Et₂SnCl₂ with sodium salts of HSp_y/ HSp_yMe₂ have been carried out to prepare complexes of formulae,

[Et₂Sn(Spy)₂]/ [Et₂Sn(SpymMe₂)Cl]. These complexes have been characterized by microanalyses and NMR (¹H, ¹³C, ¹¹⁹Sn) spectroscopy. Thermal behavior of the complexes has been studied by TGA. Thermolysis of [R₂Sn(SepymMe₂)₂] (R = Et or ^tBu) in high boiling solvents has been carried out to prepare tin selenide nanomaterials. The nanomaterials have been characterized by XRD. AACVD of [^tBu₂Sn(SepymMe₂)₂] was attempted for deposition of tin selenide at 375 °C at various flow rates and concentrations of the precursor. The best deposition was obtained at 0.4 ft³/h of argon at 375°C with 125 mg of precursor in toluene (25 ml). XRD of thin films deposited at 375 °C showed peaks corresponding to hexagonal phase of SnSe₂.

Copper tin selenide nanomaterials have been prepared by heating either [Me₂Sn(SepyMe)₂] and [Cu(SepyMe)₄] together in oleylamine at different temperatures ranging from 160-200°C for different durations or injecting [Me₂Sn(SepyMe)₂] into the flask containing [Cu(SepyMe)₄] dissolved in hot oleylamine to obtain phase pure Cu₂SnSe₄ nanoparticles. These materials have been characterized by XRD.

6. Organometallic Chemistry

6.1 Palladium and platinum complexes with chalcogenolate ligands

A polymeric complex [PdCl₂(py₂Te₂)_n] was obtained by the reaction of Na₂PdCl₄ with 4,4'-py₂Te₂ in 1:1 ratio. Addition of one equivalent of PPh₃ to [PdCl₂(py₂Te₂)_n] yielded two types of products as indicated by ³¹P NMR. One of them was crystallized as binuclear complex *cis*-[PdCl(μ-Tepy)(PPh₃)₂] as confirmed by single crystal XRD, the structure showed the pyridyl N-atom is uncoordinated and Te atom bridges two Pd centers. The second product is characterized as [Pd(PPh₃)₂(Tepy)₂]. Two macrocyclic structures [Pt₂(κ²-Se,N-4-Sepy)₂(P^oP)₂](BPh₄)₂ (P^oP = 2PEt₃, dppe) were obtained having both Se and N atoms coordinated to Pd centers containing Pt...Pt distances at ~ 7.5–7.8 Å.

Reaction of Pd(dppe)(OTf)₂ with 4,4'-py₂Te₂ in 1:1 ratio yielded a trinuclear complex of composition [Pd₃Te₂(dppe)₃](OTf)₂ which was confirmed from ³¹P NMR spectra, elemental analysis and X-ray diffraction analyses. The telluride group bridges between two Pd(II) atoms capped with dppe ligands in the trinuclear structure. Several reactions [M(P^oP)Cl₂] (M = Pt/Pd), (P^oP = dppe, dppm, 2PEt₃) with NaBPh₄ and 4-NaSepy were carried out to prepare complexes of the type [M(Sepy)(P^oP)]₂(BPh₄)₂. ³¹P NMR spectra showed two different types of phosphorus linkages in the complexes [Pt(Sepy)(dppe)]₂(BPh₄)₂ (¹J_{Pt-P} = 2888 Hz, 3196 Hz) and [Pt(Sepy)(PEt₃)₂](BPh₄)₂ (¹J_{Pt-P} = 2855 Hz, 3013 Hz).

The reaction of [PdCl(SeCH₂CH₂CH₂NMe₂)₂] with excess of AgOTf followed by treatment with NaOAc resulted in [Pd₂(SeCH₂CH₂CH₂NMe₂)₂(OAc)](OTf) as characterized by microanalysis, NMR spectra and confirmed by crystal structure. The molecular structure showed two Pd(II) atoms are held by two selenolate ligands acting in a chelating-bridging mode. The acetate group linked to the fourth co-ordination site of Pd(II) and bridges between two "Pd₂(SeCH₂CH₂CH₂NMe₂)₂" units forming 1-dimensional co-ordination polymer. [PdCl(SeCH₂CH₂NMe₂)₃] and [Pd₄(SeCH₂CH₂NMe₂)₄(OTf)](OTf)₃ were prepared. To replace the triflate ions with AcO⁻, Ph-

COO⁻, Me₃CCOO⁻ ions, the latter complex was treated with an excess of AcOH, PhCOOH (in the presence of NEt₃) and Me₃CCOONa, respectively. The triflate ion was not completely replaced in the case of acetate reaction and whereas they are replaced in the other two cases as confirmed by NMR spectra. The crystal structures of [Pd₄(SeCH₂CH₂NMe₂)₄(OOCPh)₄] and [Pd₄(SeCH₂CH₂NMe₂)₄(OOCMe₃)₄] showed that the molecules consist of four square planar Pd atoms.

6.2 Synthesis of [Pd(Ar)(S₂COR')(PR₃)₂]

The arylpalladium complexes derived from chalcogen ligands are active intermediates in several organic transformations involving arylhalides (e.g. Suzuki reaction). [Pd₂Ar₂(μ-Cl)₂(PR₃)₂] (Ar = Ph, tol) were synthesized by the reaction of Ar₃Bi with [Pd₂Cl₂(μ-Cl)₂(PR₃)₂] in benzene. Compounds of the type [PdPh(S₂COPrⁱ)(PMe₂Ph)], [Pdtol(S₂COEt)(PMe₂Ph)] and [PdPh(S₂COEt)(PMe₂Ph)] were synthesized by reacting [Pd₂Ar₂(μ-Cl)₂(PMe₂Ph)₂] with NaS₂COR' in benzene. These compounds were characterized by ¹H, ³¹P NMR spectroscopy. Crystal structures of [PhPd(S₂COEt)(PEt₃)] and [PdPh(S₂COPrⁱ)(PMe₂Ph)] revealed a four coordinated palladium with chelated xanthate ligand.

6.3 Complexation of platinum with various telluro ether ligands

The complexes, [PtCl₂(TeMes₂)₂], [PtCl₂(MesTetol-o)₂] and [PtCl₂(MesTePh)₂] were obtained by the reactions of K₂PtCl₄ with the telluro ether. Only [PtCl₂(TeMes₂)₂] gave mononuclear cycloplatinated complex in refluxing THF (¹²⁵Te δ = 338.12 ppm (J_{Te-Pt} = 618 Hz), 592.9 ppm (J_{Te-Pt} = 1539 Hz) w.r.t Me₂Te¹⁹⁵Pt δ = -4452 ppm). The molecular arrangements of [PtCl₂(TeMes₂)₂], [PtCl₂(MesTetol-o)₂], [PtCl₂(MesTePh)₂] and [PtClCH₂C₆H₂(4,6-Me₂)Mes(TeMes₂)] were revealed by single crystal X-ray diffraction studies of these complexes. From the X-ray data it was seen that the geometry of all the first three complexes are trans in nature. There is a strong agostic interaction between Pt and C-H (sp³) hydrogen of one of the ortho -CH₃ group of mesityl ring in case of [PtCl₂(TeMes₂)₂] with a characteristic Pt-H distance of 2.47 Å and Pt-H-C angle of 149°. It is evidenced that such type of interaction is responsible for the C-H bond activation.

Complexation of platinum with both symmetrical and unsymmetrical telluro ether were also carried out using [PtCl₂(PhCN)₂] as the platination source. It was noticed that [PtCl₂(PhCN)₂] on reacting with MesTePh gave the simple substitution complex *trans*-[PtCl₂(MesTePh)₂] (¹²⁵Te δ = 575.16 ppm (J_{Te-Pt} = 365 Hz), 576.51 ppm (J_{Te-Pt} = 369.5 Hz; ¹⁹⁵Pt δ = -3555.22 and -3557.30 ppm) but the chemistry changes completely on increasing the steric crowding around telluro ether ligand. [PtCl₂(PhCN)₂] on reacting with MesTetol-o in toluene at room temperature gave *trans*-[PtCl₂(PhCONTeMes₂)(PhCN)] (¹²⁵Te δ = 937.48 ppm (J_{Te-Pt} = 317 Hz); ¹⁹⁵Pt δ = -3606.26 ppm) whereas with Mes₂Te in THF gave *trans*-[PtCl₂(PhCONTeMes₂)₂] (¹²⁵Te δ = 958.83 ppm (J_{Te-Pt} = 347 Hz); ¹⁹⁵Pt δ = -3079.40 ppm) at room temperature and *trans*-[PtCl₂(PhCOC₄H₆N)(PhCONTeMes₂)] (¹²⁵Te δ = 945.12 ppm) under refluxing condition.

6.4 Synthesis of platinum(II)-selenoether complexes

The platinum(II) complexes with phenylseleno N-acetyl α -amino acid having general formulae $\text{Pt}(\text{N}^{\text{n}}\text{N})(\text{L})[\text{NO}_3]_2$, $[\text{Pt}(\text{N}^{\text{n}}\text{N})(\text{L})][\text{NO}_3][\text{OH}]\cdot\text{H}_2\text{O}$ [$\text{N}^{\text{n}}\text{N}$ = ethylenediamine or 2 NH_2 ; L = $\text{dmpzC}_6\text{H}_4\text{Se}(\text{CH}_2)_n\text{COOH}$ or $\text{dmpzCH}_2\text{CH}_2\text{Se}(\text{CH}_2)_n\text{COOH}$ ($n = 1$ and 2)] were synthesized by treatment of $[\text{Pt}(\text{N}^{\text{n}}\text{N})(\text{NO}_3)_2]$ with equimolar $\text{L} = \text{PhSeCH}_2\text{CONHCH}_2\text{COOH}$, $\text{PhSeCH}_2\text{CONH}(\text{CH})(\text{CH}_2\text{Ph})\text{COOH}$ in methanolic solution. The products were characterized by microanalyses and NMR (^1H , ^{13}C , ^{77}Se and ^{195}Pt) spectroscopy. Some of these complexes exhibit cytotoxicity.

6.5 Silver(I) complexes with chalcogen (S, Se) containing pyridyl ligands

Silver(I) coordination compounds of chalcogen (S, Se) containing pyridyl based ligands have been synthesized, characterized and their molecular structures have been elucidated by single crystal X-ray crystallography. The complex $[\text{Ag}(4\text{-SpyH}_{0.5})_2(\text{PPh}_3)_2]$ is a mononuclear complex comprising of linear hydrogen bonded chains while the complex $[\text{Ag}_3(\mu\text{-Se-4-py})_3(\text{PPh}_3)_4](\text{H}_2\text{O})$ (MeOH) is a trinuclear molecule having a six membered Ag_3Se_3 ring. The complexes $[(\text{Ph}_3\text{P})_2\text{Ag}(\mu\text{-S-4-py})_2\text{Ag}(\text{PPh}_3)_2]$ and $[(\text{Ph}_3\text{P})_3\text{Ag}(\text{Se-4-py})]$ have also been prepared and structurally characterized. The latter complex in $\text{CHCl}_3/\text{MeOH}$ solution transforms to $[\text{Ag}_3(\mu\text{-Se-4-py})_3(\text{PPh}_3)_4](\text{H}_2\text{O})$ (MeOH) after a few days. When complex $[(\text{Ph}_3\text{P})_2\text{Ag}(\mu\text{-S-4-py})_2\text{Ag}(\text{PPh}_3)_2]$ was refluxed in CHCl_3 an insoluble white complex of composition $[\text{Ag}(\text{S-4-py})(\text{PPh}_3)]$ precipitates out. This complex is probably a coordination polymer, as can be inferred from its insoluble nature in common solvents. Another complex $[(\text{Ph}_3\text{P})_3\text{Ag}(\text{S-2-py})]$, analogous to $[(\text{Ph}_3\text{P})_3\text{Ag}(\text{Se-4-py})]$, was obtained using 2-pyS⁻ as ligand. In short, discrete and polymeric complexes of silver(I) with chalcogen derived pyridyl based ligands have been isolated by subtle variation of the reaction conditions and the chalcogen ligands. The coordination number of silver varies from 3 to 4 and the observed geometries are T-shaped, distorted tetrahedral and distorted pyramidal. In all these complexes, the pyridyl-N does not participate in bonding with Ag(I).

6.6 Synthesis of organoselenium compounds for biological applications

The DHS^{red} derivatives of the types $\text{DHS}^{\text{red}}\text{-O-R}$ and $\text{DHS}^{\text{red}}(\text{O-R})_2$ ($\text{R} = \text{CH}_2\text{C}_{10}\text{H}_7$, $(\text{C}=\text{O})\text{CH}_2\text{C}_8\text{H}_6\text{N}$ and $\text{CH}_2\text{C}_6\text{H}_4\text{-Me}$) were synthesized by treatment of DHS^{red} with Ag_2O followed by reaction with the corresponding bromo functionalized moieties in DMF at room temperature. They were characterized by NMR (^1H , ^{13}C and ^{77}Se) spectroscopy. A representative compound, $\text{DHS}^{\text{red}}\text{-(OCH}_2\text{C}_{10}\text{H}_7)_2$ was crystallized from ethyl acetate-hexane mixture and its molecular structure was established by single crystal X-ray diffraction analysis. The naphthyl and indolyl substituted derivatives exhibited luminescence properties in chloroform solutions. The naphthyl derivatives, $\text{DHS}(\text{OH})\text{OCH}_2\text{C}_{10}\text{H}_7$ and $\text{DHS}(\text{OCH}_2\text{C}_{10}\text{H}_7)_2$ were excited at wavelength 340 nm and emissions at ~ 400 nm were observed. Stoke shift of ~ 60 nm was observed. While the indolyl derivatives, $\text{DHS}(\text{OH})\text{O}(\text{C}=\text{O})\text{CH}_2\text{C}_8\text{H}_6\text{N}$ and $\text{DHS}\{\text{O}(\text{C}=\text{O})\text{CH}_2\text{C}_8\text{H}_6\text{N}\}_2$ were excited at wavelength 320 nm which emit at 385 nm with Stoke shift of ~ 65 nm.

6.7 Chemistry of organo-gallium and -indium complexes

Diorganogallium hydroxides are partial hydrolysis products of triorganogallium compounds and diorganogallium complexes and their structure is influenced by the nature of organic group attached to gallium. The dimethylgallium hydroxide is the simplest in the series and is often encountered during the synthesis of methylgallium complexes. A variety of structures and their polymorphs have been isolated by re-crystallizing the complex from different solvents. $[\text{Me}_2\text{GaOH}]_n$.dioxane has one dimension helical polymeric structure with monomeric molecules bonded in head-to-tail fashion $-\text{Me}_2\text{GaOH}-\text{Me}_2\text{GaOH}-$. These polymers are held together in the crystal lattice through hydrogen bonds ($-\text{OH}\dots\text{O}-$) with intermediate dioxane molecules. The $[\text{Me}_2\text{GaOH}]_4$ is devoid of any solvent molecules and exist as discrete cyclic tetramers without any significant interactions in the solid state. The $[\text{Me}_2\text{GaOH}]_6$.dioxane. C_6H_6 exists as discrete cyclic hexameric species held together with intermolecular hydrogen bonds ($-\text{OH}\dots\text{O}-$) with dioxane molecules. This molecule also has intra-molecular hydrogen bonds between opposite $\text{OH}\dots\text{OH}$ moieties.

The photo-physical properties of organogallium and indium complexes find applications as OLED materials. Thus organogallium and indium complexes with Schiff base ligands have been synthesized by the reactions of trimethyl-/ triethyl-gallium etherates and $\text{Me}_3\text{In.OEt}_2$ with appropriate ligand and the resulting complexes, such as $[\text{R}_2\text{GaO}(\text{C}_6\text{H}_3-\text{R}')\text{CH}=\text{NCN}(\text{SC}_6\text{H}_4)]$ (where $\text{R} = \text{Me}/ \text{Et}$ and $\text{R}' = \text{H}/ \text{OMe}$) and $[\text{R}_2\text{InO}(\text{C}_6\text{H}_3-\text{R}')\text{CH}=\text{NCN}(\text{SC}_6\text{H}_4)]$ (where $\text{R} = \text{Me}$ and $\text{R}' = \text{H}/ \text{OMe}$), have been purified by re-crystallization and characterized by melting point, IR, NMR (^1H and $^{13}\text{C}\{^1\text{H}\}$) spectroscopy. The crystal structure of $[\text{Me}_2\text{GaO}(\text{C}_6\text{H}_3-\text{OMe})\text{CH}=\text{NCN}(\text{SC}_6\text{H}_4)]_2$ revealed that the gallium atom is four coordinated to give a distorted tetrahedral geometry. Photophysical studies of these complexes revealed that the complexes and free ligands are photo-emissive.

7. Catalysis: Homogeneous and Heterogeneous

7.1 Heterogeneous catalysts

Besides numerous catalysts for sulfur-iodine thermochemical cycle and photo-catalytic reaction for hydrogen generation and platinum based catalysts for hydrogen mitigation discussed earlier, several other catalysts for de-nitration, reduction of U(VI) to U(IV) and dye degradation have been developed.

7.1.1 Catalytic activity of Pt/ZrO₂ for U(VI) to U(IV) reduction reaction

Zirconia supported platinum (Pt/ZrO₂) catalytic system has been developed for reduction of U(VI) (in the form of uranyl nitrate solution) to U(IV) at ambient conditions employing hydrazine as a reductant. The performance of Pt(1wt.%)/ZrO₂ catalyst was the best among the various Pt/ZrO₂ catalysts evaluated for this reduction process. About 99.9 % conversion could be achieved in 7 h which is comparable to the performance of commercial Pt/SiO₂ catalyst. The stability of Pt/ZrO₂ is expected to be better compared to the commercial Pt/SiO₂ catalyst.

7.1.2 Reduction of CO₂ with Cu-doped TiO₂

Various compositions of Cu doped titania ($0 \leq x \leq 0.1$) photocatalysts have been synthesized by using simple sol-gel process. These photocatalysts comprise of pristine anatase phase of nanotitania. The DRS studies indicate that the samples are indirect band gap semiconductors with a large shift in the band edge from Cu-1 to Cu-10 as a function of Cu content in the TiO₂. TiO₂ showed sharp band edge which was shifted towards visible region on increasing the copper contents from Cu-1 to Cu-10. These materials have been prepared for their utility for photo-catalytic reduction of CO₂.

7.1.3 Photocatalytic degradation of methylene blue using Pd doped CdS

Photocatalytic activity of Pd doped CdS for the degradation of methylene blue (MB, concentration 10 ppm) was studied using fluorescent lamp as source of radiation. Under the natural pH of the solution (~7.0), 70% degradation of MB occurred after 6 hours of irradiation. But, when the pH of the solution is increased to 10.0, complete degradation of the solution occurred in 30 minutes. The increased photocatalytic activity at higher pH is attributed to increased adsorption of dye on the catalyst surface at alkaline conditions as MB is a cationic dye.

7.1.4 Photocatalytic activity of Pd-CdO-TiO₂ composite

Photocatalytic stability 0.5%Pd-50%CdO-TiO₂ composite was tested by using it for repeated cycles (4 cycles). The catalyst, after six hours of experiment (light source: day light fluorescent lamp), was reused by flushing it with argon gas. A slight decrease in the activity is seen in the second cycle. But in the subsequent cycles, the photocatalytic activity remained almost the same. Variation in the photocatalytic activity of this composite with change in the wavelength of the incident light was studied using different cut-off filters. The source of light used for this experiment was Xenon arc lamp (300 Watts). It is seen that with the increase in the wavelength of light, the photocatalytic activity decreased, which resembles the UV-visible absorption spectrum of this sample. This observation suggests that the reaction is truly photocatalytic. Photoluminescence spectra showed emission peaks originating from defect levels. Fluorescence lifetime studies indicated increased lifetime for the charge carriers for the CdO-TiO₂ composite compared to single phase CdO and TiO₂.

7.2 Homogeneous catalysts

The complex [PdCl₂(PhSeCH₂CH₂CH₂NMe₂)] was used as catalyst (0.1 mol%) in Suzuki coupling reactions of aryl halides and phenyl boronic acid. The yields of biaryls obtained were in the range of 80-95% with activated aryl bromides. In the case of bromotoluene, yield was 16% within 10 h. A similar coupling reaction with iodotoluene [PdCl₂(PhSeCH₂CH₂CH₂NMe₂)] (0.01 mol%) resulted in 94% yield of the product. The complex [Pd₄(SeCH₂CH₂NMe₂)₄(OTf)](OTf)₃] showed very poor yield when used in the coupling reaction between bromo toluene and phenyl boronic acid.

[Pd₄(SC₆H₄C₆H₄S)₂(dppe)₄](OTf)₄ and [Pd₈(SCH₂C₆H₄CH₂S)₄(dppe)₈](OTf)₈ were used as catalysts in Suzuki coupling reactions. With phenyl boronic acid the reaction of tolyliodide gave more than

91% yield of product within 7h. Using both the complexes as catalyst 96-97 % yield of biaryl was obtained in case of tolylbromide in 10 h of reaction. High yields (90, 70 %) were observed even lowering the catalyst concentration by 10 times. In the presence of electron donating and bulkier aryl bromide such as mesityl group and 2,6-Me₂ groups, the yield of biaryl obtained as 37 and 58 %, respectively. Under the same conditions cross-coupling of electron-poor aryl bromides gave quantitative yields of the corresponding biaryls. After lowering the catalyst concentration gradually to 10⁻⁶ mol% of Pd, the complex was found highly active to yield 85% with a very high TON of twenty million in case of bromoacetophenone as substrate.

The Suzuki C–C coupling reactions of phenylboronic acid with 2-bromo benzaldehyde and 4-bromo toluene in the presence [Pd₂(μ-Cl)₂{MesSeC₆H₂(Me₂)CH₃}]₂] and tetrabutyl ammonium hydroxide as a base and dioxane as solvent at 100 °C for 7 hrs yielded 15% and 60% of biaryls, respectively. The same reaction in the presence of K₂CO₃ as base could yield 9% of product in case of 4-bromo toluene as substrate.

8. Cluster Chemistry

8.1 Fabrication of electron energy analyzer and determination of kinetic energy of electrons produced due to multiple charging of methyl iodide clusters

Interaction of 532 nm laser pulses of intensity ~10⁹ W/cm² with methyl iodide clusters leads to generation of multiply charged atomic ions of carbon and iodine. Observation of these multiply charged atomic ions has been attributed to multiple ionization of the cluster constituents by quasi-free electrons, confined within the cluster, which is energized under the influence of laser field by inverse Bremsstrahlung process. The interaction of laser pulse with cluster ultimately results in generation of multiply charged atomic ions of carbon and iodine. In order to test this proposition, attempts have been made to detect and quantify kinetic energy of electrons, liberated upon laser-cluster interaction. For kinetic energy measurement an electron energy analyzer setup has been designed and fabricated. The analyzer is based on retarding field method, which comprises of three stainless steel grids for energy filtering and is coupled with channel electron multiplier detector. Initial experiments have been carried out with methyl iodide clusters at 532 nm laser pulses. A typical signal obtained from the setup comprises of a sharp signal due to scattered photons followed by a broad electron signal, which systematically decreases upon varying negative voltage on the central grid of the retarding field analyzer. Based on the electron energy distribution obtained from these studies, electrons with kinetic energy up to ~ 25 eV have been detected.

8.2 Structure and reactivity of Au_n clusters on α-Al₂O₃(0001) surface

To underscore the effect of support interaction, geometries of Au clusters were compared with the gas-phase structures. The structure and reactivity of Au_n (n =1-7 and 10) clusters supported on clean α-Al₂O₃(0001) surface using spin-polarized version of the plane wave based pseudo-potential method have been investigated. In general, the trend in growth pattern showed that all deposited Au clusters favor planar configurations, similar to that in the isolated case. However, due

to roughness of the $\text{Al}_2\text{O}_3(0001)$ surface the deposited Au atoms are arranged in zig-zag pattern. The binding energy of an Au on the Al_2O_3 surface is 0.79 eV and it binds with the surface Al atom. Two Au atoms favor to form a dimer on the alumina surface than adsorbing as monomer at long distance. As the size of the cluster increases the adsorption energy showed decreasing trend. The nature of chemical bonding at the interface was established by the charge distribution analysis, which suggests an overall charge transfer from the surface to the Au cluster. The additional negative charge on the deposited Au cluster corroborates the red shift of the energy levels of Au/ Al_2O_3 composite in comparison to the isolated Au_n clusters. Further investigations were carried out by interacting oxygen molecule with the $\text{Au}_n@/\text{Al}_2\text{O}_3$ system, a prototype to study oxidation mechanism. The results revealed that the interaction of O_2 with $\text{Au}_n@/\text{Al}_2\text{O}_3$ follows dissociative chemisorption route and cleavage of O-O bond.

8.3 Comparison between cluster and slab model for Pt-group atom adsorption on gold and silver substrates

The adsorption of Pt group ($M = \text{Ni}, \text{Pd}, \text{Pt}$) metal atoms on gold and silver substrate has been investigated using spin polarized density functional theory formalism. The spin orbit interactions were employed to calculate the total energy. The results showed that all tetramer clusters favors planar configuration and heptamer clusters showed both planar as well as non-planar structures. Addition of Ni to Ag_6/Au_6 is distinct as it gives dissimilar structure in comparison to what obtained by addition of Pd/Pt atom. For example, while NiAg_6 clusters form a pentagonal bipyramidal structure, PdAg_6 and PtAg_6 clusters prefer chair form structure in which six Ag atom forms chair configuration and M atom at central site. Contrary PdAu_6 and PtAu_6 favor planar hexagonal and exceptionally, NiAu_6 cluster favors 3D chair like conformation. Over all, interaction of M atom with hexamer cluster is primarily governed by relative strength of M-Ag/Au vs. Ag-Ag/Au-Au bond and consequently modifies planar triangular arrangement to different extent. In case of silver cluster, intense and narrow peaks are observed in EDOS. For gold clusters, relatively diffused peaks are seen indicating higher degrees of hybridization. In order to compare adsorption behavior of M atoms on finite-size clusters and periodic slab, M atom are adsorbed on Ag/Au(111) surface was carried out. For slab model, M atom irrespectively gets adsorbed on fcc site with small local distortion. Due to different interaction strength and deformation amount, cluster and slab model differs in absolute adsorption energy values. Further a comparison of bonding analysis through electronic density of state (EDOS) and orbital decomposed charge distribution suggest that interaction of Ni/Pd/Pt with gold substrate is relatively stronger than silver substrate.

9. Fuel Cell Materials

9.1 Thermal stability of $\text{Ba}_2\text{In}_{1-x}\text{M}_x\text{O}_{5+\delta}$ ($M = \text{W}, \text{Mo}, \text{V}$) under CO_2 atmosphere

$\text{Ba}_2\text{In}_{2-x}\text{M}_x\text{O}_{5+x}$ ($M = \text{W}, \text{Mo}, \text{V}$) are potential proton conductors that can be used as electrolytes in Intermediate Temperature Solid Oxide Fuel Cells (ITSOFC). Their stability in CO_2 atmosphere is an important parameter for their application as electrolytes. Thermogravimetric studies of $\text{Ba}_2\text{In}_{2-x}\text{M}_x\text{O}_{5+x}$ ($M = \text{W}, \text{Mo}, \text{V}$) systems were carried out under CO_2 atmosphere up to 1200°C at 10°C per

minute heating rate. TG scan of vanadium and molybdenum doped barium indate in carbon dioxide atmosphere showed increase of mass in the temperature range 400 – 600°C whereas in case of tungsten doped barium indate an increase of mass began from 750°C. Increasing of mass corresponds to CO₂ absorption, which leads to production the barium carbonate. In DTA curve endothermic peak was observed at 983°C. The expected weight gain for absorption of CO₂ was 15.3, 15.0 and 14.6% in case V, Mo and W doped barium indate respectively. Weight gain observed in TG curve within 400 - 1200°C is 14.5, 11.4 and 3.9% which indicates that tungsten doped barium indate has higher stability as compared to others.

9.2 Synthesis of Li₄Ti₅O₁₂ for high capacity lithium ion battery as anode material

Li₄Ti₅O₁₂ was prepared by sol- gel method. Titanium isopropoxide and lithium acetate was taken in 1:1 ratio. Isopropyl alcohol and water was used as solvent for titanium isopropoxide and lithium acetate respectively. Titanium isopropoxide solution was slowly mixed with lithium acetate solution with constant stirring to form gel. Formed gel was dried at 100°C on hot plate. Dried powder was ground and heated at 750°C for 20 hrs. XRD pattern of heated sample indicated the formation of Li₄Ti₅O₁₂ with an impurity of TiO₂. Further attempts were made to reduce the TiO₂ impurity by changing stoichiometric ratio of titanium isopropoxide. 93, 95 and 98% of titanium isopropoxide were mixed with same concentration of lithium acetate. Same procedure was followed as stated for 1:1 mixture. XRD pattern of resultant compounds formed in case of 95% and 98% indicate the presence of TiO₂ impurity. XRD pattern of 93% of Titanium isopropoxide indicate the formation Li₄Ti₅O₁₂ without TiO₂ impurity.

10. High Purity Materials

Process development of high purity materials for advance technologies has been one of the thrust areas of research activity. A process for purification of germanium has been developed and 2 kg germanium (7N) has been delivered to TPD for single crystal growth.

11. Thin Films/ Sensors/ Detectors

11.1 Room temperature diamond H₂S sensor

In continuation of this work, several gas sensors were fabricated tested, packaged and calibrated for H₂S sensitivity up to 20 ppm concentration. The handheld battery operated units (4 nos.) for H₂S sensors were developed. Technology transfer document of diamond H₂S sensor has been submitted to TTCD. H₂S sensor with battery operated hand held interface was displayed and demonstrated in Symposium on Advances in Control and instrumentation held in Nov 2014 and ISMC-2014 (Dec 2014).

11.2 Testing of diamond H₂S sensor at bio-fouling test loop facility, WSCD, Kalpakkam

WSCD, Kalpakkam has an ongoing program of sulfate bioremediation, where H₂S is generated by the sulfate reducing bacteria in the bioreactor. Hence it is required to monitor the concentration of H₂S in the bioreactor and the background concentration of H₂S in the bioreactor

room. Some of the packaged H₂S sensors and the portable gas alarm interface were tested at the Biofouling Test Loop Facility, WSCD. The sensors were found suitable for monitoring the background level in the bioreactor lab, which should be <10 ppm. As the sensors were highly sensitive, the sensor response saturated against the high concentration (~100 ppm) of H₂S produced in the bioreactor.

11.3 Polyaniline nanoparticle based colorimetric sensor for monitoring bacterial growth

Detection of pathogens in food and water is important for quality monitoring and disease prevention. A simple and novel colorimetric sensor was developed for detection of bacterial growth relying on estimation of its metabolic products. As a proof of the concept, utility of the sensor for detection of Escherichia coli (E. coli) was demonstrated. All major groups of micro-organisms including E. coli commonly use the glycolytic pathway for glucose degradation, eventually releasing mixed acids like succinate, acetate, malate, etc. as by-products. Polyaniline, a conducting polymer, is highly sensitive to the presence of protons in its microenvironment and its protonic doping results in a visible color change. Hence, polyaniline nanoparticles were synthesized and the sensor films were fabricated by incorporating these nanoparticles in agarose gel. The films when used for real time monitoring of bacterial growth exhibited a visible color change from blue to green. Since no specific antibodies or receptors are used, the sensor is generic in nature and has potential for adaptation to real life applications in the form of patch sensor on cartons to gauge integrity and freshness of food items and beverages in real time (In collaboration with MBD, BARC).

11.4 Development of diamond-based α -particle detector

To develop CVD diamond-based alpha particle detector for direct monitoring of actinides in highly acidic and radioactive liquids, significant progress has been made. The α -particle detector was comprehensively tested in air using alpha emitters (Pu, ²⁴¹Am) of varying activity ranging from 0.06 nCi (~133 dpm) to 0.09 μ Ci (~199800 dpm). All the counting parameters of the detector were optimized during these experiments. The response was linear over the studied concentration range which was reproducible. Having evaluated its performance in air, its suitability in acidic liquid medium (3M HNO₃) was assessed in Fuel Reprocessing Division, BARC. The testing was carried out for different type of solutions namely, 3M HNO₃ containing 1 to 10000 ppm of Pu in the presence and absence of oxalic acid, 3M HNO₃ solutions containing 40 to 1500 ppm of ²³³U, ²⁴¹Am and Pu.

The results have shown reproducible performance of the detector while measuring individual actinides in the above solutions. Calibration plots have shown linearity for Pu and ²³³U in concentration range of 1 to 1000 ppm. Deviation from linearity was observed for concentrations beyond 1000 ppm. Pu content in few process samples was also determined using these calibration plots. The results were in agreement with those obtained from the conventional radiometric method presently followed, which is tedious due to multistep involvement. The sensitivity of the detector is lower than that of the conventional solid-state α -detectors (Si-surface barrier detector, Ag-doped ZnS detector) used at present.

12. Development and maintenance activities

12.1 Development of high temperature PC- based dilatometer

The indigenous development of a fully automated PC-based high temperature dilatometer (RT to 1373 K) has been completed. Data have been recorded on standards / known materials such as NIST sapphire, high purity aluminum and nickel in the temperature range up to 1373 K, 773 K and 823 K, respectively and have been analyzed and net dilation of these materials evaluated by suitable baseline correction. The results match well with the linear expansion behavior measured on a commercial thermo mechanical analyzer (Setsys TMA, Setaram) under same experimental conditions. The overall accuracy of the system in the operational temperature range is within 4%.

12.2 Low Temperature Electrical Resistivity Measurement

Developmental work of a low temperature electrical resistivity measurement facility has been taken up. In this activity, data acquisition software has been developed to simultaneously measure the electrical resistivity of two samples in the temperature range from 4.5 to 310 K, using Lab Windows/ CVI platform. The DAS incorporates various features such as data collection, temperature control and stabilization, data storage, on-line display of experimental conditions; both numerically and graphically, etc. This software has been tested for its performance by measuring the resistance of commercially available resistors in the temperature range from 77 to 310 K.

13 Human Resource Development

Several members of Chemistry Division were actively involved in human resource development program carried out by HRDD, BARC. The activities cover preparation of question bank, conducting written test examinations and interviews for selections of trainee officers and CAT-I trainees, coordinating and delivering lectures and conducting laboratory practicals in the training courses in chemistry discipline, for OCES (OCES-58 batch: Dr. P.A. Hassan, Dr. V. Sudarsan, Dr. S. Nigam, Dr. Vinita G. Gupta, Dr. D. P. Dutta, Dr. Mainak Roy, Shri M. Jafar), HBNI PhD students, CAT-I trainees (Dr. V. K. Jain, Dr. P. A. Hassan, Dr. S.R. Bharadwaj, Dr. Vinita G. Gupta, Dr. G. Kedarnath, Dr. A. K. Tyagi, Dr. B. P. Mandal, Dr. A. M. Banerjee, Dr. K. Bhattacharya, Shri A.N. Shrishat, Shri R. Shukla and S. J. Patwe) and MU-DAE center for excellence in basic sciences (Dr. R.K. Vatsa, Dr. P.A. Hassan and Dr. V. Sudarsan), and evaluations of their performances at different stages. A number of colleagues are members of HBNI doctoral committees at BARC and RRCAT. Many of our senior colleagues are invited as specialists and core committee members in promotional cases at different levels, such as KSKRA interviews, C to D, D to E and E to F interviews, SA to SO/C or TO/C, interviews etc.

Chemistry Division organized DAE-BRNS 5th Interdisciplinary Symposium on Materials Chemistry (ISMC-2014) during 9-13 December 2014 (Convener Dr. V. K. Jain). The 5th ISMC-2104 covered research areas in materials chemistry which include: nuclear materials; high purity materials; nanomaterials and clusters; carbon based materials; fuel cell materials and other electro-ceramics; biomaterials; polymers and soft condensed matter; materials for energy conversion;

thin films and surface chemistry; magnetic materials; catalysis; chemical sensors; organic and organometallic compounds; computational material chemistry. The deliberation of the five days ISMC-2014 comprised of about 35 invited lectures, 8 short lectures and about 400 posters by researchers from India and abroad (USA, Russia, Germany, South Africa). The Royal Society of Chemistry, UK has been consented to publish invited lectures after peer review process in web version of Journal of Materials Chemistry- A/ B/ C.

13.1 Ph.D. Thesis during 2014

1. **Shri Ananda Shamrao Hodage** 'Design, synthesis and characterization of organoselenium compounds' (under the supervision of **Dr. V.K. Jain**) (Ph.D. degree awarded by Mumbai University)
2. **Shri Rakesh Kumar Sharma** 'Synthesis and characterization of single source molecular precursors for binary and ternary materials' (under the supervision of **Dr. V.K. Jain**) (Ph.D. degree awarded by Mumbai University)
3. **Parashiva Prabhu C.** 'Synthesis and physico chemical studies of organoselenium compounds with reference to their biological activities' (under the supervision of **Dr. V.K. Jain/ K.I. Priyadarsini**) (Ph.D. degree awarded by Mumbai University)
4. **Shri A. N. Shirsat**, thesis title: "Physicochemical studies in ceramic proton conductors" (under the supervision of **Dr. S.R. Bharadwaj**) (Thesis submitted to Mumbai University)
5. **Kiran Sanap**, "Development of supported noble metal catalysts for mitigation of hydrogen", (Guide **Dr. S. B. Waghmode** and Co-Guide **Dr. S. Varma**) (Thesis submitted to University of Pune)
6. **Soumitra Das** "Study of laser-cluster interaction in gas phase, (Guide **Dr. R.K. Vatsa**, Thesis submitted to Homi Bhabha National Institute)
7. **Purav Badani** "Study of ionization processes in molecular clusters using mass spectrometry" (Guide **Dr. R. K. Vatsa**, Thesis submitted to Mumbai University).

13.2 M. Sc. Thesis during 2014

1. **Shri Asheesh Kumar**, Thesis title: "Synthesis, characterization and evaluation of hydrogen storage properties of solid materials" (under the supervision of **Dr. S.R. Bharadwaj**) (Thesis submitted in October 2014)
2. **Shri Kamlesh Bairwa** (RPCD), Synthesis, characterization and dissolution of cuprous oxide, iron oxide and their derivatives relevant to BWR condenser tube decontamination (under the supervision of **Dr. A. K. Tyagi**)

14. Miscellaneous

14.1 Activities of electronic support group

Various analytical facilities in the Division were continuously maintained in good working conditions. These include repair of relay board of SIMS, zone refining unit, AFM, induction heater and FT-IR; high temperature XRD, Hiden Isochema HTP analyzers used for studying hydrogen storage; installation of two targets sputtering system; associated in the installation of XPS / AES system. Personal computers and internet and intranet related problems of various PCs have been addressed. In addition development work was also undertaken, viz., (i) designed and developed handheld battery operated interface for H₂S sensor and demonstrated, (ii) portable gas alarm system designed, developed and demonstrated for H₂S, NH₃ and SO₂, (iii) development of high temperature PC- based dilatometer, and (iv) low temperature heat capacity measurement facility.

14.2 Activities of Divisional Workshop

A total of 190 work orders including various cutting, turning, welding, brazing and fitting jobs were completed for various divisions: ChD (91), RPCD (86), ACD (7) and L&PTD (6).

14.3 Analysis Support using Divisional Facilities

Besides research activities procurement, maintenance and upgrading of the existing facilities are addressed. The various facilities in the division are used for analysis of our own samples as well as samples received from other research groups. Samples analyzed by our staffs using the divisional facilities are tabulated below. Generally 20 to 30% of the samples have been received from other research groups of BARC/DAE/outside DAE units

Name of the Instrument	No. of Samples analyzed
Single Crystal XRD (Rigaku AFC-7 S)	15
300 MHz FT NMR	1057
400 MHz FT NMR	517
HPLC	6
Micro-analyzer (CHNS analyzer)	305
FT-IR	59
Philips RT-XRD Unit	6
X'pert Pro HT-XRD unit	587
Rotating anode based XRD	955
PE Hysteresis facility	60
Steady State Emission and Excitation set-up	-
Nd:-YAG pumped OPO	-

Secondary ion Mass Spectrometer (Model-Surface Seer)	31
Resistivity and hall measurement Facility	20
Calvet calorimeter	230
Quadrupole Mass Spectrometer	15
TG-DTA With MS	186
TG-DTA (Setaram)	11
Kundsen Effusion Mass Loss Vapor pressure measurement Technique	Continuous operation
Solution Calorimeter	50
Differential scanning Calorimeter	72
Langmuir Blodgett Trough	84
Atomic Force Microscope (AFM)	23
Potentiostat Galvanostat with Impedance analyzer	211
Potentiostat galvanostat	329
Brewster Angle Microscope (BAM)	-
Wire Bonder	-
Rheometer (light scattering attachment)	4
Dynamic light scattering instrument	1303
Zeta potential analyzer	180
Scanning Electron Microscope (SEM)	306
Energy Dispersive X-Ray Spectrometer (EDX)	274
Raman Spectrometer	187
Integrated Thermo Mechanical Analyzer (TMA)	8
Temperature Modulated Differential Scanning Calorimeter (TMDSC)	105
Sample preparation furnaces	81
Induction Heater	21
Vacuum Coating (gold) Unit	15
Table Top Thermal Evaporation System (for gold)	109
Current Voltage/ photo current measurement set up	49
DR-UV-Vis spectrophotometer	11
ESCA and AES system	3

14.4 Seminars organized during 2014

	Date	Speaker	Title
1	03 January 2014	Prof. Vijay K. Ramani Illinois Institute of Technology, Chicago, USA	Advanced Materials and Diagnostics for Polymer Electrolyte Fuel Cells and Electrolyzers
2	8 January 2014	Prof. Narayan S. Hosmane, Northern Illinois University USA	Nanostructured Boron Clusters, Cages and Dendrimers: From Materials to Cancer Therapy
3	9 January 2014	Dr. C. A. Amarnath, Chemistry Division, BARC	Polyaniline Based Nanostruc- tures Super-capacitor Applica- tion
4	31 January 2014	Prof. Michio Iwaoka, Tokai University, Japan	Design of new selenium antioxidant: Achievements of 6 year collaboration between Tokai and BARC
5	25 March 2014	Dr. G. Kedarnath, Chemistry Division, BARC	Synthesis of luminescent Zn_3P_2 nanocrystals
6	23 April, 2014	Prof. K.B. Pandey, Ex-CSJM University, Kanpur	Glorious History of Chemical Science in India
7	30 July 2014	Dr. Mainak Roy, Chemistry Division, BARC	Nanoparticles Exploiting Bio- Molecules and/ Organisms
8	3 September, 2014	Dr. Kaustava Bhattacharya, Chemistry Division, BARC	Photo-Catalytic Processes: Insight via Molecular Intermediates & Structure -Activity Correlation
9	1 December 2014	Prof. Roop Mallik TIFR Mumbai	The journey of Phagosomes
10	2 December 2014	Prof. Rajdip Bandyopadhyaya, IIT Bombay	How nanoparticles enhance functionality? From water treatment to drug delivery
11	24 December, 2014	Prof. Michio Iwaoka, Tokai University, Japan	Modelling selenoenzyme active sites by using short selenopeptides

15. Technologies from Chemistry Division during 2014

S. No.	Name of the Technology	Status
1.	Dysprosium doped CaSO ₄ for TLD Phosphor	Transferred to M/s Adithisri Radiation Services, Tirupati, through TTCD on 10 January 2014
2.	Zone refining unit for purification of materials	Know-how given to TTCD for technology transfer
3.	Preparation of high purity trimethyl gallium for MOCVD	Know-how given to TTCD for technology transfer
4.	Synthesis of gallium magnesium alloy for the preparation of organogallium compounds	Know-how given to TTCD for technology transfer
5.	Diamond based H ₂ S detector	Know-how given to TTCD for technology transfer
6.	Diamond based α -particle detector	Product accepted by NRG
7.	Dry reduction process of UF ₆ to UF ₄ conversion	Chemical Technology Division, BARC
8.	ZrO ₂ -Pt catalyst for uranyl reduction	Catalyst accepted by NRG and given for large scale production to a private vendor (M/s Monarch Catalysts)
9.	Pt-Pd catalyst for hydrogen mitigation required by NPCIL	Know-how given to TTCD for technology transfer (ECIL is under consideration for large scale production)
Other activities		
1.	Process for ~8 N pure germanium has been developed (HPGe detector program)	Material (2 kg) has been supplied to TPD for single crystal growth
2.	~5 N pure gallium metal prepared	Material (3.02 kg) has been supplied to NFG on 13 August 2014

16. Awards/ Recognition during 2014

1. Dr. C. Majumder: DAE Science and Technical Excellence Award
2. Dr. G. Kedarnath: DAE Science and Technical Excellence Award
3. Dr. A. K. Tyagi: 'MRSI-ICSC Materials Science Senior Award' from Materials Research Society of India
4. Dr. A. K. Tyagi: 'CCRS Award' from Coastal Chemical Research Society, Andhra University, Visakhapatnam
5. Dr. Vinita G. Gupta: 'NASI Membership'; National Academy of Sciences India
6. Dr. Vinita G. Gupta: 'DAE-SSPS-Young Achiever Award' from Solid State Physics Symposium
7. Dr. Farheen N. Sayed : 'Fulbright Fellowship'; USA
8. Ms. K. Vasundhara: ' ISMC-2014 Best Poster Award ISMC-2014'
9. Mr. K. V. Vivekananda was selected for the "Best Poster Award (third prize)" for the poster presentation in ISMC-14
10. A.K. Tripathi -DAE Group Achievement Award for the year 2013 (on contributions made towards EXAFS beam line (BL-09) at INDUS-2, RRCAT, Indore).
11. Ms. Priyanka Ruz received the best Poster Award (2nd prize) for the poster presentation in ISMC-14.
12. Shri. J. Nuwad received the best Poster Award (1st prize) for the poster presented in DAE-SSPS-2014 held at VIT, Vellore (T. N) during Dec.16-20, 2014.

Publications of Chemistry Division (2014)

1. Synthesis, structures and DFT calculations of 2-(4,6-dimethylpyrimidyl)selenolate complexes of Cu(I), Ag(I) and Au(I) and their conversion into metal selenide nano-crystals
R. K. Sharma, A. Wadawale, G. Kedarnath, D. Manna, T. K. Ghanty, B. Vishwanadh and V. K. Jain
Dalton Trans., 43 (2014) 6525-6535. IF = 4.097

2. Cyclopalladation of telluro ether ligands: Synthesis, reactivity and structural characterization
S. Kolay, M. Kumar, A. Wadawale, D. Das and V.K. Jain
Dalton Trans., 43 (2014) 16056-16065. IF = 4.097

3. Stable selones in glutathione peroxidase like catalytic cycle of selenonicotinamide derivative
P. Prabhu, B. G. Singh, M. Nagouchi, P. P. Phadnis, V. K. Jain, M. Iwaoka and K. I. Priyadarsini
Org. Biomol. Chem., 12 (2014) 2404-2412. IF = 3.487

4. Chalcogenocarboranes: A family of multifaceted sterically demanding ligands
L. Jain, V.K. Jain, N. Kushwah, M. K. Pal, A.P. Wadawale, V.I. Bregadze and S.A. Glazum
Coord. Chem. Rev., 258-259 (2014) 72-118. IF = 12.098

5. Pyrazolato-bridged arylpalladium(II) complexes, [Pd₂Ar₂(μ-pz/dmpz)₂(PR₃)₂]: Synthesis and crystal structures
K. R. Chaudhary, A. P. Wadawale and V. K. Jain
J. Organomet. Chem., 760 (2014) 55-59. IF = 2.302

6. Pyrimidyl-2-selenolates of cadmium and mercury: Synthesis, structures and their conversion to metal selenide nano-particles
R.K. Sharma, A. Wadawale, G. Kedarnath, B. Vishwanadh and V.K. Jain
Inorg. Chim. Acta, 411 (2014) 90- 96. IF = 2.041

7. Dimethylaminoalkylchalcogenolate palladium(II) complexes as an efficient copper and phosphine-free catalyst for Sonogashira reaction
B.J. Khairnar, S. Dey, V.K. Jain and B. M. Bhanage
Tetrahedron Lett., 55 (2014) 716- 719. IF = 2.391

8. Palladium(II) chalcogenolate complexes as catalysts for C-C cross-coupling and carbonylative Suzuki coupling reactions
D. K. Paluru, S. Dey, K. R. Chaudhuri, M. V. Khedkar, B. M. Bhanage and V. K. Jain
Tetrahedron Lett., 55 (2014) 2953-2956. IF = 2.391

9. Supramolecular 3-/4-mercapto benzoic acid complexes of palladium(II) and platinum(II) stabilized by hydrogen bonding
K.V. Vivekanada, S. Dey, A. Wadawale, N. Bhuvanesh and V. K. Jain
Eur. J. Inorg. Chem., (2014) 2153- 2161. IF = 2.965

10. Organoselenium compounds based on substituted acetanilides: Synthesis, characterization and antioxidant activity
P. P. Phadnis, A. S. Hodage, K. I. Priyadarsini and V. K. Jain
Indian J. Chem., Sec. A, 53A (2014) 34- 40. IF = 0.628

11. In-vitro antioxidant studies of diselenodinitocotinamide: A potent GPx mimic
Parashiva Prabhu C., B. Adhikari, P. P. Phadnis, S. Chakravorty, V. K. Jain and K. I. Priyadarsini
Indian J. Chem. Sec. A, 53A (2014) 781- 786. IF = 0.628

12. Synthesis, characterization and structures of α-substituted selenenyl acetophenones
S. Hodage, P.P. Phadnis, A. Wadawale, K.I. Priyadarsini and V.K. Jain
Phosphorus, Sulfur, Silicon and Related Elements, 189 (2014) 700-710. IF = 0.827

13. Dimethylgallium/-indium complexes derived from bis(2-hydroxybenzylidene)-1,4-phenylenediamine and bis(2-hydroxybenzylidene)-4,4'-methylenedianiline: Synthesis and structural characterization
N. Kushwah, M.K. Pal, A.P. Wadawale and V.K. Jain
Proceedings of the National Academy of Sciences, Sec.-A 84 (2014) 179-187. IF = 0.179
14. Synthesis, structures and utility of organogallium and indium complexes with oxo- and thio-ligands
V. K. Jain, A. Wadawale, N. P. Kushwah and M. K. Pal
Izv. Akad. Nauk. Ser. Khim., (2014) 781-787; Russian Chem. Bull., 63 (2014) 781-787. IF = 0.509
15. Cyto-genotoxicity assessment of potential radioprotector, 1,3'-diselenodipropionic acid (DSePA) in Chinese Hamster ovary (CHO) cells and human peripheral blood lymphocytes
R. K. Chaurasia, S. Balakrishnan, A. Kunwar, U. Yadav, N. Bhat, K. Anjaria, R. Nairy, B. K. Sapra, V. K. Jain and K. I. Priyadarsini
Mutation Research/Genetics Toxicology and Environmental Mutagenesis, 774 (2014) 8-16. IF = 2.481
16. Pulse radiolysis studies of 3,5-dimethylpyrazole derivatives of seleno ethers
Atnu Barik, B.G. Singh, A. Sharma, V.K. Jain and K.I. Priyadarsini
J. Phys. Chem.-A, 118 (2014) 10179 – 10187. IF = 2.775
17. Silver(I) coordination polymer of 4,4'-dipyridyl selenide and its solvothermolysis
G.K. Kole, K.V. Vivekananda, M. Kumar, S. Dey and V.K. Jain
International J. Chem., 3 (2014) 263-268. IF = 1.438
18. Electrochemical characterization of Mn: Co₃O₄ Thin films prepared by spray pyrolysis via aqueous route
R.C. Ambare, S. R. Bharadwaj and B. J. Lokhande
Current Applied Physics, 14 (2014) 1582-1590. IF = 2.026
19. Supported Pt nanoparticles for the hydrogen mitigation application
Kiran K. Sanap, S. Varma, S.B. Waghmode and S.R. Bharadwaj
International Journal of Hydrogen Energy, 39 (2014) 15142-15155. IF = 2.930
20. Effect of Mo-Incorporation in the TiO₂ Lattice: A Mechanistic Basis for Photocatalytic Dye Degradation.
K. Bhattacharyya, J. Majeed, K.K. Dey, P. Ayyub, A.K. Tyagi and S.R. Bharadwaj
J. Phys. Chem. C, 118 (2014) 15946-15962. IF = 4.835
21. Thermodynamic stability and impedance measurements of perovskite LuRhO₃(s) in the Lu–Rh–O system
Aparna Banerjee, Pooja Sawant, R. Mishra, S. R. Bharadwaj and A. R. Joshi
RSC Advances, 4 (2014) 19953–19959. IF = 3.708
22. Photocatalytic hydrogen generation from water using a hybrid of graphene nanoplatelets and self doped TiO₂-Pd
Fareen N. Sayed, R.Sasikala, O.D. Jayakumar, R. Rao, C.A. Betty, A. Chokkalingam, R.M. Kadam, Jagannath, S.R. Bharadwaj, Ajayan Vinu and A.K. Tyagi,
RSC Advances, 4 (2014) 13469-13476. IF = 3.708
23. Effect of Ni Concentration on Phase Stability, Microstructure and Electrical Properties of BaCe_{0.8}Y_{0.2}O_{3-δ} Ni Cermet SOFC Anode and its application in proton conducting ITSOFC
Pooja Sawant, S. Varma, M. R. Gonal, B. N. Wani, Deep Prakash and S. R. Bharadwaj
Electrochimica Acta, 120 (2014), 80-85. IF = 4.086
24. Thermal Optimization and Supercapacitive Application of Electrodeposited Fe₂O₃ Thin Films
B. J. Lokhande, R. C. Ambare, S. R. Bharadwaj
Measurement, 47 (2014) 427-432. IF = 1.526
25. Hydrothermal synthesis of Ag@TiO₂-Fe₃O₄ nanocomposites using sonochemically activated precursors: magnetic, photocatalytic and antibacterial properties,
Anuja Bokare, Hema Singh, Mrinal Pai, Roopa Nair, Sushma Sabharwal and Anjali A Athawale
Materials Research Express, 1 (2014) 046111. IF = ----

26. Pd-TiO₂-SrIn₂O₄ Heterojunction Photocatalyst: Enhanced Photocatalytic Activity for Hydrogen Generation and Degradation of Methylene Blue
Sanjay B. Kokane, S. D. Sartale, C. A. Betty and R. Sasikala
RSC Adv., 4 (2014) 55539-55547. IF = 3.708
27. Enhanced photocatalytic activity of TiO₂ assisted by Nb, N and S multidopants
Sachin G. Ghugal, Suresh S. Umare and R. Sasikala
Mater. Res. Bull., 61 (2014) 298–305. IF = 1.968
28. Enhanced photodegradation of dyes on Bi₂O₃ microflakes: Effect of GeO₂ addition on photocatalytic activity
Charanpahari, S. S. Umare and R. Sasikala
Sep. Purif. Technol., 133 (2014) 438–442. IF = 3.065
29. Vanadium doped TiO₂ :An efficient visible light active photocatalyst
S.S. Arbuj, K.M.Kale, V.S.Patil, P.K. Chattise, R.R.Hawaladar and B. N. Wani,
J. Nanoengineering & Nanomanu, 4 (2014) 1-8. IF = -----
30. Effect of annealing environment on low temperature magnetic dielectric properties of EuCo_{0.5}Mn_{0.5}O₃
V. Katari, S. N. Achary, S. K. Deshpande, P. D. Babu, H. G. Salunke, N. Gupta, and A. K. Tyagi
J. Phys. Chem. C, 118 (2014) 17900–17913. IF = 4.835
31. Effect of grain size and microstructure on radiation stability of CeO₂: An extensive study
V. Grover, R. Shukla, Renu Kumari, B. P. Mandal, P. K. Kulriya, S. K. Srivastava, S. Ghosh, A. K. Tyagi and D. K. Avasthi
Phys. Chem. Chem. Phys., 16 (2014) 27065-27073. IF = 4.198
32. Improved magnetic and ferroelectric properties of Sc and Ti codoped multiferroic nano BiFeO₃ prepared via sonochemical synthesis
D. P. Dutta, B. P. Mandal, M. D. Mukadam, S. M. Yusuf and A. K. Tyagi
Dalton Trans. 43 (2014) 7838-7846. IF = 4.097
33. High adsorption capacity for cationic dye removal and antibacterial properties of sonochemically synthesized Ag₂WO₄ nanorods
A. Singh, D. Dutta, A. Ballal and A. K. Tyagi
Eur. J. Inorg. Chem., 2014) 5724-5732. IF = 2.965
34. Improvement of magnetodielectric coupling by surface functionalization of nickel nanoparticle in Ni and polyvinylidene fluoride nano-hybrids
B. P Mandal, K. Vasundhara, E. Abdelhamid, G. Lawes, H. G. Salunke and A. K. Tyagi
J. Phys. Chem. C, 118 (2014) 20819–20825. IF = 4.835
35. Quest for lead free relaxors in YIn_{1-x}Fe_xO₃ (0.0 ≤ x ≤ 1.0) system: Role of synthesis and structure
R. Shukla, F. N. Sayed, V. Grover, S. K. Deshpande, A. Guleria and A. K. Tyagi
Inorg. Chem., 53 (2014) 10101–10111. IF = 4.794
36. Phonons, lithium diffusion and thermodynamics of LiMPO₄ (M = Mn, Fe)
P. Goel, M. K. Gupta, R. Mittal, S. L. Chaplot, S. Rols, S. J. Patwe, S. N. Achary and A. K. Tyagi
J. Mater. Chem. A, 2 (2014) 14729-14738. IF = pending
37. Sorption of dyes and Cu(II) ions from waste water by sonochemically synthesized MnWO₄ and MnMoO₄ nanostructures
Dimple P. Dutta, A. Mathur, J. Ramakumar and A. K. Tyagi
RSC Advances 4 (2014) 37027-37035. IF = 3.708
38. Nano-Cerium Vanadate: A Novel Inorganic Ion Exchanger for Removal of Americium and Uranium from Simulated Aqueous Nuclear Waste
C. Banerjee, N. Dudwadkar, S. C. Tripathi, P. M. Gandhi, V. Grover, C. P. Kaushik and A. K. Tyagi
J. Hazard. Mater., 280 (2014) 63-70. IF = 4.331

39. Structural and luminescence studies on barium sodium borosilicate glasses containing uranium oxides
R. K. Mishra, V. Sudarsan, S. Jain, C. P. Kaushik, R. K. Vatsa and A. K. Tyagi
J. Am. Ceram. Soc. 97 (2014) 427–431. IF = 2.428
40. Disorder-induced Room Temperature Ferromagnetism in Glassy Chromites
C. Moyses Araujo, Sandeep Nagar, Muhammad Ramzan, R. Shukla, O.D. Jayakumar, A.K. Tyagi, Yi-Sheng Liu, Jeng-Lung, Per-Anders Glans, Chinglin Chang, Andreas Blomqvist, Raquel Lizárraga, Erik Holmström, Lyubov Belova, Jinghua Guo, Rajeev Ahuja, K.V.Rao
Scientific Reports Nature 4 (2014) 4686 (6 pp) IF = 5.078
41. Phase evolution and microstructural studies in CaZrTi₂O₇ (zirconolite)-Sm₂Ti₂O₇ (pyrochlore) system
M. Jafar, P. Sengupta, S. N. Achary and A. K. Tyagi
J. Eur. Ceram. Soc., 34 (2014) 4337-4381. IF = 2.307
42. Standard Molar Enthalpy of Formation of Ce₂Zr₂O₈
S. Phapale, R. Shukla, R. Mishra and A. K Tyagi
J. Alloys and Comp., 615 (2014) 792-794. IF = 2.726
43. Enhanced specific absorption rate in silanol functionalized Fe₃O₄ core - shell nanoparticles: study of Fe leaching in Fe₃O₄ and hyperthermia in L929 and HeLa cells
J. Majeed, L. Pradhan, R. S. Ningthoujam, R. K. Vatsa, D. Bahadur and A. K. Tyagi
Colloids and Surfaces B: Biointerfaces 122 (2014) 396-403. IF = 4.287
44. Role of annealing atmosphere on structure and magnetic properties of La₂CoMnO₆ and La₂MgMnO₆ double perovskites
Farheen N. Sayed, S. N. Achary, S. K. Deshpande, B. Rajeswari, R. M. Kadam, S. Dwibedi, A. K. Nigam and A. K. Tyagi
Z. Anorg. Allg. Chem., 640 (2014) 1907-1921. IF = 1.251
45. Phase Transitions in Delafossite CuLaO₂ at High Pressures
N. P. Salke, A. B. Garg, Rekha Rao, S. N. Achary, M. K. Gupta, R. Mittal and A. K. Tyagi
J. Appl. Phys., 115 (2014) 133507. IF = 2.186
46. Low temperature Neutron Diffraction Study of Nd_{1-x}Sr_xCrO₃ (0.05 ≤ x ≤ 0.15)
Keka R. Chakraborty, S. Mukherjee, S. D. Kaushik, S. Rayaprol, C. L. Prajapat, M. R. Singh, V. Siruguri, A. K. Tyagi and S. M. Yusuf
J. Magn. Magn. Mater., 361 (2014) 81–87. IF = 2.002
47. Sorption of Americium from low level liquid wastes by nanocrystalline MnO₂
K. Bhagyashree, A. Kar, S. Kasar, S. Kumar, R. K. Mishra, C. P. Kaushik, R. Shukla, A. K. Tyagi and B. S. Tomar
J. Radioanal. Nucl. Chem., 299 (2014) 1433-1437. IF = 1.415
48. Structural and oxide ion conductivity studies on Yb_{1-x}Bi_xO_{1.5} (0.00 ≤ x ≤ 0.50) composites
K. Vasundhara, S. N. Achary, S. J. Patwe, A. K. Sahu, N. Manoj and A. K. Tyagi,
J. Alloys Comp., 596 (2014) 151-157. IF = 2.726
49. Sonochemical synthesis, characterization and photocatalytic properties of Bi_{2-x}Sb_xWO₆ nanorods
A. Singh, Dimple P. Dutta, M. Roy, A. K. Tyagi and M. H. Fulekar
J. Mater. Science, 49 (2014) 2085-2097. IF = 2.305
50. Visible light driven photocatalysis and antibacterial activity of AgVO₃ and Ag/AgVO₃ Nano wires
A. Singh, D. P. Dutta, A. Ballal, A. K. Tyagi and M. H. Fulekar
Mater. Res. Bull., 51 (2014) 447–454. IF = 1.968
51. Efficient photocatalytic degradation of rhodamine B dye by aligned arrays of self-assembled hydrogen titanate nanotubes
Sriparna Chatterjee, A. K Tyagi and Pushan Ayyub
J. Nanomaterials (2014), Article ID 328618, 7 pages IF = 1.611

52. Morphology and luminescence characteristics of combustion synthesized Y_2O_3 : (Eu, Dy, Tb) nanoparticles with various amino-acid fuels.
Srirupa T. Mukherjee, V. Sudarsan, P. U. Sastry, A. K. Patra and A. K. Tyagi
J. Lumin., 145 (2014) 318-323. IF = 2.367
53. Facile synthesis of flower like FePt@ZnO core-shell structure and its bifunctional properties
J. Majeed, O. D. Jayakumar, H. G. Salunke, B. P. Mandal, R. Naik, and A. K. Tyagi
J. Alloys Comp., 597 (2014) 95-100. IF = 2.726
54. Ag incorporated nano $BiPO_4$: Sonochemical synthesis, characterization and improved visible light Photocatalytic properties.
M H Fulekar, A. Singh, D. Dutta, M. Roy, A. Ballal and A. K. Tyagi
RSC Advances, 4 (2014) 10097-10107. IF = 3.708
55. Phase evolution and Microstructural studies in $CaZrTi_2O_7$ - $Nd_2Ti_2O_7$ system
M. Jafar, P. Sengupta, S. N. Achary and A. K. Tyagi
J. Am. Ceram., Soc., 97 (2014) 609-616. IF = 2.428
56. Optical properties of sonochemically synthesized rare earth ions doped $BaTiO_3$ nanophosphors: Probable candidate for white light emission
Dimple P. Dutta, A. Ballal, J. Nuwad and A. K. Tyagi
J. Lumin., 148 (2014) 230-237. IF = 2.367
57. Experimental evidence for pressure-driven isostructural and symmetry breaking phase transitions on $Bi_{14}CrO_{24}$
D. Errandonea, D. Santamaria-Perez, S.N. Achary and A.K. Tyagi
Solid State Commun., 182 (2014) 50-54. IF = 1.698
58. In situ high-pressure synchrotron X-ray diffraction study of the structural stability in $NdVO_4$ and $LaVO_4$
D. Errandonea, C. Popescu, S. N. Achary, A. K. Tyagi and M. Bettinelli
Mater. Res. Bull., 50 (2014) 279-284. IF = 1.698
59. Enhanced thermoelectric properties of selenium-deficient layered $TiSe_{2-x}$: a charge-density-wave material.
Ranu Bhatt, Shovit Bhattacharya, Ranita Basu, Sajid Ahmad, A. K. Chauhan, G. S. Okram, Pramod Bhatt, Mainak Roy, M. Navaneethan, Y. Hayakawa, A. K. Debnath, Ajay Singh, D. K. Aswal, and S. K. Gupta
ACS Appl. Mater. Interfaces, 6 (2014) 8619-18625. IF = 5.900
60. Improved thermoelectric performance of hot pressed nanostructured n-type SiGe bulk alloys
Ranita Basu, Shovit Bhattacharya, Ranu Bhatt, Mainak Roy, Sajid Ahmad, Ajay Singh, M. Navaneethan, Y Hayakawa, D. K. Aswal and S. K. Gupta
J. Mater. Chem. A, 2 (2014) 6922-6930. IF = pending
61. Phase transformation in relaxor-ferroelectric single crystal $[Pb(Sc_{1/2}Nb_{1/2})O_3]_{0.58}[PbTiO_3]_{0.42}$
S. V. Rajasekaran, S. N. Achary, S. J. Patwe, R. Jayavel and G. Mangamma
J. Mater. Res., 29 (2014) 1054-1061. IF = 1.815
62. Photophysical, band structural, and textural properties of o- $FeNbO_4$ in relation to its co-catalyst assisted photoactivity for water oxidation
R. Babu, S. Kelkar, V. Kashid, S. N. Achary, H. G. Salunke and N. M. Gupta
RSC Advances, 4 (2014) 33435-33445. IF = 3.708
63. Photoinduced Second Harmonic Generation for the In_2O_3 Nanoparticles Embedded into the PMMA Polymers
A.H.Reshak, Anshu Singhal, Sipra Choudhury, Z. A. Alahmed, A.O.Fedorchuk, A.Wojciechowki and H. Kamarudin
Int. J. Electrochem. Sci., 9 (2014) 6370-6377. IF = 1.956
64. Preferential leaching of Sr from mixed (Th/Sr) oxide
C. K. Vyas, P.M. Joshirao, R. Shukla, V. Natarajan and V.K. Manchanda
Desalin. Wat. Treat., 52 (2014) 476-480. IF = 0.987

65. Carbon-Doped Boron Nitride Nanomesh: Stability and Electronic Properties of Adsorbed Hydrogen and Oxygen
G.C. Loh, S. Nigam, G. Mallick and R. Pandey
J. Phys. Chem. C, 118 (2014) 23888-23896. IF = 4.835
66. The structural and electronic properties of Au_n clusters on the α -Al₂O₃(0001) surface: A first principles study
C. Rajesh, S. Nigam, and C.Majumder;
Phy. Chem. Chem. Phys., 16 (2014) 26561-26569. IF = 4.198
67. Comparison between cluster and slab model for Pt-group atom adsorption on gold and silver substrate
S. Nigam and C.Majumder
Surface Science 630 (2014) 78–84. IF = 1.870
68. A theoretical study of structural and electronic properties of alkaline-earth fluoride clusters,
R. K. Pandey, K. Waters, S. Nigam, H. He, S. S. Pingale, A. C. Pandey, R.Pandey
Computational and Theoretical Chemistry, 1043 (2014) 24-30. IF = 1.368
69. Nano-size effects on the nature of bonding in Y₂Sn₂O₇: EXAFS and Raman spectroscopic investigation
C. Nayak, S. Nigam, M.Pandey, C Majumder, S N Jha, D Bhattacharyya and R. K. Vatsa
Chem. Phys. Lett., 597 (2014) 51-56. IF = 1.991
70. Synthesis, Characterization and Biocompatibility of Chitosan functionalized superparamagnetic nanoparticles for heat activated curing of cancer cells
N. D. Thorat, S. V. Otari, R. M. Patil, R. A. Bohara, H. M. Yadav, V. B. Koli, A. K. Chaurasia and R. S. Ningthoujam
Dalton Trans., 43 (2014) 17343-17351. IF = 4.097
71. Enhanced up-conversion and temperature-sensing behaviour of Er³⁺ and Yb³⁺ co-doped Y₂Ti₂O₇ by incorporation of Li⁺ ions
B. P. Singh, A. K. Parchur, R. S. Ningthoujam, P. V. Ramakrishna, R. Maalej, P. Singh and S. B. Rai
Phy. Chem. Chem. Phys., 16 (2014) 22665-22676. IF = 4.198
72. Structured superparamagnetic nanoparticles for high performance mediator of magnetic fluid hyperthermia: Synthesis, colloidal stability and biocompatibility evaluation
N. D. Thorat, S. V. Otari, R. A. Bohara, H. M. Yadav, V. M. Khot, A. B. Salunkhe, M. R. Phadatar, A. I. Prasad, R. S. Ningthoujam and S. H. Pawar
Materials Science and Engineering: C, 42 (2014) 637-646. IF = 2.736
73. Multifunctional hybrid nanomaterials from water dispersible CaF₂:Eu³⁺, Mn²⁺ and Fe₃O₄ for luminescence and hyperthermia application
L. P. Singh, S. K. Srivastava, R. Mishra and R. S. Ningthoujam
J. Phys. Chem. C, 118 (2014) 18087-18096. IF = 4.837
74. Is higher ratio of monoclinic to tetragonal in LaVO₄ a better luminescence host? Redispersion and polymer film formation
R. Okram, N. Yaiphaba, R. S. Ningthoujam and N. R. Singh
Inorg. Chem., 53 (2014) 7204-7213. IF = 4.794
75. Ce³⁺ sensitized GdPO₄:Tb³⁺ nanorods: An investigation on energy transfer, luminescence switching and quantum yield
N. K. Sahu, N. S. Singh, R. S. Ningthoujam and D. Bahadur
ACS Photonics, 1 (2014) 337-346. IF = -----
76. Colloidal stability of polyethylene glycol functionalized Co_{0.5}Zn_{0.5}Fe₂O₄ nanoparticles: effect of pH, sample and salt concentration for hyperthermia application
D. S. Nikam, S. V. Jadhav, V. M. Khot, R. S. Ningthoujam, C. K. Hong, S. S. Mali and S. H. Pawar,
RSC Advances, 4 (2014) 12662-12671. IF = 3.708

77. Enhanced photoluminescence in $\text{CaMoO}_4:\text{Eu}^{3+}$ by Gd^{3+} co-doping
B. P. Singh, A. K. Parchur, R. S. Ningthoujam, A. A. Ansari, P. Singh and S. B. Rai
Dalton Trans., 43 (2014) 4779-4789. IF = 4.090
78. Influence of Gd^{3+} co-doping on structural property of $\text{CaMoO}_4:\text{Eu}$ nanoparticles
B. P. Singh, A. K. Parchur, R. S. Ningthoujam, A. A. Ansari, P. Singh and S. B. Rai
Dalton Trans., 43 (2014) 4770-4778. IF = 4.097
79. Non-aqueous to aqueous phase transfer of oleic acid coated iron oxide nanoparticles for hyperthermia application
R. M. Patil, P. B. Shete, N. D. Thorat, S. V. Otari, A. I. Prasad, R. S. Ningthoujam, B. Tiwale and S. H. Pawar
RSC Advances, 4 (2014) 4515-4522. IF = 3.708
80. Enhanced luminescence of $\text{CaMoO}_4:\text{Eu}$ by core@shell formation and its hyperthermia study after hybrid formation with Fe_3O_4 : Cytotoxicity assessing on human liver cancer cells and mesenchymal stem cells
A.K. Parchur, A. A. Ansari, B. P. Singh, T. N. Hasan, N. A. Syed, S. B. Rai and R. S. Ningthoujam
Integrative Biology, 6 (2014) 53-64. IF = 3.996
81. Superparamagnetic iron oxide/chitosan core/shells for hyperthermia application: Improved colloidal stability and biocompatibility
R. M. Patil, P. B. Shete, N. D. Thorat, S. V. Otari, K. C. Barick, A. Prasad, R. S. Ningthoujam, B. M. Tiwale and S. H. Pawar
J. Magn. Magn. Mater., 355 (2014) 22-30. IF = 2.002
82. Magnetic Chitosan Nanocomposite For Hyperthermia Therapy Application: Preparation, Characterization and In Vitro Experiments
P. B. Shete, R. M. Patil, N. D. Thorat, A. Prasad, R. S. Ningthoujam, S. J. Ghosh and S. H. Pawar
Applied Surface Science, 288, (2014) 149-157 IF = 2.538
83. Evidence for charge-induced dipole reaction in laser ionized van der Waals clusters: A case of Fe^{2+} reacting with argon atoms inside a cluster
P.M. Badani, S. Das, P. Sharma, KRS Chandra Kumar and R.K. Vatsa
RSC Advances, 4 (2014) 2339-2345. IF = 3.708
84. Generation of multiply charged tin and carbon ions in low intensity Coulomb explosion of tetramethyl tin clusters: Role of screening effects
P.M. Badani, S. Das, P. Sharma and R.K. Vatsa
Int. J. Mass Spectrom., 358 (2014) 36-42. IF = 2.227
85. Fabrication of a novel biocompatible magnetic biomaterial with hyperthermia potential
R. Karunamoorthi, G.Suresh Kumar, R.K.Vatsa, A.Thamizhavel and E.K. Girija
J. Amer. Ceram. Soc., 97 (2014) 1115-1122. IF = 2.428
86. Nature of WO_4 tetrahedra in blue light emitting CaWO_4 probed through the EXAFS technique
S. Basu, B.S. Naidu, B. Viswanadh, V. Sudarsan, S. N. Jha, D. Bhattacharyya and R. K. Vatsa
RSC Advances, 4 (2014) 15606-15612. IF = 3.708
87. Characterization of composites of Beryllia and Lithium titanate produced by sol gel route
B N Rath, S J Ghanwat, R. Mishra, S. Bhattacharya, S. Kaity, C. Danani, S. Kumar, V. D. Alur, N. Kumawat, D Sathiyamoorthy and S Anantharama
Ceram-Silikaty, 58 (2014) 123-131. IF = 0.418
88. Interaction of Alumina with $\text{Pb}_{83}\text{Li}_{17}$ Alloy
Uttam Jain, Abhishek Mukherjee, Sanjay Kumar, Ratikanta Mishra and Nagaiyar Krishnamurthy
Fusion Engineering and Design, 89 (2014) 2554–2558. IF = 1.149
89. Synthesis and characterization of composites of beryllia and lithium-titanate produced by solid state route
B. N. Rath, S. J. Ghanwat, R. Mishra, S. Bhattacharya, S. Kaity, C. Danani, S. Kumar and V. D. Alur
J.Modern Chemistry & Chemical Technology, 5 (2014) 17-27. IF = -----

90. Phase Equilibria in the Ternary Ni-Sb-Sn System: Experiments and Calculations
Ratikanta Mishra, Divakar Rajamohan, Hans Flandorfer, Andrew Watson, Herbert Ipser, and Ales Kroupa
CALPHAD: Computer Coupling of Phase Diagrams and Thermochemistry, 45 (2014) 151–166. IF = 1.394
91. Standard molar enthalpy of formation of FeGe (s) and FeGe₂(s) intermetallic compounds
S. Phapale, P. Samui, P. U. Sastry P. K. Mishra and R. Mishra
J. Alloys and Compounds, 591 (2014) 170-173. IF = 2.726
92. Partial Phase diagram of BaO-TeO₂ System
R. Mishra, S. Phapale, P. Samui and S. R. Dharwadkar
J. Phase Equilibria and Diffusion, 35 (2014) 127-136. IF = 0.490
93. Determination of thermodynamic stability of Lanthanum chloride hydrates (LaCl₃.xH₂O) by dynamic transpiration method
D. K. Sahoo, R. Mishra, H. Singh and N. Krishnamurthy
J Alloys and Compounds, 588 (2014) 578-584. IF = 2.726
94. Phase separations in aerosol OT reverse micellar solutions in dodecane: A curious case of polar domain composition driven transition from lower consolute temperature (LCT) to upper consolute temperature (UCT) regime.
R. Ganguly
J. Colloid Inter. Sci., 430 (2014) 234-238. IF = 3.552
95. Reliability studies of highly sensitive and specific multi-gas sensor based on nanocrystalline SnO₂ film.
C.A. Betty, Sipra Choudhury and K.G. Girija
Sensors and Actuators B, 193 (2014) 484– 491. IF = 3.840
96. Multistep hydrothermal (MSH) route for nanocoral architecture of anatase TiO₂: Synthesis and characterization of dye-sensitized solar cell performance
Sawanta S. Mali, Pravin S. Shinde, C. A. Betty, Popatrao N. Bhosale, Won J. Lee and P. S. Patil
Progress in Photovoltaics: Research and applications, 22 (2014) 525-539. IF = 9.696
97. From nanocorals to nanorods to nanoflowers nanoarchitecture for efficient dye-sensitized solar cells at relatively low film thickness: All Hydrothermal Process
Sawanta S. Mali, C. A. Betty, P. N. Bhosale, P. S. Patil and C. K. Hong
Scientific Reports: Nature publishing group, 4 (2014) 5451. IF = 5.078
98. Water dispersible Ag@polyaniline-pectin as supercapacitor electrode for physiological environment
C. A. Amarnath, V. Nandakumar, M. Doble and S. N. Sawant
J. Mater. Chem. B, 2 (2014) 5012–5019. IF = pending
99. Pectin coated polyaniline nanoparticles for an amperometric glucose biosensor
B. Thakur, C. A. Amarnath and S. N. Sawant
RSC Adv., 4 (2014) 40917–40923. IF = 3.708
100. Sum frequency generation spectroscopy of an adsorbed monolayer of mixed surfactants at an air-water interface
A. Saha, H. P. Upadhyaya, Awadhesh Kumar, Sipra Choudhury and P. D. Naik
J Phys Chem. C, 118 (2014) 3145-3155. IF = 4.835
101. Nanobrick-like WO₃ Thin Films: Hydrothermal Synthesis and Electrochromic Application
Vijay Kondalkar; R R Kharade, S S Mali, R M Mane, P B Patil, P S Patil, S. Choudhury and P.N. Bhosale
Superlattices and Microstructures, 73 (2014) 290-295. IF = 1.979
102. Microwave-assisted rapid synthesis of highly porous TiO₂ thin films with nanocrystalline framework for efficient photoelectrochemical conversion.
V. V. Kondalkar, S. S. Mali, N. B. Pawar, R. M. Mane, S. Choudhury, C. K. Hong, P. S. Patil, S. R. Patil, P. N. Bhosale and J. H. Kim
Electrochimica Acta, 143 (2014) 89-97. IF = 1.529

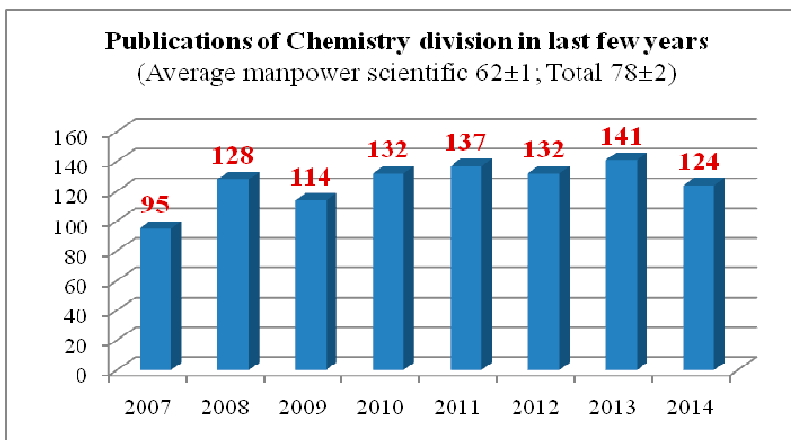
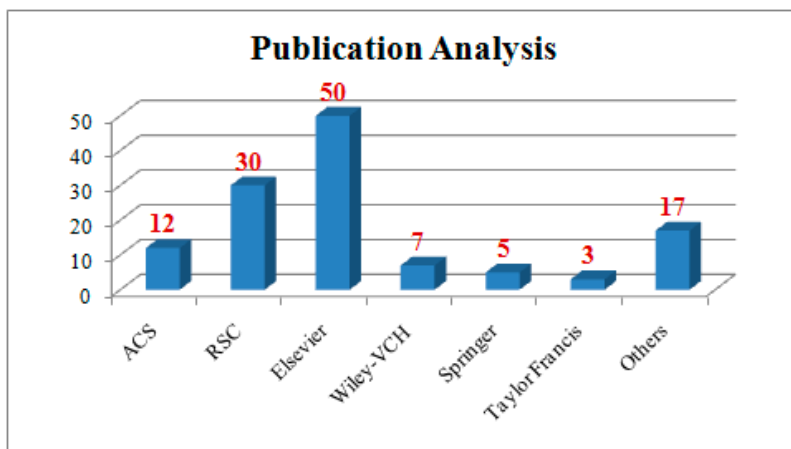
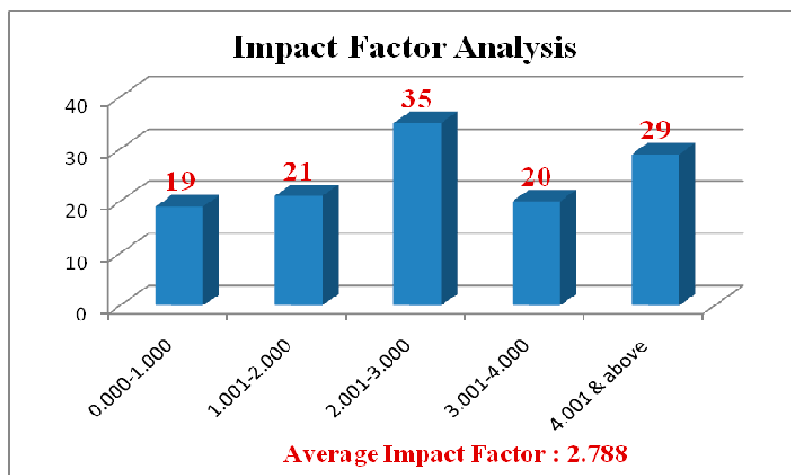
103. Probing the annealing induced molecular ordering in bulk heterojunction polymer solar cells using in-situ Raman spectroscopy
P. Veerender, Vibha Saxena, A. K. Chauhan, S. P. Koiry, P. Jha, Abhay Gusain, Sipra Choudhury, D. K. Aswal and S. K. Gupta
Solar Energy Materials and Solar Cells, 120 (2014) 526-535. IF = 5.030
104. Dynamic interfacial behaviour of poly(oxyethylene) lauryl ether based surfactant mixtures
A. Goswami, Gunjan Verma, P. A. Hassan, V. K. Aswal and S. S. Bhagwat
J. Disper. Sci. Technol., 35 (2014) 1717-1726. IF = 0.705
105. Effect of ethylene glycol on the special counter ion binding and microstructures of sodium dioctylsulfosuccinate micelles
J. Dey, S. Kumar, A. Srivastava, G. Verma, P. A. Hassan, V. K. Aswal, J. Kohlbrecher and K. Ismail
J. Colloid & Interface Sci., 414 (2014) 103-109. IF = 3.552
106. Biocompatible phosphate anchored Fe₃O₄ nanocarriers for drug delivery and hyperthermia
P. Sharma, S. Rana, K. C. Barick, C. Kumar, H. G. Salunke and P. A. Hassan
New. J. Chem., 38 (2014) 5500-5508. IF = 3.159
107. Polyaniline shell cross-linked Fe₃O₄ magnetic nanoparticles for heat activated killing of cancer cells
S. Rana, N. V. Jadhav, K. C. Barick, B. N. Pandey and P. A. Hassan
Dalton Trans., 43 (2014) 12263-12271. IF = 4.097
108. Protein nanoparticle electrostatic interaction: Size dependent counterions induced conformational change of hen egg white lysozyme
G. Ghosh, L. Panicker and K. C. Barick
Colloids Surf. B: Biointerfaces, 118 (2014) 1-6. IF = 4.287
109. Selective binding of proteins on functional nanoparticles via reverse charge parity model: An in vitro study
G. Ghosh, L. Panicker and K. C. Barick,
Mater. Res. Express 1 (2014) 015017. IF = -----
110. Fabrication and properties of Co doped ZnO assemblies
K. C. Barick, M. Aslam and D. Bahadur
J. Alloys Comp., 587 (2014) 282-286. IF = 2.726
111. Carboxyl decorated Fe₃O₄ nanoparticles for MRI diagnosis and localized hyperthermia
K. C. Barick, S. Singh, D. Bahadur, M. A. Lawande, D. P. Patkar and P. A. Hassan
J. Colloids Interf. Sci., 418 (2014) 120-125. IF = 3.552
112. Radiolytic preparation, characterization and catalytic properties of Pt/AlMCM-41
R. Vijayalakshmi, V. Sudarsan, G. K. Dey and S. K. Kulshreshtha
Ind. J. Chem. Sec. A, 53 (2014) 1338-1343. IF = 0.628
113. Concentration dependent luminescence studies on Eu³⁺ doped telluro fluoroborate glass
R. Vijayakumar, K. Maheshvaran, V. Sudarsan and K. Marimuthu
J. Lumin., 154 (2014) 160-167. IF = 2.367
114. The impact of lattice strain on optical properties of CdS nanocrystals
N. Pote, C. Phadnis, K. Sonawane, V. Sudarsan and S. Mahamuni
Solid State Commun., 192 (2014) 6-9. IF = 1.698
115. Disordered Self Assembled Monolayer Dielectric Induced Hysteresis in Organic Field Effect Transistors
N. Padma, V. Saxena, V. Sudarsan, H. Raval and S. Sen
J. Nanosci & Nanotec., 14 (2014) 4418-4423. IF = 1.339
116. Influence of Al³⁺ ions on self up-conversion in Ho³⁺ doped lead silicate glasses
K. Bhargavi, M. Sundara Rao, V. Sudarsan, Ch. Srinivasa Rao, M. Piasecki, I.V. Kityk, M. Srinivasa Reddy and N. Veeraiah
Opt. Mater., 36 (2014) 1189-1196. IF = 2.075

117. A study of charge transfer mechanism and optical properties of Au-CdS core-shell nanocrystals
S. V. Kahane, V. Sudarsan and S. Mahamuni
J. Lumin., 147 (2014) 353-357. IF = 2.367
118. Ultrasensitive, highly selective and naked eye colorimetric recognition of D-penicillamine in aqueous media by CTAB capped AgNPs: applications to pharmaceutical and biomedical analysis
L. S. Walekar, U. R. Kondekar, A. H. Gore, S. P. Pawar, V. Sudarsan, P. V. Anbhule, S. R. Patil and G. B. Kolekar
RSC Adv., 4 (2014) 58481-58488. IF = 3.708
119. Electron energy level engineering in Zn_{1-x}Cd_xSe nanocrystals
K. G. Sonawane, C. Phadnis, L. Tatikondewar, V. Sudarsan, A. Kshirsagar and S. Mahamuni
J. Mater. Chem. C, 2 (2014) 8077-8082. IF = pending
120. Mesoporous SAPO-5 (MESO-SAPO-5): a potential catalyst for hydroisomerisation of 1-octene
A. K. Singh, R. Yadav, V. Sudarsan, K. Kishore, S. Upadhyayula and A. Sakthivel
RSC Adv., 4 (2014) 8727-8734. IF = 3.708
121. Hydrogen absorption characteristics and Mössbauer spectroscopic study of Ti_{0.67}Nb_{0.33-x}Fe_x (x = 0.00, 0.13, 0.20) alloys
Priyanka Ruz, Asheesh Kumar, Seemita Banerjee, S.S. Meena and C.G.S. Pillai
J. Alloys Compounds, 585 (2014) 120-128. IF = 2.726
122. Core-Shell Prussian Blue Analogue Molecular Magnet Mn_{1.5}[Cr(CN)₆]•mH₂O@Ni_{1.5}[Cr(CN)₆]•nH₂O for Hydrogen Storage
Pramod Bhatt, Seemita Banerjee, Sharmistha Anwar, Mayuresh D. Mukadam, Sher Singh Meena, and Seikh M. Yusuf,
ACS Appl. Mater. Interfaces, 6 (2014) 17579-17588. IF = 5.900
123. Improvement on the Hydrogen Storage Properties of ZrFe₂ Laves Phase Alloy by Vanadium Substitution
Seemita Banerjee, A. Kumar and C. G. S. Pillai,
Intermetallics, 51 (2014) 30-36. IF = 2.119
124. An electrochemical pathway to prepare circular planar ⁹⁰Sr/⁹⁰Y sources for the calibration of surface contamination monitors
Manoj Kumar, Shyamala S. Gandhi, J. Nuwad, J. Udhayakumar and A. Dash
J. Radioanal. Nucl. Chem., 302 (2014) 709-719. IF = 1.415

Other Publications

1. Materials Challenges in Renewable Hydrogen Production
A. M. Banerjee, M. R. Pai, A. K. Tripathi and S. R. Bharadwaj
SMC Bulletin, Volume 5 (2014) 17-29.
2. Chemical Vapor Deposited Diamond Thin Films: A Brief Overview on Synthesis and Characterization
J. Nuwad, Dheeraj Jain, C.G.S. Pillai and V. Sudarsan
SMC Bulletin 5 (2014) 15-25.
3. Application of Metal Hydride System for Hydrogen Storage
Seemita Banerjee, Priyanka Ruz, Asheesh Kumar, C. G. S. Pillai,
SMC Bulletin, 5 (2014) 8-16.
4. Phase Transition and Thermal Stability studies of Materials used as electroceramics, Catalyst and superconductors
B N Wani
BARC Newsletter Founder's Day Special Issue Oct 2014 P-180.

5. Catalysts For Hydrogen Mitigation By Passive Autocatalytic Recombiner,
Salil Varma,
BARC Newsletter Founder's Day Special Issue Oct 2014, P-165.
6. Platinum atomic wire encapsulated in gold nanotubes: A first principle study
S. Nigam, S. K. Sahoo, P. Sarkar and C. Majumder
AIP Conf. Proc. 1591 (2014)468-469.
7. Synthesis and photoluminescence study of Er-doped SnO₂
S. Nigam, A.I. Prasad, V. Sudarsan, and R. K. Vatsa
AIP Conf. Proc. 1591 (2014) 524-525.
8. Structural investigations of Ga₂O₃nanorods
R.M. Pandey, B.S. Naidu, V. Sudarsan, M. Pandey, R.J. Kshirasagar and R.K. Vatsa,
AIP Conference Proceedings 1591 (2014) 426-428.
9. Size induced structural modifications in Y₂Sn₂O₇
M. Pandey, S. Nigam, V. Sudarsan, R.J. Kshirasagar and R.K. Vatsa
AIP Conference Proceedings 1591 (2014) 432-433.
10. Folate-conjugated luminescent Fe₃O₄ nanoparticles for magnetic hyperthermia
K. C. Barick, S. Rana, P. A. Hassan
AIP Conference Proceedings , 1591 (2014) 561-562.
11. Self assembled nanostructured materials for drug delivery
Gunjan Verma, P. A. Hassan,
A book chapter in "Nanotechnology for Biomedical Applications" by Atlantic Publishers, New Delhi, (2014),
259-283



Society for Materials Chemistry

(Reg. No. - Maharashtra, Mumbai/1229/2008/GBBSD)
C/O Chemistry Division, BARC, Mumbai 400 085

Dear Colleagues,

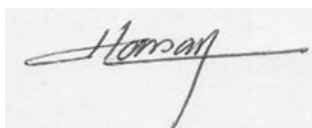
Materials Chemistry has emerged as an important area in Chemistry cutting across the traditional boundaries of Inorganic, Organic and Physical Chemistry. Chemists have been making remarkable contributions to the development of materials for applications in areas as microelectronics, energy technologies, polymer science, catalysis, nanotechnology etc. With ever increasing demand for improved quality of life and depleting natural resources, there is a growing need to develop advanced materials for alternative energy sources such as hydrogen generation and storage, photovoltaic materials, fuel cells, sensor materials, super capacitors, optical materials etc. Some other important materials are in the field of drug delivery systems, soft-matter, biomaterials, multi-ferroics, spintronics and high purity materials. The advent of nanomaterials has brought the new concepts of size and shape dependent functionalities of materials. Likewise, there is a need to develop new materials for Nuclear Technologies as well, in particular from the point of view of new generation reactors such as Advanced Heavy Water Reactor, Compact High Temperature Reactor, Accelerator Driven sub-critical systems and Fast Reactors with shorter doubling time.

Materials Chemistry has been playing significant role in search of novel materials for advanced applications. Novel functional materials emerge as a result of concerted effort of chemists, physicist and materials scientists in general using the basic information in optimization of the structure through compositional as well as particle size variation for improved characteristics for a particular application. The latest trend in Chemistry is to use soft-chemical methods instead of conventional high temperature methods. Nature has been synthesizing a large number of compounds at ambient or very close to ambient conditions using self-assembly.

In view of this, it was felt since long that there is a need to form a society primarily dedicated to Materials Chemistry, but encompassing other disciplines also such as Condensed Matter Physics and Life Sciences. The idea of Society for Materials Chemistry was first germinated during National Workshop on Materials Characterization (NWMC) organized by Chemistry Division, BARC in Sept, 2004. This was further strengthened during 1st DAE-BRNS International Symposium on Materials Chemistry (December, 2006) organized by Chemistry Division BARC. In the valedictory function of ISMC-2006, several delegates supported the need of such scientific interactions for augmenting materials chemistry research in India. With these initial efforts, SMC was founded in early 2008. We are happy to inform you that through our persistent efforts the "Society for Materials Chemistry (SMC)" has been registered under the Mumbai registration act. This society hopes to provide a common platform to young researchers and active scientists in the area of material chemistry to exchange their ideas, develop

interdisciplinary collaborations and share costly instruments / techniques available at premier institutes. SMC will also provide linkages with university researchers and other national laboratories with Department of Atomic Energy. The 2nd, 3rd, 4th and 5th DAE-BRNS International Symposia on Materials Chemistry (December 2008, 2010, 2012 and 2014 respectively) were organized by Chemistry Division, BARC in association with SMC. The Department of Atomic Energy has kindly approved the organization of ISMC series biennially. The next ISMC will be held in Dec. 2016. It was also decided to organize biennial National Workshops on Materials Chemistry (NWMC) under the auspices of SMC. The first NWMC workshop is being held during 7-8 Dec. 2011 at BARC under the theme "functional materials" and the second one being organized under "Catalytic Materials" during 22-23 Nov, 2013. The present one on "Optical Materials" is being organized to celebrate the International Year of Light (IYL 2015). SMC also arranges series of lectures on various contemporary topics by eminent scientists across the globe.

The current life membership of the society stands close to 1000 researchers from different institutes of India. We do hope for further enrichment of the strength and activities of this society and look forward for your active participation to take the society to greater heights.



(Dr. P. A. Hassan)
President
(hassan@barc.gov.in)



(Dr. S. K. Sarkar)
Secretary
(sarkarsk@barc.gov.in)

Society for Materials Chemistry

Society for Materials Chemistry was mooted in 2007 with following aims and objectives:

- to help the advancement, dissemination and application of the knowledge in the field of materials chemistry,
- to promote active interaction among all material scientists, bodies, institutions and industries interested in achieving the advancement, dissemination and application of the knowledge of materials chemistry,
- to disseminate information in the field of materials chemistry by publication of bulletins, reports, newsletters, journals.
- to provide a common platform to young researchers and active scientists by arranging seminars, lectures, workshops, conferences on current research topics in the area of materials chemistry,
- to provide financial and other assistance to needy deserving researchers for participation to present their work in symposia, conference, etc.
- to provide an incentive by way of cash awards to researchers for best thesis, best paper published in journal/national/international conferences for the advancement of materials chemistry,
- to undertake and execute all other acts as mentioned in the constitution of SMC.

Executive Committee

President

Dr. S. K. Sarkar
Bhabha Atomic Research Centre
Trombay, Mumbai, 400 085
sarkarsk@barc.gov.in

Vice-Presidents

Dr. V. K. Jain
Bhabha Atomic Research Centre
Trombay, Mumbai, 400 085
jainvk@barc.gov.in

Prof. Sandeep Verma

Indian Institute of Technology
Kanpur
sverma@iitk.ac.in

Secretary

Dr. P. A. Hassan
Bhabha Atomic Research Centre
Trombay, Mumbai, 400 085
hassan@barc.gov.in

Treasurer

Dr. Sandeep Nigam
Bhabha Atomic Research Centre
Trombay, Mumbai, 400 085
snigam@barc.gov.in

Members

Dr. K. Ananthasivan
Indira Gandhi Centre for Atomic
Research
Kalpakkam, 603102

Dr. (Smt.) A. Banerjee

Bhabha Atomic Research Centre
Trombay, Mumbai-400085

Dr. K. Bhattacharya

Bhabha Atomic Research Centre
Trombay, Mumbai-400085

Dr. D. Das

Bhabha Atomic Research Centre
Trombay, Mumbai-400085

Dr. G. K. Dey

Bhabha Atomic Research Centre
Trombay, Mumbai-400085

Dr. P. Sujata Devi

CSIR Central Glass & Ceramic Re-
search Institute, Kolkata-700032

Dr. C. P. Kaushik

Bhabha Atomic Research Centre
Trombay, Mumbai-400085

Dr. T. Mukherjee

Bhabha Atomic Research Centre
Trombay, Mumbai-400085

Dr. M. C. Rath

Bhabha Atomic Research Centre
Trombay, Mumbai-400085

Dr. (Smt.) S. S. Rayalu

CSIR National Environmental
Engineering Research Institute, Nagapur

Prof. S. D. Samant

Institute of Chemical Technology
Mumbai

Dr. A. K. Tyagi

Bhabha Atomic Research Centre
Trombay, Mumbai-400085

Dr. R. K. Vatsa

Bhabha Atomic Research Centre
Trombay, Mumbai-400085

Co-opted Members

Prof. A. Ajayaghosh
CSIR - National Institute for
Interdisciplinary Science and Technology
Thiruvananthapuram
ajayaghosh@niist.res.in

Prof. A. K. Ganguli

Director, Institute for Nanoscience and
Technology
ashok@chemistry.iitd.ernet.in

Prof. S. Ram

Indian Institute of Technology - Kharagpur
sram @ matsc.iitkgp.ernet.in

Dr. A. K. Tripathi

Bhabha Atomic Research Centre
Trombay, Mumbai-400085
catal@barc.gov.in

Contact address

Society for Materials Chemistry

C/o Chemistry Division, Bhabha Atomic Research Centre, Trombay, Mumbai, 400 085, India
Tel: +91-22-25592001, E-mail: socmatchem@gmail.com

Notes

Notes

Notes

Notes

Notes

Notes

Notes

Notes

Notes

Notes

Notes

Notes

Notes

Notes

Notes

Notes

Notes

Notes

Notes

Notes

Notes

Notes

Notes

Notes

Notes

Notes

Notes

Notes

Notes

Notes

Notes

Notes

Notes

Notes

Notes

Notes

Notes

Notes

Notes

Notes

Notes

3rd cover

